論文 / 著書情報
Article / Book Information

題目(和文)	
Title(English)	Discovering Surface Markers and Functional Characterization of MDSC-like Adherent Cells
著者(和文)	CoSoriano John
Author(English)	Johnclyde Cosoriano
出典(和文)	学位:博士(工学), 学位授与機関:東京工業大学, 報告番号:甲第12627号, 授与年月日:2023年12月31日, 学位の種別:課程博士, 審査員:門之園 哲哉,越川 直彦,山本 直之,小俣 透,小倉 俊一郎,近藤 科江
Citation(English)	Degree:Doctor (Engineering), Conferring organization: Tokyo Institute of Technology, Report number:甲第12627号, Conferred date:2023/12/31, Degree Type:Course doctor, Examiner:,,,,,
学位種別(和文)	博士論文
Type(English)	Doctoral Thesis

Tokyo Institute of Technology
Graduate School of Life Science and Technology
Department of Life Science and Technology

Discovering Surface Markers and Functional Characterization of MDSC-like Adherent Cells

John Clyde L. Co Soriano

Academic adviser: Assoc. Prof. Tetsuya Kadonosono

-2023-

Table of Contents

List of Abbreviations

APC: Average peptide count

BMDC: Bone marrow-derived cells

BMDM: Bone marrow-derived macrophages

CCL: C-C motif ligand

CD: Cluster of differentiation

C/EBPs: CCAAT-enhancer-binding proteins

cGMP: Cyclic guanosine monophosphate

CXCL: C-X-C motif chemokine ligand

FACS: Fluorescence activated cell sorting

FSC: Forward scatter

GM-CSF: Granulocyte-macrophage colony-stimulating factor

CSF: Granulocyte-colony-stimulating factor

GSEA: Gene set enrichment analysis

GO: Gene ontology

HSC: Hematopoietic stem cells

IFN γ : Interferon γ

IgCAM: Immunoglobulin super family cell adhesion molecules

IL: Interleukin

iNOS: Inducible nitric oxide synthase

ITAM: Immunoreceptor tyrosine-based activation motif

LC-MS/MS: Liquid chromatography tandem mass spectrometry

Lck: Lymphocyte-specific protein tyrosine kinase

M-MDSC: Monocytic myeloid derived suppressor cells

MAPK: Mitogen activated protein kinase

MMP: Matrix metallopeptidase

M-CSF: Macrophage colony stimulating factor

MDSC: Myeloid derived suppressor cells

MFI: Relative median fluorescence intensity

MHC: Major histocompatibility complex

MLAC: MDSC-like adherent cell

NGS: Next generation sequencing

NK: Natural killer

PI: Propidium iodide

PMN-MDSC: Polymorphonuclear myeloid derived suppressor cells

qRT-PCR: Real-time quantitative reverse transcription PCR

RIN: RNA integrity

RIPA: Radioimmunoprecipitation assay

ROS: Reactive oxygen species

SDS-PAGE: Sodium dodecyl-sulfate polyacrylamide gel electrophoresis

SSC: Side scatter

STAT: Signal transducer and activator of transcription

TAM: Tumor associated macrophage

TCR: T cell receptor

TME: Tumor microenvironment

TNF α : Tumor necrosis factor α

TPM: Transcripts per million

Treg: Regulatory T cell

TRM: Tissue resident macrophage

VEGF: Vascular endothelial growth factor

UMAP: Uni-form manifold approximation and projection

RRHO: Rank-rank hypergeometric overlap

Chapter 1

General Introduction

1-1. Tumor microenvironment

The tumor microenvironment (TME) is a dynamic and complex environment that includes the tumor cells, vasculature, and surrounding stroma. The development of the TME has an essential role in tumor malignant progression such as invasion, metastasis and treatment resistance[1]. The physical and biochemical environment within the TME promotes the invasion and continuous division of cancer cells. Immune cells such as neutrophils, monocytes, macrophages, T lymphocytes, dendritic cells and natural killer (NK) cells are usually recruited into tumors in order to attack tumors and promote anti-tumor immune responses[2]. In TME, however, lymphocyte infiltration does not always correlate with tumor clearance due to the emergence of cells with immunosuppressive functions: Cells that initially have anti-tumor effect can be reprogrammed into immunosuppressive cells as tumor grows. The immunosuppressive cells in tumor-bearing host include regulatory T (T_{reg}) cells, tumor associated macrophages (TAM) and myeloid derived suppressor cells (MDSC)[3].

During tumor progression, the TME is characterized by chronic inflammation and hypoxia. The biochemical environment in the TME is composed of a complex mixture of different cytokines, chemokines and growth factors that promote inflammation, recruitment of immune cells, and the division of cancer cells[4]. The immune and cancer cells under chronic inflammation and hypoxic microenvironments further release cytokines and chemokines that recruit and activate immunosuppressive cells in a positive feedback loop[5]. Many cancer cells secrete cytokines and growth factors such as platelet derived growth factor (PDGF), transforming growth factor (TGF β), C-C motif ligand (CCL) 2, and C-X-C motif chemokine ligand (CXCL) 8[6] to increase tumor growth in an autocrine manner. Cytokines such as IL-3, CXCL5, CCL3, CXCL1, and CXCL2 recruit MDSCs and TAMs[4,6] while granulocyte-macrophage colony-

stimulating factor (GM-CSF), granulocyte colony-stimulating factor (G-CSF), IL-3, vascular endothelial growth factor (VEGF), and tumor necrosis factor (TNF) α [8] can promote the growth of MDSCs and induce them to differentiate into TAMs[9,10] (Fig. 1-1).

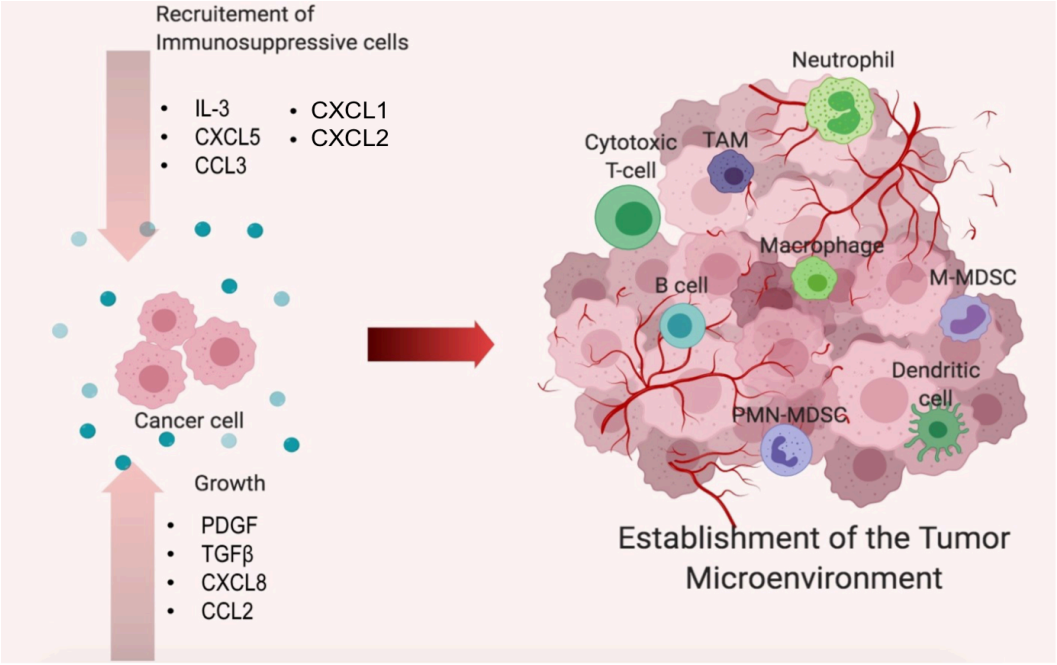

Fig. 1-1. Schematic diagram of the tumor microenvironment. Various factors secreted from cancer cells stimulate further tumor growth and recruit immunosuppressive cells. The immunosuppressive cells (violet) build up an immunosuppressive network and prevents of tumor cell killing by inhibiting the anti-tumor activities of some immune cells (green).

1-2 Myeloid derived suppressor cells

MDSCs are a heterogeneous population of myeloid cells that are involved in tumor-dependent immune dysfunction. Their most significant effect in the TME is the inhibition of T-cell anti-tumor response. It is also one of the most intensely studied mechanism of immunosuppression in the TME in recent years[11–13]. MDSCs can be found in the liver, spleen, blood and tumor samples in various tumor models and in cancer patients[14,15]. The amount of circulating MDSCs in cancer patients have been correlated with severity of tumor prognosis, reduced survival[16] and unresponsiveness to cancer therapy[17].

1-2-1. Differentiation and recruitment of MDSCs

MDSCs are rarely detected in healthy humans but are expanded during chronic infection and cancer. Their presence was hypothesized to reduce immune-pathological damage during extended periods of inflammation[18]. They can also be transiently found in neonates; and may have a role in the reduction of immune reactivity during fetal development[19]. The development of MDSCs and myeloid cells are influenced by tumor-derived soluble factors such as inflammatory cytokines and growth factors[20]. The combination and changes of these factors due to chronic inflammation increases myelopoiesis in cancer patients.

MDSCs originate from the hematopoietic stem cells (HSC) in the bone marrow which differentiate into the common lymphoid progenitor (Fig. 1-2)[21]. This development is mediated by the growth factors: GM-CSF, G-CSF, and M-CSF. In the spleens of healthy individuals, these cells continue to differentiate into macrophages, neutrophils, and dendritic cells. However, the continuous inflammation causes rapid myelopoiesis because the body is trying to control the emergence of tumor. Consequently, a significant amount of these cells are unable to completely differentiate to mature neutrophils of phagocytic monocytes; some of these are MDSC[21,22]. These MDSCs are also arrested in different stages of development. MDSCs are also produced in healthy individuals, but their numbers are very small and they immediately differentiate into mature granulocytes and monocytes. Studies have shown that HSC can be induced to differentiate into MDSCs through treatment with GM-CSF and IL-6 or GM-CSF and IL-1 β [24]. M-MDSCs can differentiate into PMN-MDSCs[25]. Both M-MDSC and PMN-MDSC have the capacity to differentiate into TAM[15,26].

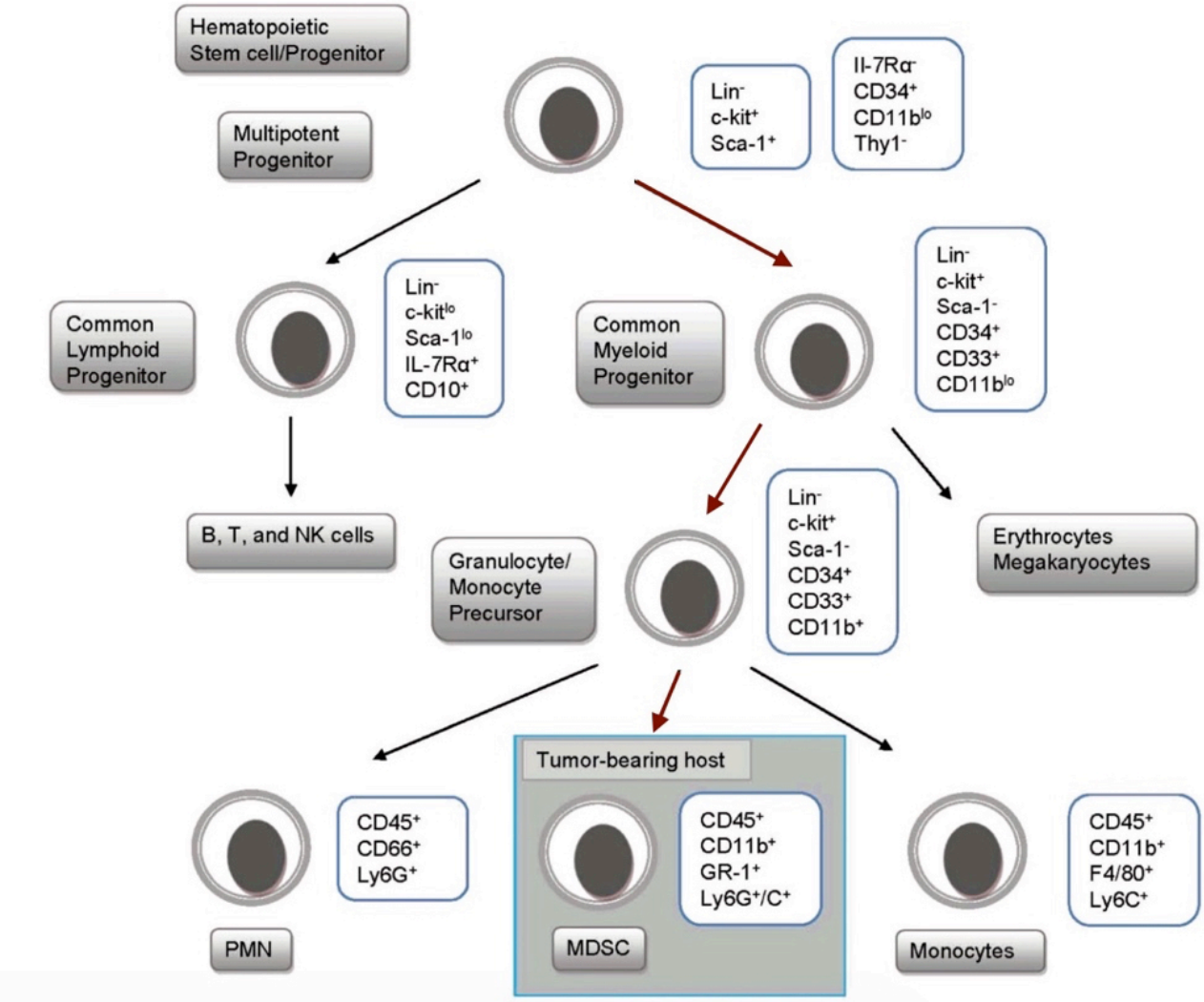

Fig. 1-2. Differentiation lineage of Myeloid Derived Suppressor Cells. MDSCs originated from the common lymphoid progenitor which becomes the granulocyte/monocyte precursor. Figure adapted from Goedegebuure et al. 2011[21].

Several transcription factors have been discovered that orchestrate MDSC development. The signal transducer and activator of transcription (STAT) family of transcription factors is directly involved in the production and expansion of MDSC. STAT3 may be activated by several tumor-derived factors such as GM-CSF[27], G-CSF[28], IL-6, and IL-11[29]. STAT3 inhibitor drugs such as axitinib have been shown to be able to decrease MDSC accumulation[23]. CCAAT-enhancer-binding proteins (C/EBPs) are a family of transcription regulators that contain a basic-region-

leucine zipper domain and are key regulators of granulocyte production[30]. C/EBPs are upregulated in cluster of differentiation (CD) $11b^+$ myeloid cells such as MDSCs as a response to inflammatory signals[31]. Conditional knockout of C/EBPs using *Cebpb*$^{flox/flox}$*;Tie2cre* mice reduced the immunosuppressive ability of the $CD11b^+$ myeloid cells[9].

1-2-2. Subsets of MDSCs

MDSC population is heterogeneous, but these cells can be broadly divided into two subpopulations: monocytic MDSCs (M-MDSC) and polymorphonuclear or granulocytic MDSCs (PMN-MDSC). The key function of MDSCs is to suppress the activity and proliferation of T cell, but M-MDSCs and PMN-MDSCs have different mechanisms of immune suppression. M-MDSCs suppress T cell responses through the production of inducible nitric oxide synthase （iNOS） and the immunosuppressive cytokines IL-10 and TGF-β. iNOS leads to the production of nitric oxide from L-arginine[32]. This causes a deficiency in L-arginine and leads to the reduction in CD3ζ expression and inhibition of T cell proliferation[33]. Furthermore nitric oxide can also impair T cell receptor signaling though targeting of cyclic guanosine monophosphate (cGMP) dependent protein kinase and IL-2 signaling which is necessary for T-cell activation[34–36]. PMN-MDSC, on the other hand produces arginase, coded by (*Arg1* and *Arg2*) and reactive oxygen species (ROS)[26,37] (Fig. 1-3). Arginase, hydrolyzes L-arginine to urea and L-ornithine consequently leading to deficiency in L-arginine. Another consequence of this production of L-ornithine is that it is used as a nutrient source for further growth of tumors[38]. ROS production is mediated by NADPH oxidase 2 and prevents the recognition between T cell receptor (TCR) and major histocompatibility complex (MHC)-peptide complex of antigen specific T cells. Another effect of ROS is the generation of peroxynitrite through the reaction of

NO with superoxide, which nitrates TCRs and T cell response to cognate antigen-MHC complexes[39].

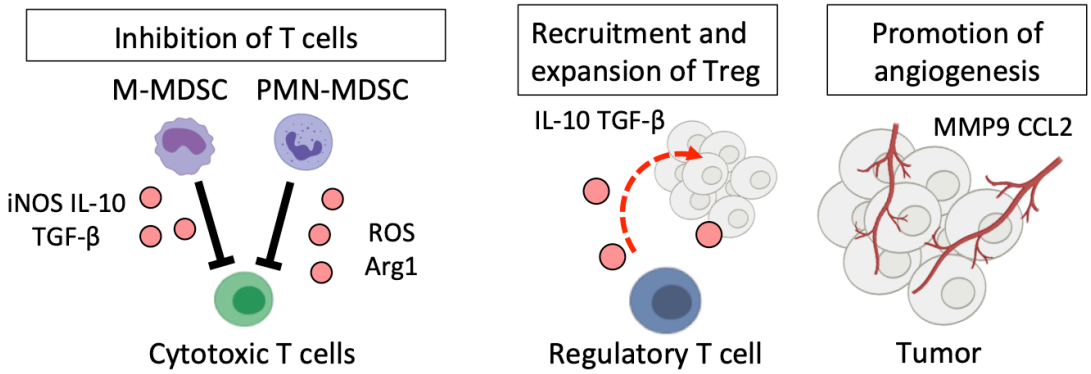

Fig. 1-3. Summary of contribution of MDSC on tumor progression.

Previous studies have compared the immunosuppressive abilities between PMN-MDSCs and M-MDSCs[40]. PMN-MDSCs isolated from tumors were more immunosuppressive to T cells than tumor derived M-MDSCs[41]. Furthermore, tumor derived M-MDSCs and PMN-MDSCs were more immunosuppressive when compared to the same population isolated from the spleen. MDSCs can also promote T_{reg} activation and expansion through interaction of CD40–CD40L and secretion of interferon (IFN) γ, IL-10, and TGF β [42]. MDSCs can also stimulate tumor angiogenesis by producing VEGF, Basic fibroblast growth factor, prokineticin 2, matrix metallopeptidase (MMP) 9, and CCL2[43,44] (Fig. 1-3).

The presence of MDSC correlates to poor phagocytic activity of antigen presenting cells and poor T cell infiltration due to their immunosuppressive activities[5]. Hence several therapeutic strategies involving specific targeting of MDSCs were formulated. Many of these show an improvement in the anti-tumor activities of T cells and NK cells within the TME[45,46].

1-2-3. Specific surface markers of MDSC

The most commonly used markers to differentiate the two types of MDSCs in mice is through the markers: CD11b, Ly6C, Ly6G, and Gr-1. M-MDSC are $CD11b^{+}$ $Gr\text{-}1^{low}$ $Ly6G^{-}$ $Ly6C^{hi}$ while PMN-MDSCs are $CD11b^{+}$ $Gr\text{-}1^{hi}$ $Ly6G^{+}$ $Ly6C^{low}$[25] (Fig. 1-4). CD11b is a myeloid cell marker; Ly6C is a monocyte marker while Ly6G is a granulocyte marker[25]. Gr-1, which is a combination of the Ly6G and Ly6C, has been commonly used to characterize MDSCs[47]. Anti-Gr-1 antibody binds with different affinities to Ly6C and Ly6G[7]. The $Gr\text{-}1^{high}$ tumor infiltrating cell population is mainly composed of PMN-MDSCs and $Gr\text{-}1^{int}$ population contains M-MDSCs and other immature myeloid cells. The Gr-1 antigen is not present in humans. Instead, human M-MDSC are defined as $CD11b^{+}CD14^{+}CD33^{+}$, and PMN-MDSCs are defined as $CD11b^{+}$ $CD15^{+}CD66b^{+}$ [26].

Several markers have been discovered and employed to more clearly distinguish MDSC subsets, such as CD1d[48] for M-MDSCs and LOX-1[49] for PMN-MDSCs in humans. For mice, CD49d has been found to be a specific marker for M-MDSCs[50] (Fig. 1-4). At present, Alshetaiwi, et al, have discovered junctional adhesion molecule (JAML) as the most comprehensive marker to label both subsets of MDSCs in both humans and mice through single cell RNA sequencing in mouse and human tumor samples. Furthermore, they have found that CD84 can label M-MDSC in both humans and mice[51] (Fig. 1-4).

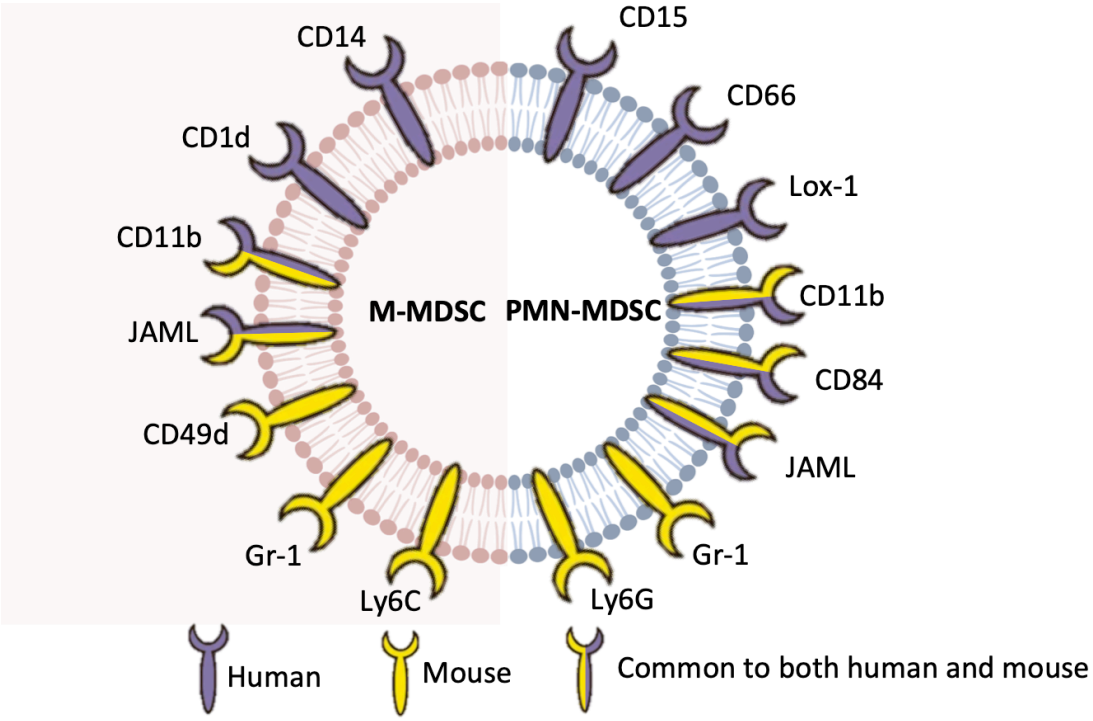

Fig. 1-4. Summary of known surface markers for M-MDSC and PMN-MDSC in humans and mice.

A heterodimer of S100A8 and S100A9 (S100A8/A9, also known as calprotectin) is a calcium binding protein. Its main function is in inflammation where it promotes the recruitment of leukocytes. They are expressed predominantly by granulocytes, monocytes, and macrophages that are in the early differentiation stages[52]. This protein is highly expressed by MDSC in the tumor and is indicative of MDSC function[53].

1-3. Tumor associated macrophages

TAMs are dysregulated macrophages that have a very different activity from physiologically healthy macrophages, which have phagocytic and antigen presenting abilities[54]. In contrast to classically activated macrophages, TAMs have pro-tumor activities such as promoting tumor progression and metastasis[55]. Furthermore, in the clinical setting, TAMs have been found to

contribute to resistance to chemotherapy and radiotherapy[56], provide a protective niche for cancer stem cells[57], and promotion of metastasis[58]. TAMs may originate from either the bone marrow-derived macrophages (BMDMs) or tissue resident macrophages (TRMs). BMDMs are recruited to tumors through CCR2 signaling, where they start to differentiate to TAMs. They increase expression of CXCR4 as they attach to blood vessels[59], and by the time they reach the tumor, they have already acquired the TAM phenotype. On the other hand, the presence of a tumor causes transcriptional changes in genes related to antigen presentation and remodeling of extracellular matrix in the TRMs[60]. In addition, the increased production of IL-4 and CSF-1 from tumor cells stimulate the proliferation of TRMs with this transcriptional change and promotes differentiation into TAMs[61].

TAMs promote tumor growth, angiogenesis, or metastasis through several secreted factors: vascular endothelial growth factor (VEGF), platelet-derived growth factor (PEGF), and endothelial growth factor (EGF)[62], MMP9 and MMP7[63], or CSF-1[64], respectively. In addition, TAMs facilitate the development of immunosuppressive TME by recruiting T_{reg} cells by secreting IL-10 and by blocking the effector function of cytotoxic T cells[65].

1-4. MDSC-like adherent cells

A previous report has isolated and characterized a previously unknown subset of MDSCs termed MDSC-like adherent cells (MLAC) from multiple tumor mouse models[66]. MLAC possess strong adhesion to culture dish like macrophages, but they express less of the macrophage marker F4/80 and more of the MDSC marker Gr-1 (Fig. 1-5). They were reported to be present even at the early stage of solid tumors and promote tumor growth through secretion of CXCL1, CXCL2, and CXCL5 and promote angiogenesis. Co-injection of MLACs and cancer cells have

shown that MLAC increases the rate of tumor establishment and tumor growth[66]. They can also recruit MDSCs through CCL2/5 and CXCL1/2/5 signaling (Fig. 1-6).

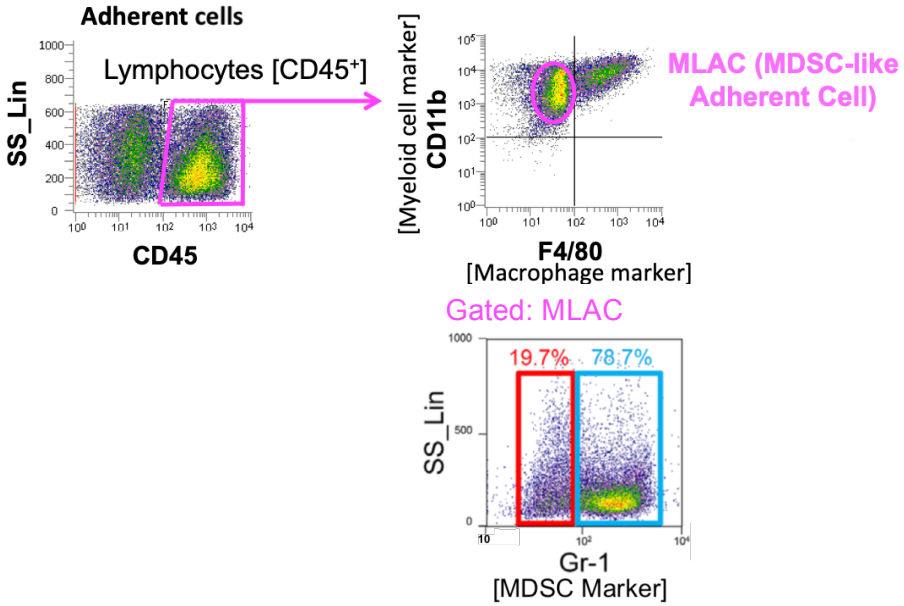

Fig. 1-5. Gating of MLAC from adherent cells from tumor.

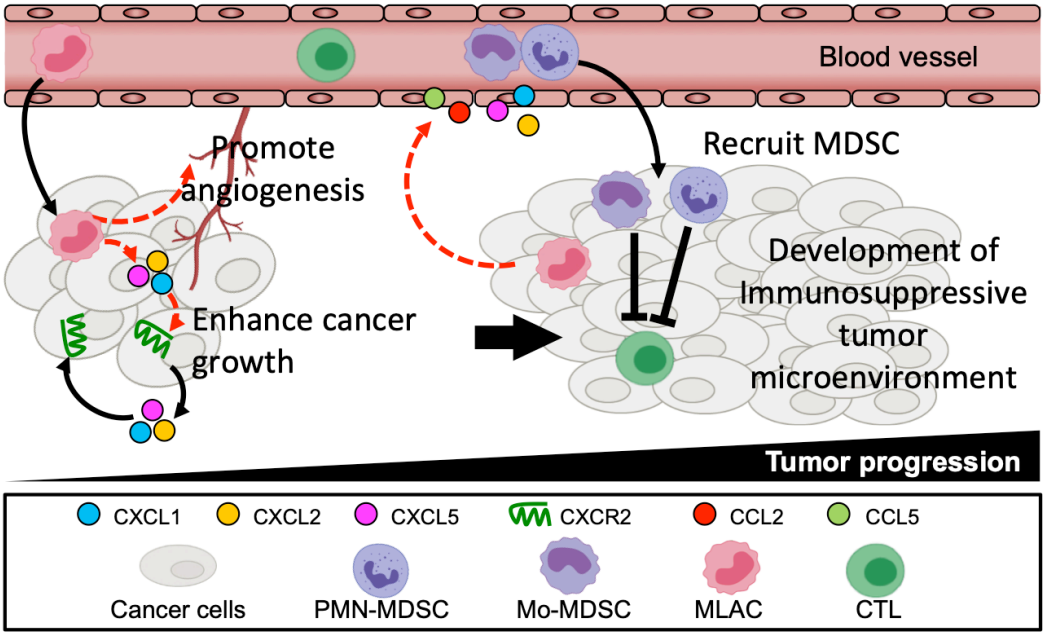

Fig. 1-6. Mechanisms of action of MLACs to promote tumor development. Adopted from Tsubaki, et al[66].

MLACs also did not show any ability to differentiate into other cells, unlike some populations of MDSCs, which can differentiate into TAM[25]. There are currently no known specific markers for MLACs which is a hurdle towards elucidating this cell further. Conceptually, MLAC is similar to the study of Shen, et al, 2014[67], wherein they analyzed the adherent and non-adherent cells while generating MDSCs from bone marrow cells using GM-CSF and tumor conditioned medium. They have found that the non-adherent cells suppressed T cell proliferation but adherent cells were co-cultured with stimulated T cells showed weak suppressive activity. Their analyses suggested that the adherent cells were immature myeloid cells.

1-4-1. Previously known surface markers of MLACs

Both MLACs and MDSCs contain a mixture of $Ly6C^+$ (monocyte marker) and $Ly6G^+$ populations (granulocyte marker). Because Gr-1 is a collective antigen for Ly6C and Ly6G, MLACs and MDSCs are both $CD11b^+Gr\text{-}1^+$ populations[68]. However the proportion of monocytic and granulocytic cells differ between MLACs and MDSCs. Through staining of Ly6G and Ly6C, previous research has found that the majority of the composition of MLACs and MDSCs are granulocytic cells (Figs. 1-7, 1-8), but the percent of monocyte population within MLACs may be greater than MDSCs (Figs. 1-7, 1-8). Hence these 2 populations have slightly different compositions, which highlight their heterogeneity.

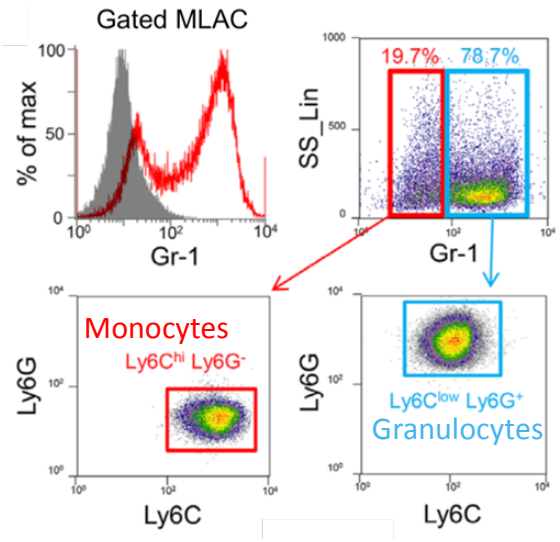

Fig. 1-7. Analysis of the granulocytic and monocytic cell composition of MLACs. MLACs have heterogeneous expression of Gr-1. The granulocytic and monocytic subsets of MLACs were determined through Ly6G and Ly6C expression, respectively. Adopted from Tsubaki, et al, 2018[1].

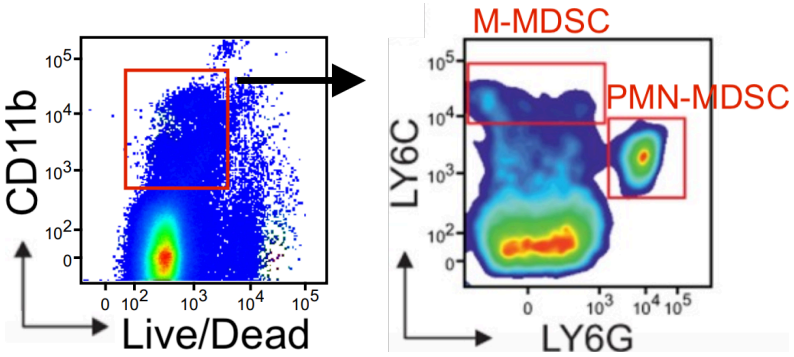

Fig 1-8. Analysis of the granulocytic and cell composition of MDSCs. MDSCs were gated from living $CD11b^+$ cells of solid tumors. Monocytic M-MDSC and granulocytic PMN-MDSC subpopulations were determined through $Ly6G^+$ and $Ly6C^+$ staining, respectively. Figure adopted from Damuzzo, et al[3].

1-4-2. Initial analysis of cellular identity of MLACs

The expression of common cell surface markers on myeloid cells were tested by flow cytometry[66]. MLACs were found to not express monocyte (CD68, CX3CR1), mast cells (c-Kit), eosinophils (Siglec-F), or basophils (Fc ε RI α) markers, and MLACs only weakly expressed the monocyte marker CCR2 and the hematopoietic progenitor cell marker (CD34) (Fig. 1-9).

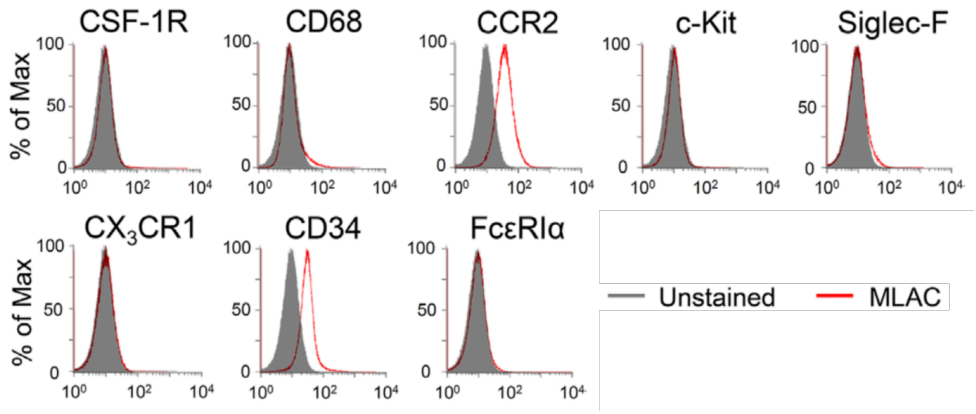

Fig. 1-9. General surface marker expression analysis of MLACs through flow cytometry analysis. Expression of indicated surface markers on MLACs were shown by red histograms. Gray-filled histograms indicate negative controls (unstained cells).

In order to determine the relationship of MLACs with other myeloid cells, MLACs were also screened for marker genes from different myeloid cells[66]. MLACs expressed *Cebpa* and *Cebpb* which immature myeloid cell markers and had a low expression of the MDSC gene marker *S100a8*. MLACs had low expression of the marker genes of TAMs (*Mertk, Mafb*) but have weak expression of DC markers (*Zbtb46, Irf8*) (Fig. 1-10). These suggest that MLACs possess some similarities to immature myeloid cells or dendritic cells.

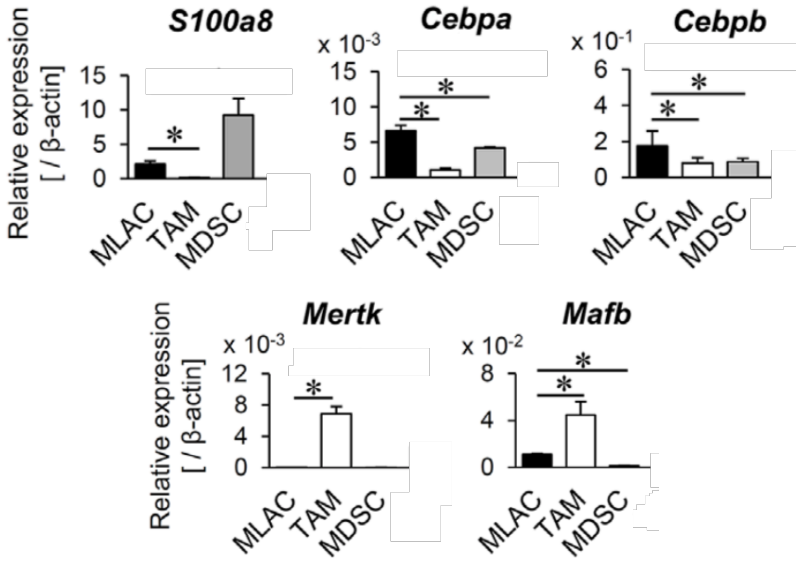

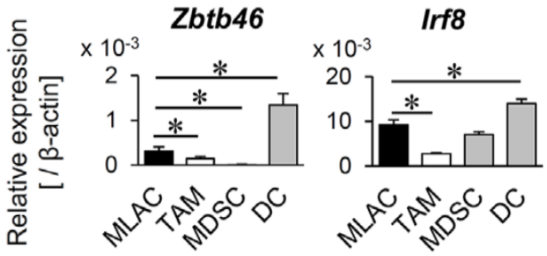

Fig 1-10. Transcript levels of myeloid cells marker genes in MLACs, TAMs, MDSCs, and DCs. Indicated gene expressions were examined by qRT-PCR. Error bars indicate standard deviation; *, $p<0.05$ vs. MLACs. $n = 3$.

1-5. Cell adhesion molecules

Adhesion proteins are responsible for many cellular functions such as anchorage, signal transduction, differentiation, growth, and many others. The interaction of cellular adhesion proteins to the extracellular matrix components, such as collagen and fibronectin allow for the remodeling of physiological structures in the body[69]. The major classifications of adhesion proteins are the integrins, immunoglobulin super family cell adhesion molecules (IgCAM), selectins, and cadherins[70] (Table 1-1).

Table 1-1. Major classifications of adhesion proteins

Classification*	Members	Function
Integrins	24 known αβ-heterodimers, 18 α-subunits, and 8 β-subunits	Connection between the extracellular matrix and actin cytoskeleton of cells
Immunoglobulin super family cell adhesion molecules (IgCAM)	ICAM1	Cell–cell adhesion by binding to specific ligands in the ECM and surrounding cells
	NCAM	
	VCAM	Leukocyte adhesion to endothelial cells
	PECAM	Adhesion and accumulation of platelets
Selectins	E-Selectin	Adhesion between epithelial cells
	P-Selectin	Adhesion between epithelial cells
	L-Selectin	Tumor intercellular adhesions and Adhesive connections between endothelial cells
Cadherins	E-Cadherin	Adhesion of platelets to tumor cells, lymphocyte homing, endothelial cells-
	P-Cadherin	

	N-Cadherin	tumor cells, interaction of tumor cells
	VE-Cadherin	

*Adopted from Lin, et al[70].

Integrin is a large family of adhesion proteins that are abundantly expressed on the cell surface to allow for strong adhesion of cells to the extracellular matrix. They are composed of an alpha (α) and a beta (β) subunit to form a ligand binding head[71]. There is great diversity in the combinations of the α and β subunits to form different integrin molecules. $\alpha_M\beta_2$ (CD11b), a myeloid cell marker, is able to bind to a wide variety of unrelated ligands such as ICAMs and fibrinogen[72]. Other major leukocyte integrins are summarized in Table 1-2. Individually, integrins exhibit relatively low affinities for their ligands (dissociation constants K_D between 10^{-6} and 10^{-8} M) when compared with cell-surface hormone receptors (K_D values of 10^{-9} to 10^{-11} M)[73], but the binding of several hundred thousand integrin molecules would allow the cell to firmly adhere on their substrate.

Table 1-2. Major leukocyte integrins

Integrin*	**Ligands**
CD11a/CD18 ($\alpha_L\beta_2$)	ICAMs (1-5), JAM-1
CD11b/CD18 ($\alpha_M\beta_2$)	ICAMs (1, 2, 4), fibrinogen
CD49d ($\alpha_4\beta_1$)	VCAM-1, fibronectin, JAM-2
CD11c/CD18 ($\alpha_X\beta_2$)	collagen I, iC3b, fibrinogen, ICAMs (1, 2, 4)
CD11d/CD18 ($\alpha_D\beta_2$)	fibronectin, fibrinogen, vitronectin and plasminogen

*Adopted from Hyun, et al and Mezu, et al[74,75].

Selectins are a group of adhesion proteins that have an essential role in immune response. L-selectin (CD62L) is usually expressed by leukocytes including T cells and myeloid cells; P-selectin (CD62P) is usually expressed by platelets; and E-selectin is usually expressed in endothelial cells[76]. The main function of selectins is to allow the cell to adhere to the blood vessel while the blood is still flowing. Leukocytes undergo a process of rolling, anchoring and

then transmigrating to the sites of inflammation or infection. In this study, I characterized whether MLACs have a different adhesion protein profile compared to MDSCs, which may be able to explain its strongly adherent nature.

1-6. Research purpose

The aims of this study are: *1. Determine novel surface markers of MLACs in order to isolate MLACs using fluorescence activated cell sorting (FACS).* To identify the markers, I used a strategy combining RNA-sequencing analysis and Shotgun proteomics. *2. Identify the molecular identity of MLACS and determine a MLAC-specific gene signature, by using public single cell RNA-seq dataset.* This will be used as a tool to distinguish MLACs from MLACs. *3. Confirm the marker positive MLAC population isolated with FACS is the same as previously reported MLAC by confirming the expression of MLAC gene signature and through functional in vitro analyses.*

References

1. Larsen, J. E. & Minna, J. D. Molecular biology of lung cancer: clinical implications. *Clin. Chest Med.* 32, 703–740 (2011).

2. Vinay, D. S. *et al.* Immune evasion in cancer: Mechanistic basis and therapeutic strategies. *Seminars in Cancer Biology* 35, S185–S198 (2015).

3. Shurin, G. V, Ma, Y. & Shurin, M. R. Immunosuppressive Mechanisms of Regulatory Dendritic Cells in Cancer. *Cancer Microenviron.* 6, 159–167 (2013).

4. Jin, M.-Z. & Jin, W.-L. The updated landscape of tumor microenvironment and drug repurposing. *Signal Transduct. Target. Ther.* 5, 166 (2020).

5. Kumar, V. *et al.* Cancer-associated fibroblasts neutralize the anti-tumor effect of CSF1 receptor blockade by inducing PMN-MDSC infiltration of tumors. *Cancer Cell* 32, 654-668.e5 (2017).

6. Zhang, X., Nie, D. & Chakrabarty, S. Growth factors in tumor microenvironment. *Front. Biosci. (Landmark Ed.* 15, 151–165 (2010).

7. Serafini, P. *et al.* Derangement of immune responses by myeloid suppressor cells. in *Cancer Immunology, Immunotherapy* 53, 64–72 (2004).

8. Sade-Feldman, M. *et al.* Tumor Necrosis Factor-α Blocks Differentiation and Enhances Suppressive Activity of Immature Myeloid Cells during Chronic Inflammation. *Immunity* 38, 541–554 (2013).

9. Marigo, I. *et al.* Tumor-induced tolerance and immune suppression depend on the C/EBP β transcription factor. *Immunity* 32, 790–802 (2010).

10. Melani, C., Chiodoni, C., Forni, G. & Colombo, M. P. Myeloid cell expansion elicited by the progression of spontaneous mammary carcinomas in c-erbB-2 transgenic BALB/c mice suppresses immune reactivity. *Blood* 102, 2138–2145 (2003).

11. Youn, J.-I. & Gabrilovich, D. I. The biology of myeloid-derived suppressor cells: The blessing and the curse of morphological and functional heterogeneity. *Eur. J. Immunol.* 40, 2969–2975 (2010).

12. Tavazoie, M. F. *et al.* LXR/ApoE Activation Restricts Innate Immune Suppression in Cancer. *Cell* 172, 825-840.e18 (2018).

13. Kumar, V., Patel, S., Tcyganov, E. & Gabrilovich, D. I. The nature of myeloid-derived suppressor cells in the tumor microenvironment. *Trends Immunol.* 37, 208–220 (2016).

14. Ilkovitch, D. & Lopez, D. M. The Liver is a Site for Tumor Induced Myeloid-Derived Suppressor Cell Accumulation and Immunosuppression. *Cancer Res.* 69, 5514–5521 (2009).

15. Corzo, C. A. *et al.* HIF-1α regulates function and differentiation of myeloid-derived suppressor cells in the tumor microenvironment. *J. Exp. Med.* 207, 2439–2453 (2010).

16. Peng, S., Aijuan, W., Mengye, H., Qingqing, W. & Shusen, Z. Increased circulating $Lin^{-/low}CD33^{+}HLA\text{-}DR^{-}$ myeloid‐derived suppressor cells in hepatocellular carcinoma patients. *Hepatol. Res.* 44, 639–650 (2014).

17. Pitt, J. M. *et al.* Resistance mechanisms to immune-checkpoint blockade in cancer: tumor-intrinsic and -extrinsic factors. *Immunity* 44, 1255–1269 (2018).

18. Dorhoi, A. & Du Plessis, N. Monocytic myeloid-derived suppressor cells in chronic infections. *Front. Immunol.* 8, 1895 (2018).

19. He, Y.-M. *et al. Transitory presence of myeloid-derived suppressor cells in neonates is critical for control of inflammation*. *Nature Medicine* (2018). doi:10.1038/nm.4467

20. Gimeno, R. & Barquinero, J. Myeloid-derived suppressor cells (MDSC): Another player in the orchestra. *Inmunología* 30, 45–53 (2011).

21. Goedegebuure, P. *et al.* Myeloid-derived suppressor cells: general characteristics and relevance to clinical management of pancreatic cancer. *Curr. Cancer Drug Targets* 11, 734–751 (2011).

22. Wynn, T. A. Myeloid-cell differentiation redefined in cancer. *Nat. Immunol.* 14, 197–199 (2013).

23. Condamine, T., Mastio, J. & Gabrilovich, D. I. Transcriptional regulation of myeloid-derived suppressor cells. *J. Leukoc. Biol.* 98, 913–922 (2015).

24. Lechner, M. G., Liebertz, D. J. & Epstein, A. L. Characterization of cytokine-induced myeloid-derived suppressor cells from normal human peripheral blood mononuclear cells. *J. Immunol.* (2010). doi:10.4049/jimmunol.1090100

25. Youn, J.-I., Nagaraj, S., Collazo, M. & Gabrilovich, D. I. Subsets of myeloid-derived suppressor cells in tumor bearing mice. *J. Immunol.* 181, 5791–5802 (2008).

26. Bronte, V. *et al.* Recommendations for myeloid-derived suppressor cell nomenclature and characterization standards. *Nat. Commun.* 7, 1–10 (2016).

27. Furuya, M. Y. *et al.* Tofacitinib inhibits granulocyte–macrophage colony-stimulating factor-induced NLRP3 inflammasome activation in human neutrophils. *Arthritis Res. Ther.* 20, 196 (2018).

28. Chakraborty, A. & Tweardy, D. J. Stat3 and G-CSF-induced myeloid differentiation. *Leuk. Lymphoma* 30, 433–442 (1998).

29. Johnson, D. E., O'Keefe, R. A. & Grandis, J. R. Targeting the IL-6/JAK/STAT3 signalling axis in cancer. *Nat. Rev. Clin. Oncol.* 15, 234–248 (2018).

30. Satake, S. *et al.* C/EBP β is involved in the amplification of early granulocyte precursors during candidemia-induced 'emergency' granulopoiesis. *J. Immunol.* 189, 4546–4555 (2012).

31. Wang, W., Xia, X., Mao, L. & Wang, S. The CCAAT/Enhancer-Binding Protein Family: Its Roles in MDSC Expansion and Function. *Front. Immunol.* 10, 1804 (2019).

32. Gabrilovich, D. I. & Nagaraj, S. Myeloid-derived suppressor cells as regulators of the immune system. *Nat. Rev. Immunol.* 9, 162–174 (2009).

33. Rodriguez, P. C., Zea, A. H., Culotta, K. S., Zabaleta, J. & Ochoa Augusto C Ochoa, J. B. Regulation of T cell receptor CD3 ζ chain expression by L-arginine. *J. Biol. Chem.* (2002). doi:10.1074/jbc.M110675200

34. Albeituni, S. H., Ding, C. & Yan, J. Hampering immune suppressors: therapeutic targeting of myeloid-derived suppressor cells in cancer. *Cancer J.* 19, 490–501 (2013).

35. Gnipp, S. *et al.* Nitric oxide dependent signaling via cyclic GMP in dendritic cells regulates migration and T-cell polarization. *Sci. Rep.* 8, 10969 (2018).

36. Mazzoni, A. *et al.* Myeloid suppressor lines inhibit T cell responses by an NO-dependent mechanism. *J. Immunol.* 168, 689–695 (2002).

37. Chen, X., Song, M., Zhang, B. & Zhang, Y. Reactive Oxygen Species Regulate T Cell Immune Response in the Tumor Microenvironment. *Oxid. Med. Cell. Longev.* 2016, 1580967 (2016).

38. Bronte, V., Serafini, P., Mazzoni, A., Segal, D. M. & Zanovello, P. L-arginine metabolism in myeloid cells controls T-lymphocyte functions. *Trends Immunol.* 24, 302–306 (2003).

39. Nagaraj, S. *et al.* Altered recognition of antigen is a mechanism of $CD8^+$ T cell tolerance in cancer. *Nat. Med.* (2007). doi:10.1038/nm1609

40. Haverkamp, J. M. *et al.* Myeloid-derived suppressor activity is mediated by monocytic lineages maintained by continuous inhibition of extrinsic and intrinsic death pathways. *Immunity* 41, 947–959 (2014).

41. Li, K. *et al.* Myeloid-derived suppressor cells as immunosuppressive regulators and therapeutic targets in cancer. *Signal Transduct. Target. Ther.* 6, 362 (2021).

42. Serafini, P., Mgebroff, S., Noonan, K. & Borrello, I. Myeloid derived suppressor cells promote cross-tolerance in B cell lymphoma by expanding regulatory T cells. *Cancer Res.* 68, 5439–5449 (2008).

43. Shojaei, F. *et al.* G-CSF-initiated myeloid cell mobilization and angiogenesis mediate tumor refractoriness to anti-VEGF therapy in mouse models. *Proc. Natl. Acad. Sci. U. S. A.* 106, 6742–6747 (2009).

44. Bruserud, O. & Kittang, A. O. The chemokine system in experimental and clinical hematology. *Curr. Top. Microbiol. Immunol.* 341, 3–12 (2010).

45. Tavazoie, M. F. *et al.* LXR/ApoE Activation Restricts Innate Immune Suppression in Cancer. *Cell* 172, 825-840.e18 (2018).

46. Lindau, D., Gielen, P., Kroesen, M., Wesseling, P. & Adema, G. J. The immunosuppressive tumour network: myeloid-derived suppressor cells, regulatory T cells and natural killer T cells. *Immunology* 138, 105–115 (2013).

47. Wang, J.-X. *et al.* Ly6G ligation blocks recruitment of neutrophils via a β2-integrin-dependent mechanism. *Blood* 120, 1489–1498 (2012).

48. An, B. *et al.* CD1d is a novel cell-surface marker for human monocytic myeloid-derived suppressor cells with T cell suppression activity in peripheral blood after allogeneic hematopoietic stem cell transplantation. *Biochem. Biophys. Res. Commun.* 495, 519–525 (2018).

49. Condamine, T. *et* al. Lectin-type oxidized LDL receptor-1 distinguishes population of human polymorphonuclear myeloid-derived suppressor cells in cancer patients. *Science immunology* 1, (2016).

50. Korangy, F., Greten, T. F., Haile, L. A., Gamrekelashvili, J. & Manns, M. P. Subpopulations in mice myeloid-derived suppressor cell cd49d is a new marker for distinct cd49d is a new marker for distinct myeloid-derived suppressor cell subpopulations in mice. *J. Immunol.* 185, 203–210 (2017).

51. Alshetaiwi, H. *et al.* Defining the emergence of myeloid-derived suppressor cells in breast cancer using single-cell transcriptomics. *Sci. Immunol.* 5, eaay6017 (2020).

52. Zhao, F. *et al.* S100A9 a new marker for monocytic human myeloid-derived suppressor cells. *Immunology* 136, 176–183 (2012).

53. Gielen, P. R. *et al.* Elevated levels of polymorphonuclear myeloid-derived suppressor cells in patients with glioblastoma highly express S100A8/9 and arginase and suppress T cell function. *Neuro. Oncol.* 18, 1253–1264 (2016).

54. Cassetta, L. *et al.* Human tumor-associated macrophage and monocyte transcriptional landscapes reveal cancer-specific reprogramming, biomarkers, and therapeutic targets. *Cancer Cell* 35, 588-602.e10 (2019).

55. Larionova, I. *et al.* Interaction of tumor-associated macrophages and cancer chemotherapy. *Oncoimmunology* 8, 1596004 (2019).

56. Mantovani, A., Marchesi, F., Malesci, A., Laghi, L. & Allavena, P. Tumour-associated macrophages as treatment targets in oncology. *Nat. Rev. Clin. Oncol.* 14, 399–416 (2017).

57. Aramini, B. *et al.* Cancer stem cells and macrophages: molecular connections and future perspectives against cancer. *Oncotarget* 12, 230–250 (2021).

58. Fujimura, T., Kambayashi, Y., Fujisawa, Y., Hidaka, T. & Aiba, S. Tumor-Associated Macrophages: Therapeutic Targets for Skin Cancer. *Front. Oncol.* 8, (2018).

59. Arwert, E. N. *et al.* A unidirectional transition from migratory to perivascular macrophage is required for tumor cell intravasation. *Cell Rep.* 23, 1239–1248 (2018).

60. Casanova-Acebes, M. *et al.* Tissue-resident macrophages provide a pro-tumorigenic niche to early NSCLC cells. *Nature* 595, 578–584 (2021).

61. Kumari, N. & Choi, S. H. Tumor-associated macrophages in cancer: recent advancements in cancer nanoimmunotherapies. *J. Exp. Clin. Cancer Res.* 41, 68 (2022).

62. Lewis, C. E. & Pollard, J. W. Distinct role of macrophages in different tumor microenvironments. *Cancer Research* 66, 605–612 (2006).

63. Rogers, T. L. & Holen, I. Tumour macrophages as potential targets of bisphosphonates. *J.*

Transl. Med. 9, 177 (2011).

64. Lin, E. Y., Nguyen, A. V., Russell, R. G. & Pollard, J. W. Colony-stimulating factor 1 promotes progression of mammary tumors to malignancy. *J. Exp. Med.* 193, 727–740 (2001).

65. Gentilcore, G. *et al.* Ipilimumab treatment results in an early decrease in the frequency of circulating granulocytic myeloid derived suppressor cells as well as their arginase1 production. *J. Transl. Med.* 12, O9 (2014).

66. Tsubaki, T. *et al.* Novel adherent $CD11b^+$ $Gr\text{-}1^+$ tumor-infiltrating cells initiate an immunosuppressive tumor microenvironment. *Oncotarget* 9, 11209–11226 (2018).

67. Shen, X. Z. *et al.* Myeloid expression of angiotensin-converting enzyme facilitates myeloid maturation and inhibits the development of myeloid-derived suppressor cells. *Lab. Invest.* 94, 536–544 (2014).

68. Lee, P. Y., Wang, J.-X., Parisini, E., Dascher, C. C. & Nigrovic, P. A. Ly6 family proteins in neutrophil biology. *J. Leukoc. Biol.* 94, 585–594 (2013).

69. Wolfenson, H., Lavelin, I. & Geiger, B. Dynamic regulation of the structure and functions of integrin adhesions. *Developmental Cell* 24, 447–458 (2013).

70. Lin, X., Zhang, K., Wei, D., Tian, Y. & Gao, Y. The impact of spaceflight and simulated microgravity on cell adhesion. 1–20

71. Harburger, D. S. & Calderwood, D. A. Integrin signalling at a glance. *J. Cell Sci.* 122, 159–163 (2009).

72. Yakubenko, V. P., Yadav, S. P. & Ugarova, T. P. Integrin α D β 2, an adhesion receptor up-regulated on macrophage foam cells, exhibits multiligand-binding properties. *Blood* 107, 1643–1650 (2006).

73. Lodish, H. *et al. Molecular Cell Biology. 4th edition*. *New York: W. H. Freeman* (2000). doi:10.1017/CBO9781107415324.004

74. Hyun, Y.-M., Lefort, C. T. & Kim, M. Leukocyte integrins and their ligand interactions. *Immunol. Res.* 45, 195–208 (2009).

75. Mezu-Ndubuisi, O. J. & Maheshwari, A. The role of integrins in inflammation and angiogenesis. *Pediatr. Res.* 89, 1619–1626 (2021).

76. Ley, K. & Kansas, G. S. Selectins in T cell recruitment to non-lymphoid tissues and sites of inflammation. *Nat. Rev. Immunol.* 4, 325–336 (2004).

Chapter 2

Transcriptome analysis of MLAC and MDSC

Abstract

The tumor microenvironment is a complex mixture composed of cancer cells, tumor infiltrating bone marrow-derived cells (BMDC) and a mixture of tissue-resident immune cells. Myeloid-derived suppressor cell (MDSC)-like adherent cells (MLACs) are a recently identified $CD11b^{+}F4/80^{-}Gr\text{-}1^{+}$ myeloid cell that infiltrate tumors early in tumor development and promote tumor growth. MLACs alone are not immunosuppressive but they recruit MDSCs through secretion of cytokines and can directly accelerate tumor growth and angiogenesis. However, the lack of MLAC-specific markers has hampered further characterization of MLACs. I aimed to identify novel cell-type-specific surface biomarkers for MLAC through transcriptome analysis. I identify the gene signature of MLACs by analyzing RNA-sequencing (RNA-seq) and public single-cell RNA-seq data. The comparison of transcriptome profile between MLACs and MDSCs show that MLACs are a distinct cell population that expresses several unique plasma membrane proteins and inflammatory factors. Furthermore, MLACs were found as a distinct intratumoral myeloid cell population. These newly discovered cell surface markers for MLACs may be used to further aid in the isolation and characterization of MLACs as a target for cancer therapy.

2-1. Introduction

2-1-1. Isolation of MLAC, MDSC, and TAM populations with adhesion-based separation

MLACs are isolated by using adhesion-based separation method. First, solid tumors are resected from tumor bearing mice and are physically and chemically disaggregated in order to obtain a tumor cell suspension. Next, the single cell tumor suspensions are seeded onto culture dishes. Strongly adherent cells will attach to the culture dish during incubation, while non-adherent cells remain suspended. Strongly adherent cells can then be collected to produce the adherent fraction containing MLACs and TAMs. The non-adherent cells is also collected as the non-adherent fraction containing MDSCs (Fig. 2-1).

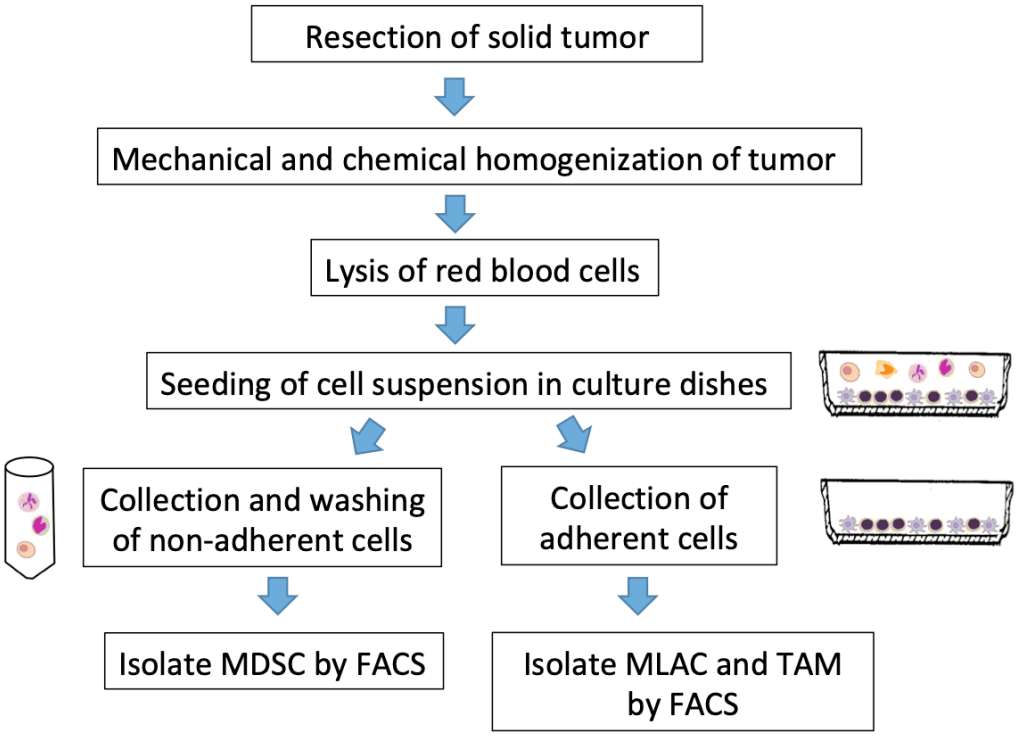

Fig. 2-1. Schematic diagram of adhesion-based separation.

The adherent and non-adherent fractions obtained were sorted and analyzed using FACS (Fig. 2-2). All the cells were gated from the initial forward scatter (FSC) vs side scatter (SSC)

plot. Single cells were then gated by using FSC-Width vs FSC-Height and SSC-Width vs SSC-Height. Propidium iodide (PI) was added to differential viable from dead deads. Viable cells are PI-negative. MLACs and TAMs were then isolated from the adherent fraction as $CD11b^{+}F4/80^{-}$ and $CD11b^{+}F4/80^{+}$ populations, respectively, and MDSCs were isolated from the non-adherent fraction as $CD11b^{+}Gr\text{-}1^{+}$ population. About 3.1×10^{5} MLACs, for 2.85×10^{5} MDSCs, and 4.62×10^{5} TAMs could be isolated from each LLC solid tumor.

When comparing the FSC and SSC properties of MLACs, MDSCs and TAMs, MLAC appeared to be slightly less granular than TAMs and MDSCs (Fig. 2-3). Furthermore, MLACs generally appear slighlty smaller than TAMs but lager than MDSCs. MLACs and MDSCs appear to be more granular than TAMs.

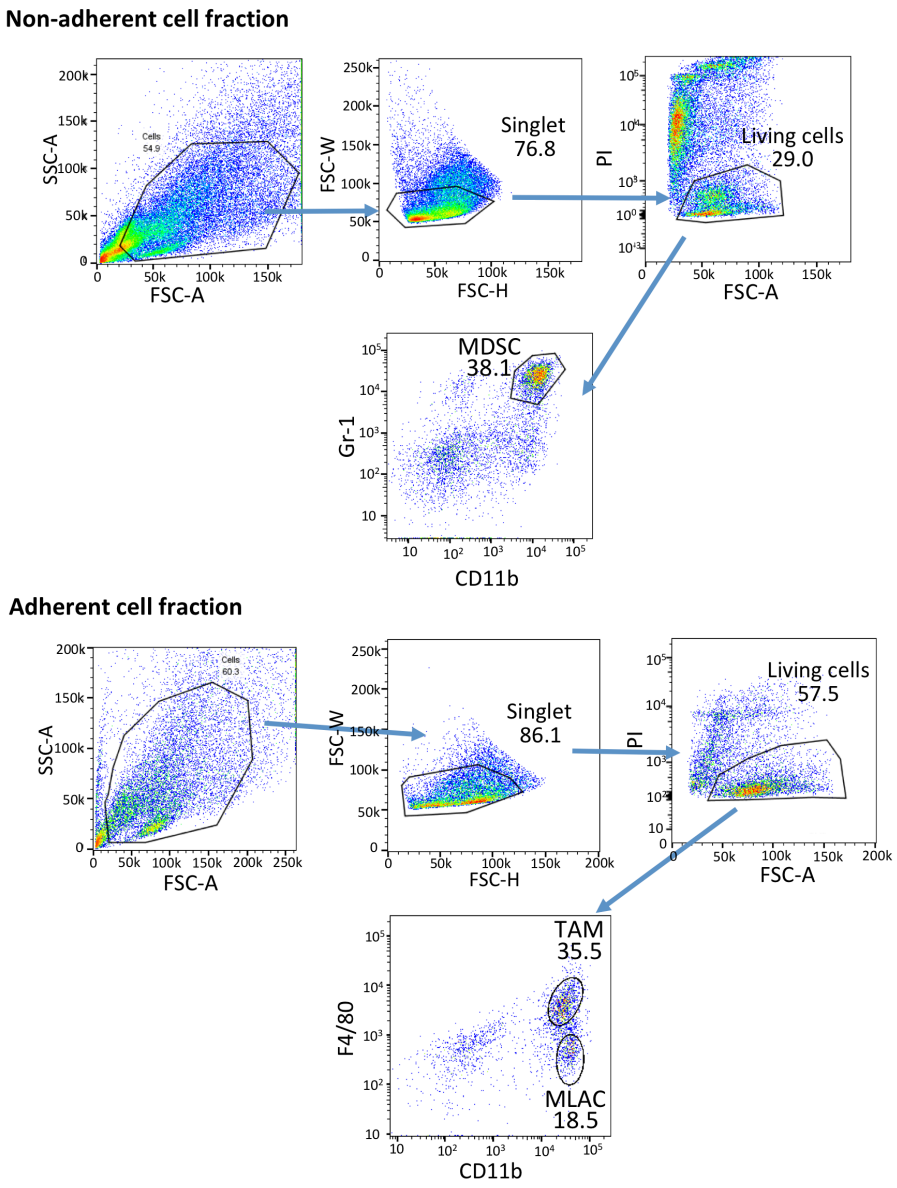

Fig. 2-2. Gating scheme for TAMs, MLACs, and MDSCs cell sorting. Gating scheme of MDSCs from non-adherent cell fraction and MLACs and TAMs from adherent cell fraction of digested LLC tumors.

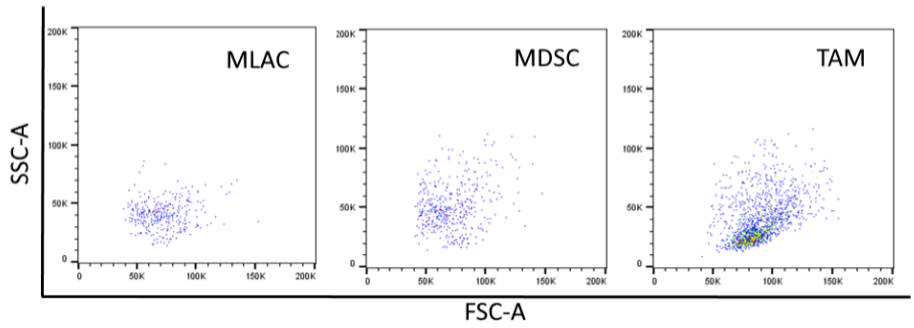

Fig. 2-3. Size and granularity of MLACs, MDSCs, and TAMs. Cells were compared based on forward scatter area (FSC-A) for size and side scatter area (SSC-A) for granularity.

2-1-2. Comparative transcriptome analysis between MLACs, MDSCs, and TAMs

RNA-seq was performed previously to determine difference in transcriptome between MLACs, MDSCs, and TAMs. Hierarchical clustering analysis and Pearson correlation analysis show that these 3 cell types are distinct from one another (Figs. 2-4 and 2-5). Based on this, the relationship between the transcriptomes of MDSCs and TAMs was closer than that between MDSCs and MLACs.

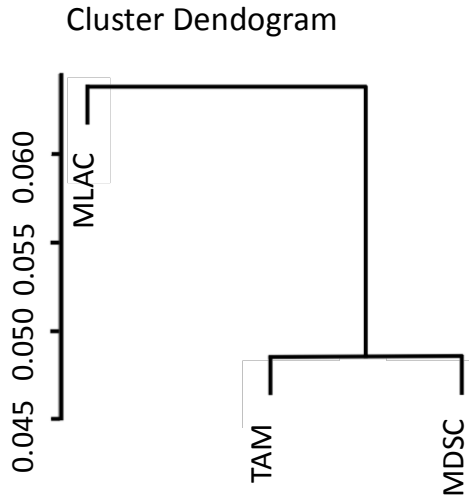

Fig 2-4. Hierarchical clustering analysis of transcriptome profile among MLAC, MDSC, and TAM. Clustering was based on the expression value of 6803 detected genes expressed in all three cell populations.

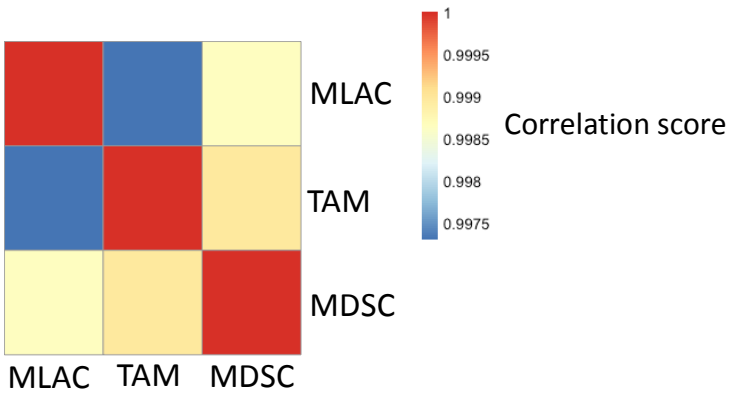

Fig. 2-5. Pearson correlation analysis between MLAC, MDSC and TAM.

Since MLACs and TAMs could be clearly separated from each other through F4/80 expression, the key differences between the transcriptomes of MLACs and MDSCs became a greater point of interest. Differential gene expression analysis between MLACs and MDSCs showed that 348 were upregulated and 2,331 genes were downregulated at least 2-fold in MLACs compared to MDSC (Fig. 2-6). In this study, more thorough analysis of the biological significance of there differentially expressed genes was performed. Furthermore, plasma membrane protein encoding genes were analyzed in order to determine surface markers for MLAC.

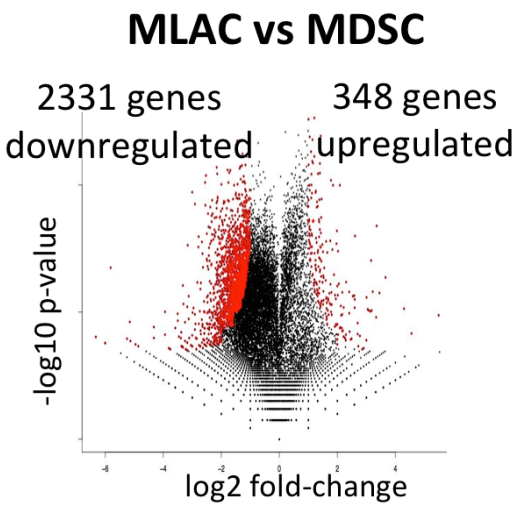

Fig. 2-6. Volcano plot of RNA-seq analysis between MLACs and MDSC. Red dots indicate genes that were significantly upregulated or downregulated in MLACs compared to MDSCs.

2-1-3. Next Generation RNA-sequencing

High throughput next-generation sequencing (NGS) is a powerful analysis tool to study the transcriptomes and genomes of organisms. It is commonly used to identify and quantify all of the genes that are expressed in a sample[1]. Library preparation for NGS shares some similar processes with real-time quantitative reverse transcription PCR (qRT-PCR) such as reverse transcription in order to convert the mRNA to cDNA and replication of cDNA for quantification. To sequence all the cDNA, the cDNA is fragmented and all the DNA fragments are sequenced simultaneously. In Illumina's sequence technology platform, which is the most commonly used platform, oligonucleotide tags are used during fragmentation of cDNA. The tags bind to oligonucleotides coated on the flow cell. All the bound DNA fragments undergo the process of "strand synthesis" where fluorescently labelled nucleotides are incorporated and detected for the whole flow cell. This allows for all the fragments on the flow cell to be sequenced all at once. The advantage of NGS is its high throughput with high sensitivity and relatively low cost per sequence read. RNA-seq also have other applications such as discovering novel transcripts or

different splice variants of the same gene. It can also be used to other RNA molecules like micro RNA and long non-coding RNA[2].

After sequencing, further bioinformatics analyses are done in order to convert raw counts of nucleotides into annotated gene transcript counts. The general steps of RNA-seq analysis involve the use of several bioinformatics software pipelines; many of which are open source. In general, the RNA-seq analysis could be divided into: determining the quality of reads, alignment of reads to a genome, assigning reads to transcripts, and estimating transcript abundance[3]. After that, differentially expression analysis may be performed. Further analysis through Gene set enrichment analysis (GSEA) or Gene ontology (GO) can also be employed to infer functional characteristics that are of biological significance[4].

2-1-4. Single-Cell RNA-seq Analysis

scRNA-seq analysis is a relatively new tool used to analyze the expression profiles at single cell resolution. It can analyze and dissect cell heterogeneity and identify rare populations that cannot be detected from bulk RNA-seq[5]. This generally involves the isolation of single cells through the use of FACS or microfluidic devices. Once single cells have been isolated, the generation of cDNA for sequencing is generally similar with bulk RNA-seq. The unique feature of scRNA-seq is that each cell obtains a distinct nucleotide barcode during the generation of cDNA. Hence every transcript contains the barcode of its cell during sequencing. This will allow the user to segregate the transcriptome information that belongs to each cell in the sample.

2-1-5. Gene signature

Gene signatures are lists of genes that are involved together or associated in a specific biological relationship[6]. A representative gene set can be utilized as a prognostic or detection tool to infer the identity or presence of a biological process from a sample[7]. In this study, highly elevated genes of MLACs compared with MDSCs were utilized to form a MLAC gene signature.

2-2. Materials and Methods

2-2-1. Mice

Male B6(Cg)-*Tyr*$^{c\text{-}2J}$/*J* (B6 albino) albino mice were obtained from Charles River Laboratories, Japan (Yokohama, Japan). All mice were housed in specific pathogen free conditions in the animal facilities at Tokyo Institute of Technology. Animal experiments were performed with the approval of the Animal Ethics Committees of Tokyo Institute of Technology (no. D2020008) and in accordance with the Ethical Guidelines for Animal Experimentation of Tokyo Institute of Technology.

2-2-2. Subcutaneous tumor formation

The experiment was performed using 6 to 9-week-old male B6 albino mice. The mice were anesthetized with pentobarbital sodium (Somnopentyl, Kyouritsu Seiyaku, Tokyo, Japan). Murine Lewis lung carcinoma cell line LLC obtained from American Type Culture Collection (ATCC) (Maryland, USA) maintained with 5% fetal bovine serum-Dulbecco's Modified Eagle's medium (FBS-DMEM) (Nacalai Tesque, Kyoto, Japan) supplemented with penicillin (100 units/mL) and streptomycin (100 mg/mL). The cultured LLC cells were collected by

trypsinization and adjusted to a concentration of 1×10^6 cells/ 20 μL. Cells were mixed with an equal volume of Geltrex® (Thermo Fisher Scientific, Waltham, MA) and then injected subcutaneously into the ventral part of the hind limb of mice.

2-2-3. Isolation of tumor infiltrating lymphocytes from tumors

Subcutaneous tumors of 15-20 mm in diameter were resected, minced using a scalpel blade and digested in RPMI medium (Thermo Fisher Scientific) supplemented with 2% FBS and 2.6 U Liberase DH (Roche Applied Science, IN, USA) at 37°C for 60 min, and then sequentially passed through 250, 100, and 40 μm strainers (Greiner Bio-One, Kremsmünster, Austria) to obtain single-cell suspensions. Cells were then resuspended in PharmLyse™ solution (BD Bioscience, Franklin Lakes, NJ, USA) and incubated for 10 min at room temperature to lyse red blood cells. To select for the adherent cells, the cells were seeded into culture dishes with 2% FBS-RPMI at a seeding density of 2×10^7 cells/10 cm culture dish (Thermo Fischer Scientific) and incubated at 37°C for 20 min to allow adherent cells to attach to the surface of the dish. The non-adherent cells were collected and seeded again onto another culture dish in order to remove more adherent cells. The non-adherent cells remaining from that dish were collected for further analysis as the non-adherent fraction. The plate containing adherent cells were washed three times with PBS containing 0.68 mM EDTA. Strongly adherent cells were dislodged using PBS containing 2.5 mM EDTA and were collected with light scraping: these cells are the adherent fraction. Cells were resuspended in FACS buffer (PBS containing 1.2 mM EDTA and 5% FBS) in preparation for FACS.

2-2-4. FACS

Cells were blocked with anti-FcγRII/III and stained with anti-CD11b (BioLegend, San Jose, CA, USA), Gr-1 (BioLegend) and anti-F4/80 (Bio-Rad, Hercules, CA, USA). MLACs, MDSCs and TAMs were sorted using FACSaria (BD Bioscience) or by SH800S (Sony Biotechnology Tokyo, Japan). Information on antibodies is listed in Table 2-1. FACS was done with the technical assistance of the FACS Core Laboratory, Institute of Medical Science, and Tokyo University and Joint Research Laboratory, Faculty of Medicine, Keio University.

Table 2-1. Antibodies used for FACS and flow cytometry analysis

Antibodies	Fluorochrome	Manufacturer	Clone number	Concentration
Gr-1	PE, Pe-Cy7	BioLegend	RB6-8C5	1:100
CD11b	PE/Cy7, AF488	BioLegend	M1/70	1:200
F4/80	AF647, AF488	Bio-Rad	C1:A3-1	1:50

2-2-5. Total RNA preparation

RNA was extracted using the RNeasy Mini Kit (Qiagen, Hilden, Germany). RNA concentration was quantified using Nanodrop (Thermo Fischer Scientific). RNA samples were pooled from 10 tumor bearing mice and were concentrated by ethanol precipitation. RNA from each cell sample were pooled together and were precipitated by adding 1:10 volumes of 7.5 M ammonium acetate and 2.5 volumes of 100% ethanol and were incubated at -20°C for 2 hours. The RNA sample was then centrifuged at 15,000 rpm, 4°C 15,000 rpm for 25 min. The pellet was washed with 70% ethanol and centrifuged at 15,000 rpm, 4°C for 15 min. Finally, the RNA pellet was dissolved in RNAse free water.

2-2-6. RNA-seq analysis

The RNA-seq data of MLACs, MDSCs, and TAMs was previously analyzed using the R Noiseq package[8]. The differentially expressed genes were filtered out and was further subjected to Gene set enrichment analysis (GSEA) through the R ClusterProfiler[9] package by referencing to the Molecular Signatures Database (MSigDB)[10]. Plasma membrane encoding genes were determined through gene ontology (GO) analysis from the University of California Santa Cruz (UCSC) Genome Browser database[11].

2-2-7. scRNA-seq dataset processing

The dataset (Accession number: GSE121861 and GSE121478) was downloaded from Gene Expression Omnibus (GEO)[12]. The raw counts were loaded in an Rstudio project session and analyzed by Seurat Ver 3.0[13]. *Ptprc* (CD45)-expressing cells were selected for further analysis. Raw counts were normalized, and Uniform Manifold Approximation and Projection (UMAP) clustering analysis was performed to identify major cell clusters. For cell subset analyses, clusters with high *Itgam* (CD11b) and low *Adgre1* (F4/80) expression levels were grouped together and reanalyzed using UMAP. Specific markers for each cluster were identified using the "FindAllMarkers" function. MLAC and MDSC cluster identities were determined using known marker expression. Heatmaps and violin plots were generated using built-in Seurat commands[14].

2-2-8. qRT-PCR

cDNA was generated from total RNA using the ReverTra Ace (Toyobo Co, Osaka, Japan) reverse transcriptase. The reaction mixture included 4 μL reaction buffer, 200 ng RNA sample,

2 μL Oligo(dT)$_{20}$ primers (10 pmol/μL), 2 μL dNTP (10mM), 40 U RNase inhibitor, and 100 U reverse transcriptase and the total volume was made up to 20 μL with nuclease free water. Reverse transcription was performed using the following conditions: 30°C for 10 min, 42°C 20 min, and 99°C for 5 min using WK0232 Thermal cycler (Wako, Osaka, Japan).

The Thunderbird SYBR qPCR mix (Toyobo Co.) was used to quantify the expression levels of various genes. The reaction mixture contained 0.4 μM of each primer, 5 μL of diluted cDNA, and nuclease free water for a total volume of 20 μL. The reaction mixtures were preheated at 95°C for 10 min to activate the enzyme and then underwent 40 cycles of melting at 95°C for 15 sec and annealing/extension at 60°C for 1 min in a TP800 Thermal Cycler Dice Real Time System (Takara Bio, Shiga, Japan). The primers used are listed in Table 2-2.

Table 2-2. Primers used in the study

Gene name	Sequence
Klrd1	F: CAGGAAGTTTCTGAATGC TGTGT
	R*:* TGGATTGGGGCTGAAGAAGG
Mgl2	F: ACTTCCAGAACTTGGAGCGG
	R: CTGGGAAGGAACTGTTAGAGCA
CD209a	F: CACTGCCTGCCACAATGT
	R: CCCAGTACCATGTAGACTCC
CD74	F: CCGAAATCTGCCAAACCTGTG
	R: CAGGCCCAAGGAGCATGTTA

2-2-9. Statistical analysis

All data are presented as means ± standard deviation and were statistically analyzed with unpaired t-test. *P*-values of 0.05 or less were considered statistically significant.

2-3. Results

2-3-1. Identification of plasma membrane encoding gene markers

Transcriptome analysis through RNA-seq and public scRNA-seq analysis was performed to compare MLACs and MDSCs and to determine novel biomarkers for MLAC. Both analyses were performed in parallel in order to determine differentially expressed genes for MLAC. Gene ontology enrichment analysis was used to select for genes that are localized in the plasma membrane. Common differentially expressed genes from both RNA-seq and public scRNA-seq analysis were combined to select for surface marker candidates. Differentially expressed genes were then subjected to GSEA in order to understand more deeply the molecular processes that are unique to MLAC (Fig. 2-7).

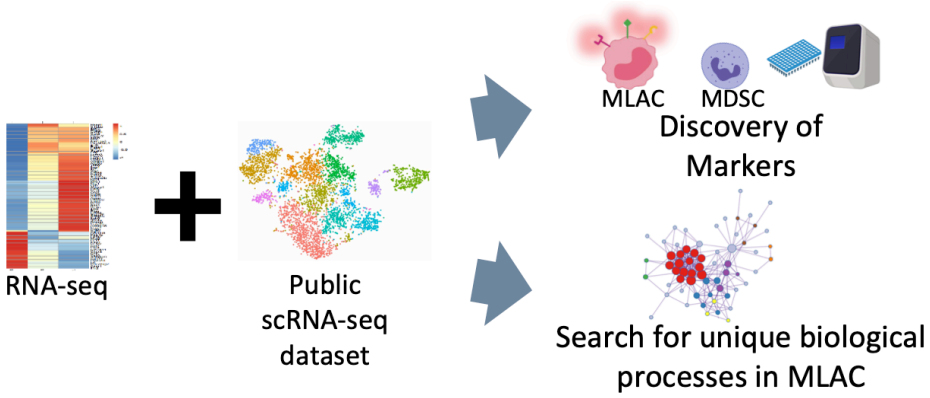

Fig. 2-7. Workflow of transcriptome analysis of MLAC for marker discovery.

Differential expression analysis was previously performed between MLACs and MDSCs, and these expressed genes were used in gene set enrichment analysis (GSEA) in order to determine unique biological prcesses for MLACs when compared with MDSCs. MLACs possess unique enrichment of genes which have a function in inflammation through cytokine production and granulocyte migration (Fig. 2-8, Table 2-3). These results support the previous finding that MLACs recruit MDSCs through secreted factors[25].

Since MLACs and MDSCs display differences in adhesion properties, differentially expressed genes encoding plasma membrane proteins (GO:0005886) were analyzed using QuickGO's gene ontology database. I extracted the plasma membrane proteins in order to narrow down the number of candidate genes for MLAC-specific marker. There were 56 plasma membrane protein genes were expressed at least two-fold higher in MLAC than in MDSC; in contrast, 101 plasma membrane protein genes were expressed at least two-fold less in MLAC than in MDSC (Fig. 2-9).

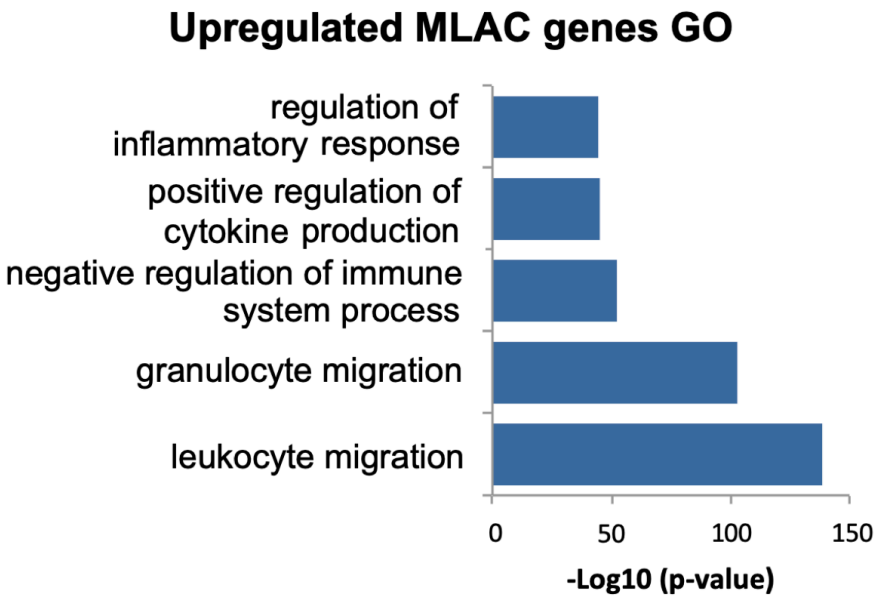

Fig. 2-8. Gene set enrichment analysis using of significantly upregulated genes between MLAC and MDSC.

Table 2-3. Upregulated genes of inflammatory proteins and receptors for MLAC

Gene name	MLAC (TPM*)	MDSC (TPM)	MLAC/MDSC
Ccl17	55.03	5.91	9.31
Ccl22	168.87	42.67	3.96
Ccl3	14345.30	5340.29	2.69
Cxcr1	74.20	28.43	2.61
Cxcr2	505.61	212.86	2.38
Cxcl2	21548.87	9338.80	2.31

Cxcr5	9.70	4.60	2.11
Ccl4	2474.82	1273.94	1.94

*Transcript count is expressed in TPM (transcript per million).

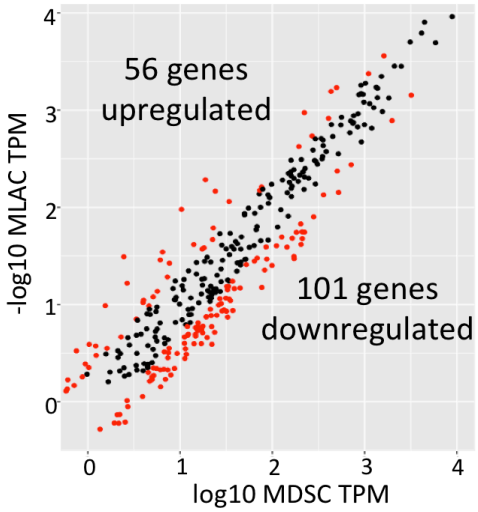

Fig 2-9. Scatterplot of normalized transcript counts of plasma membrane protein encoding genes between MLACs and MDSCs. Red dots indicate genes upregulated or downregulated at least 2-fold in MLACs compared to MDSCs.

I searched for potential markers of MLACs by selecting plasma membrane protein genes with that were strongly upregulated in MLACs and had high transcript counts. The highly upregulated surface marker genes for MLACs include adhesion proteins, like *Selp* and *Sell*, MHC associated proteins, like *Cd74, H2-Eb1, and H2-Q10,* and cytokine receptors like *Cxcr1*, *Cxcr2,* and *Ccrl2* (Fig. 2-10, Table 2-4). RNA-seq analysis has revealed that the most upregulated plasma membrane encoding genes in MLACs were *CD209a* (DC-SIGN), *Ctsk* (Cathepsin K), and *H2-Dmb2* (histocompatibility 2, class II, locus Mb2). On the other hand, *Itga1* (Integrin Subunit Alpha 1), *Sdc1* (Syndecan 1), *CD180*, and *Lpxn* (Leupaxin) were the most upregulated for MDSC (Table 2-5). These transcriptome analyses confirm that MLACs are a distinct myeloid cell population from MDSCs and TAMs, highlighting MLAC-specific surface marker candidates.

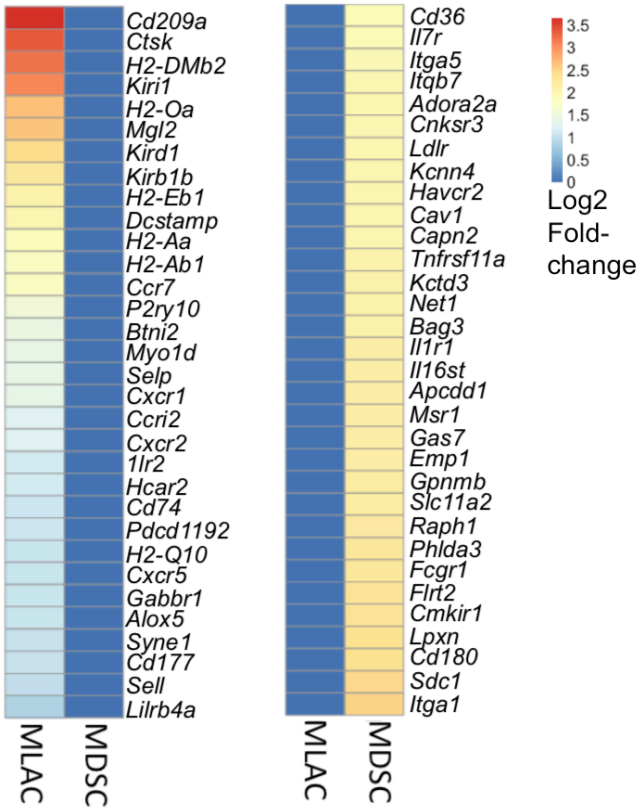

Fig. 2-10. Heatmap of differentially expressed genes based on gene ontology enrichment. Gene ontology enrichment analysis was used to enrich for genes that encode plasma membrane protein. Data was normalized by log2 fold-change and then plotted.

Table 2-4. Top differentially expressed *plasma membrane protein encoding* genes *for MLAC*

Gene name	**MLAC (TPM*)**	**MDSC (TPM)**	**Fold change MLAC/MDSC**
Cd209a	31.01	2.46	12.62
Ctsk	192.19	18.80	10.22
H2-DMb2	95.30	10.36	9.20
Klri1	17.96	2.17	8.26
H2-Oa	16.55	2.66	6.21
Mgl2	146.63	24.07	6.09
Klrd1	34.63	6.45	5.37
Klrb1b	28.70	6.10	4.71
H2-Eb1	942.36	222.26	4.24
Dcstamp	20.10	5.03	4.00
H2-Aa	1558.28	432.48	3.60

H2-Ab1	1703.84	496.60	3.43
Ccr7	114.70	33.96	3.38
P2ry10	32.17	11.05	2.91
Btnl2	11.08	4.03	2.75
Myo1d	61.28	22.93	2.67
Selp	19.17	7.28	2.63
Cxcr1	74.20	28.43	2.61
Ccrl2	746.41	311.56	2.40

*Transcript count is expressed in TPM (transcript per million).

Table 2-5. Top differentially expressed plasma membrane protein encoding genes for MDSC

Gene name	MLAC (TPM*)	MDSC (TPM)	Fold change MDSC/MLAC
Itga1	3.90	22.12	5.676
Sdc1	31.23	171.24	5.484
Cd180	14.98	76.74	5.123
Lpxn	23.37	118.74	5.082
Cmkir1	17.79	88.75	4.987
Flrt2	2.24	11.16	4.981
Fcgr1	41.50	204.95	4.938
Phlda3	1.90	8.95	4.699
Raph1	5.57	26.00	4.671
Slc11a2	5.17	23.65	4.575
Gpnmb	48.04	215.81	4.492
Emp1	218.62	973.86	4.455
Gas7	20.91	93.12	4.452
Msr1	47.64	211.28	4.434
Apcdd1	5.94	25.66	4.317
Il1r1	3.95	16.96	4.290

*Transcript count is expressed in TPM (transcript per million).

2-3-2. Identifying MLAC cluster using public scRNA-seq dataset

To further explore the gene signature and markers of MLACs, public scRNA-seq data were examined for cells with similar gene expression patterns to those observed in RNA-seq analysis. The scRNA-seq data set[12] composed of syngeneic mouse tumors such as B16-F10 (melanoma), CT26 (colon), EMT6 (breast cancer), LLC (lung), MC38 (colon), and SA1N (fibrosarcoma) was

analyzed for tumor-infiltrating immune cells. Distinct cell clusters were determined through calculations of "distance metric" and visualized through Uniform Manifold Approximation and Projection (UMAP)[14] (Fig. 2-11). To confirm the presence of MLACs in the scRNA-seq data, the $CD11b^{+}F4/80^{-}$ population, containing MLACs and MDSCs, was first defined as high expression of *Itgam* (CD11b) and low expression of *Adgre1* (F4/80) (Fig. 2-12A). I subsetted and analyzed the $CD11b^{+}F4/80^{-}$ cells and identified five distinct clusters (clusters 1 to 5) (Fig. 2-12B). In order to identify the MLAC, M-MDSC, and PMN-MDSC clusters, I firstly identified the monocytic and granulocytic populations. Clusters 1, 3, and 5 expressed the monocyte markers *Mafb* and *Ccr2*[15,16] while cluster 4 expressed the neutrophil marker *Csf3r*[17]. Cluster 2 only had low expression of *Ccr2* (Fig. 2-13). These findings suggest that clusters 1, 2, 3, and 5 were monocytic cells while cluster 4 was granulocytic cells.

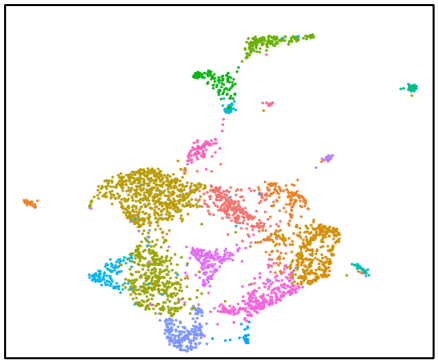

Fig. 2-11. scRNA-seq analysis through Seurat shows different clustered cell populations and visualized in a UMAP plot.

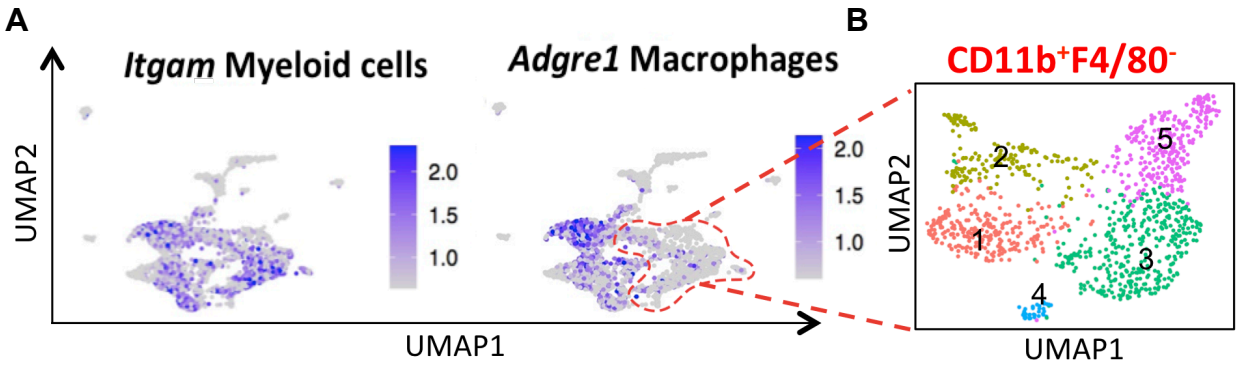

Fig. 2-12. Identification of CD11b^{+}F4/80^{-} cells through the Featureplot command. **A.** Expression of *Itgam* (CD11b) and *Adgre1* (F4/80) projected onto the UMAP plot was used to identify potential MLAC clusters. **B.** CD11b^{+}F4/80- clusters were shaded and were composed of five clusters.

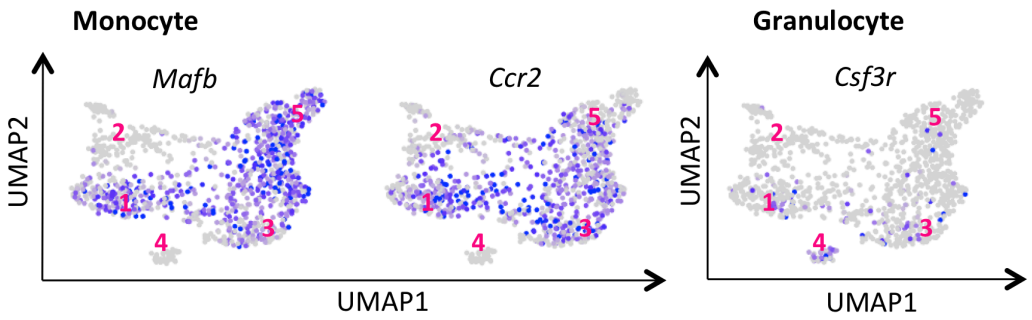

Fig. 2-13. Identification of monocytic and granulocytic clusters in CD11b^{+}F4/80^{-} cells. Monocytes were outlined based on *Ccr2* and *Mafb* expression while granulocytes were outlined based on *Csf3r* expression.

I next used the FindMarkers function of Seurat in order to perform differential expression analysis to search for the top upregulated genes of each of the CD11b^{+}F4/80^{-} cell clusters. I utilized the upregulated marker genes from the RNA-seq results to identify the MLAC cluster (Fig. 2-10). Cluster 2 uniquely expressed *Cd209a, Klrd1, Cd74, Il1r2, H2-Ab1, H2-Eb1,* and *Mgl2,* which were also significantly upregulated in MLACs in the RNA-seq analysis (Fig. 2-14).

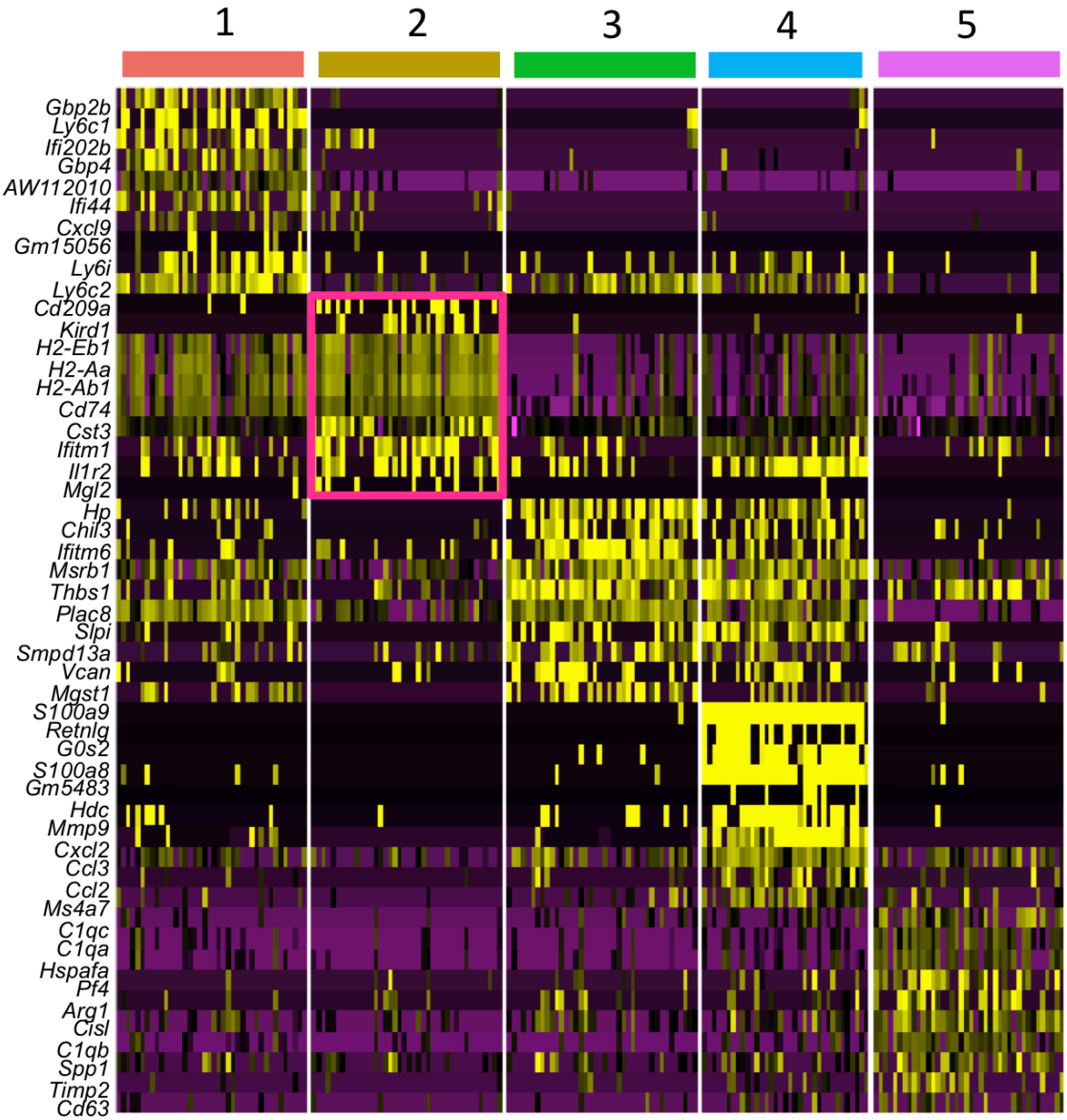

Fig. 2-14. Heatmap showing top 10 differentially expressed genes in between the CD11b^{+}F4/80^{-} cell clusters. MLAC cluster is boxed in red.

In the RNA-seq analysis, I was able to define upregulated genes for MLACs, but I also wanted to determine if MLAC did not express MDSC marker genes. I distinguished between MLAC and MDSC clusters by using a combination of immunosuppressive factors and MDSC marker genes. In general, all the other subsets had higher expression levels of immunosuppressive factors than cluster 2. Arginase coded by *Arg1* was highly expressed in

clusters 4 and 5 while *Arg2*[18] was highly expressed in clusters 1, 3, and 4. Furthermore, cluster 4 had the highest expression levels of *S100a8/S100a9*, genes encoding S100 calcium binding proteins S100a8 and S100a9, respectively[19,20]. These proteins are known to be involved in the immunosuppressive mechanisms of PMN-MDSCs (Fig. 2-15). These data suggest that all the *CD11b*$^{+}$*F4/80*$^{-}$ cells but cluster 2 may some immunosuppressive activity. Clusters 1, 3, 4, and 5 expressed several MDSC marker genes, such as *Cd33, Clec4d, Clec4e, Cd84, Ctsd,* and *Cd300ld*[21,22], while cluster 2 showed lower expression of these genes (Fig. 2-16*)*. In the RNA-seq analysis, MDSC marker genes were also expressed less in MLAC than MDSC (Table 2-6). From these analyses, clusters 1, 3, and 5 were defined as M-MDSCs because they are monocytic populations (Fig. 2-13), cluster 4 was defined as PMN-MDSCs, and cluster 2 was defined as MLACs from their lack of gene expression of immunosuppressive factors and MDSC marker gene expression. Fig. 2-17 summarizes the analysis and shows the cluster that were defined. The MLAC cluster were more related to the M-MDSC clusters than the PMN-MDSC clusters based on UMAP clustering.

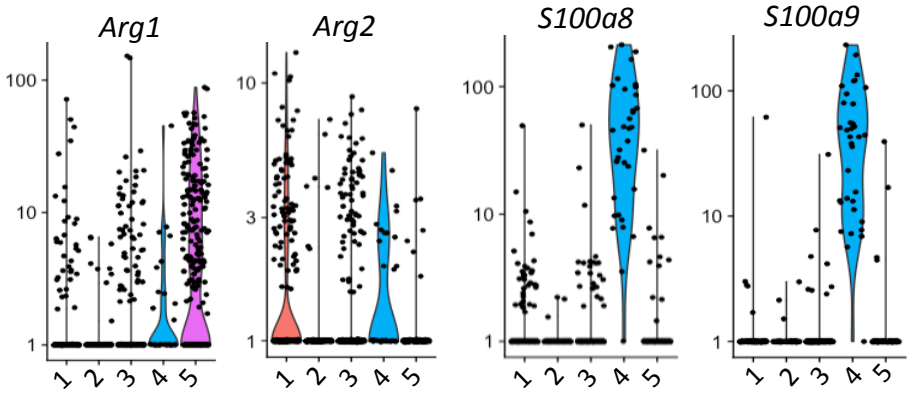

Fig. 2-15. Violin plot showing the differential expression of immunosuppressive factors in CD11b^{+}*F4/80*$^{-}$ *populations.*

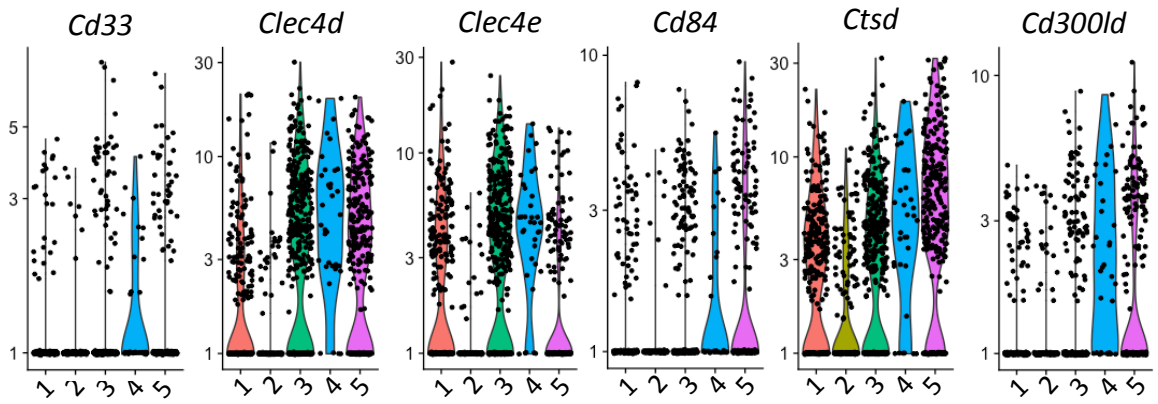

Fig. 2-16. Violin plot showing the differential expression of MDSC marker genes in CD11b^{+}F4/80^{-} populations.

Table 2-6. Expression of MDSC marker genes for MLAC and MDSC

Gene name	MLAC (TPM*)	MDSC (TPM)	Fold-change (MLAC/MDSC)
Cd33	70.57	506.07	0.14
Clec4d	2094.36	5021.13	0.42
Clec4e	1624.32	2836.51	0.57
Cd84	83.36	86.75	0.96
Cd300ld	245.98	479.74	0.51

*Transcript count is expressed in TPM (*t*ranscript per million).

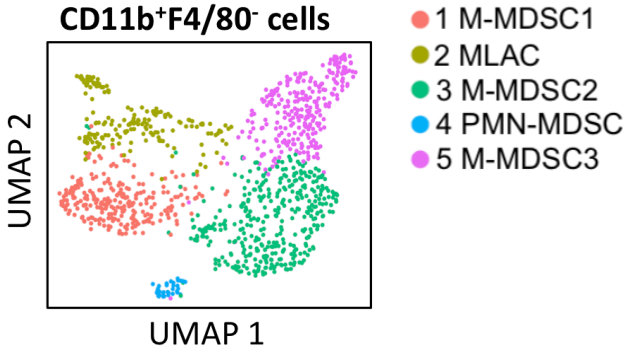

Fig. 2-17. UMAP plot of CD11b^{+}F4/80^{-} cells with cluster names identified.

I next established MLAC signature genes as a tool to identify the presence of MLACs. I selected *CD209a, Mgl2, Klrd1,* and *CD74,* as they were consistently upregulated for MLAC in

RNA-seq and public scRNA-seq analyses. I verified these genes and tested their differential expression between MLACs and MDSCs by qRT-PCR. The magnitude of fold-change was relatively consistent with the RNA-sequencing analysis data (Table 2-4). *CD209a* and *Mgl2* were the most highly expressed for MLAC. *CD209a (DC-SIGN)* was expressed about 8.2-fold more in MLAC than in MDSC and *Mgl2 (CD301b)* was expressed was expressed about 9.1-fold more MLAC than in MDSC (Fig. 2-18).

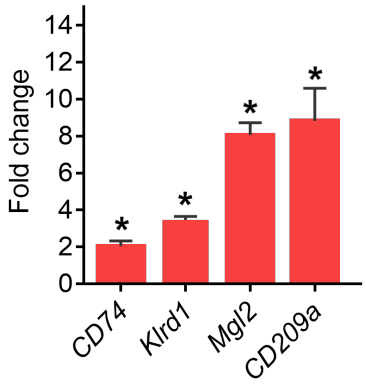

Fig 2-18. Gene expression analysis of MLAC marker candidate genes by qRT-PCR. Expression of genes of interest were normalized to actin and fold-change in expression of MLAC over MDSC was calculated. Fold change of expression was compared to 1-fold, denoting that genes were consistently upregulated. $n = 3$. $*p < 0.05$.

I next verified the consistency of the MLAC gene signature through the analysis of another public scRNA-seq dataset, which focused on B16-F10 tumors[23]. I used the same analysis method such as the identification and reclustering of the $CD11b^{+}F4/80^{-}$ cell populations (Fig. 2-19). I analyzed for the expression by gene expression analysis and found that cluster 2 highly expressed MLAC signature genes in addition to other top MLAC marker genes and had low expression of genes encoding immunosuppressive factors (Fig. 2-20). Cluster 2 also had low expression of MDSC signature genes (Fig. 2-21), and can be identified as MLAC.

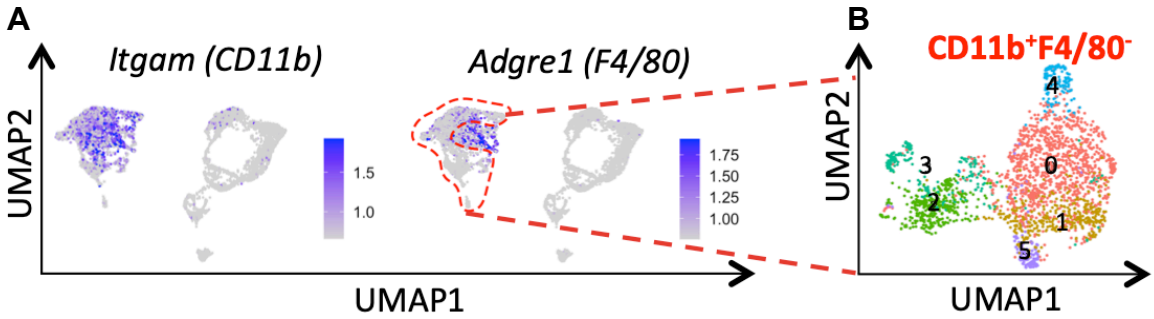

Fig. 2-19. Identification of CD11b^{+}F4/80^{-} cells in melanoma scRNA-seq dataset. The same methodology from Fig. 2-12 was applied to search for MLAC in B16-F10 tumor dataset. **A.** Expression of *Itgam* (CD11b) and *Adgre1* (F4/80) projected onto the UMAP plot was used to identify potential MLAC clusters. **B.** CD11b^{+}F4/80^{-} clusters were shaded and were composed of five clusters.

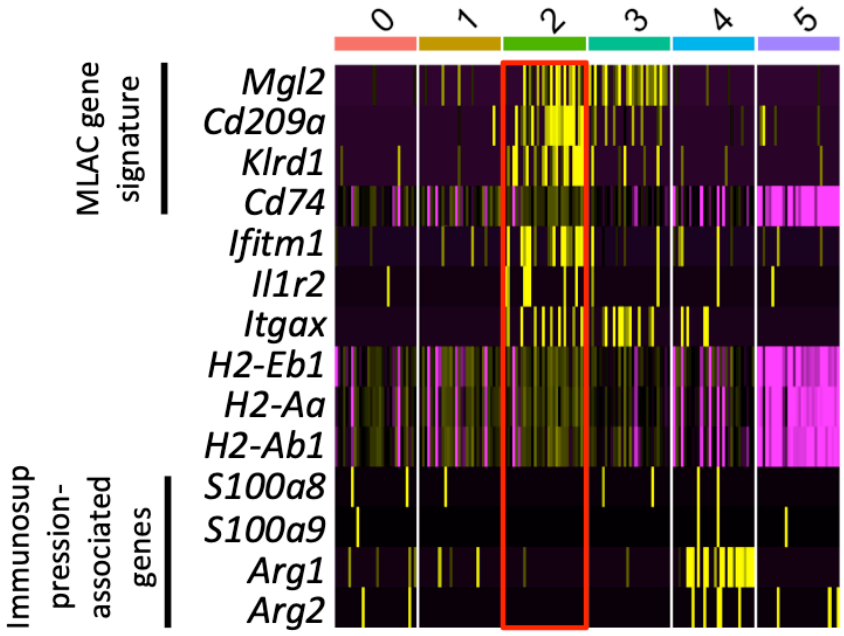

Fig. 2-20. Heatmap showing expression of MLAC signature genes and immunosuppression associated genes in the B16-F10 tumor scRNA-seq dataset. CD11b^{+}F4/80^{-} cell clusters were analyzed and hypothesized MLAC cluster is boxed in red.

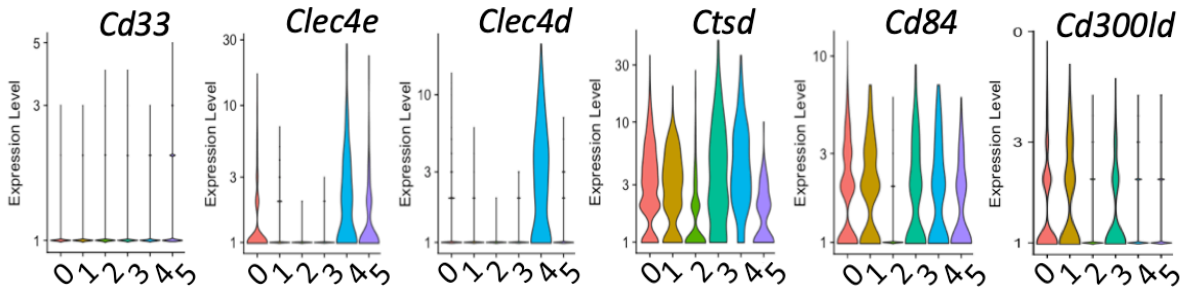

Fig. 2-21. Violin plot showing the differential expression of MDSC marker genes in CD11b^{+}F4/80^{-} populations from B16-F10 scRNA-seq dataset.

Overall, this transcriptome analysis has highlighted MLAC as a distinct myeloid cell population from other tumor infiltrating cells. I assigned selected MLAC gene markers as MLAC signature genes, which can be used as a molecular barcode to identify MLAC population and will be used in the next chapters.

2-4. Discussion

In this study, I combined public scRNA-seq data analysis with transcriptome analysis to reveal MLAC marker genes. Despite previous studies suggesting that MLACs are similar to MDSCs, my analysis of hierarchical cluster distance has shown that TAMs and MDSCs were more related. This may be explained through the capacity of MDSCs to differentiate into TAMs. Some MDSCs may be in the process of differentiating into TAMs, particularly in larger tumors[24]; in contrast, MLACs do not differentiate into TAMs[25].

My integrated analysis of RNA-seq and scRNA-seq analysis confirmed that MLACs has a distinct transcriptome profile from MDSCs, despite previous reports suggesting that it shares several markers with MDSCs[25]. I identified a set of genes that were uniquely expressed in MLACs, namely *Mgl2, CD209a, CD74,* and *Klrd1* to be used as the MLAC gene signature to distinguish MLACs from other CD11b^{+}F4/80^{-} cells in tumors. Majority of the top upregulated genes of MLACs have a biological role in antigen presentation, like *CD74* and *H2-Ab1*, or have

been associated with dendritic cells such as *Mgl2* and *CD209a*[26]. Furthermore, several MHCII subunits were found to be upregulated in MLACs, suggesting that MLACs may have functions as an auxiliary regulator of immune response. Huang et al[27] have previously described a $CD11b^{+}F4/80^{-}$ tumor infiltrating cell population that highly expresses MHCII which may have corresponded to MLACs.

Gene set enrichment analysis of RNA-seq data of MDSCs and MLACs suggests that several biological processes such as cytokine production and granulocyte migration were more active in MLACs compared to MDSCs. High expression of *CXCL1, CXCL2, CXCR1,* and *CXCR2* in MLACs suggests the activation of CXCR1-CXCR2/CXCL8 axis that is involved in the recruitment of MDSCs and tumor growth[28], which is consistent with previous studies on the tumor-promoting function of MLAC[25]. RNA-seq analysis also found increased expression of other cytokines and chemokines previously detected in MLACs such as *CCL17,* which can directly stimulate the proliferation of cancer cells[25,29] and *CCL22*, a cytokine that attracts T_{reg}[30]. These may be auxiliary drivers of tumor growth and immunosuppression. These further highlight the ability of MLACs to employ different mechanisms to promote tumor development.

References

1. Reuter, J. A., Spacek, D. V & Snyder, M. P. High-throughput sequencing technologies. *Mol. Cell* 58, 586–597 (2015).

2. Kukurba, K. R. & Montgomery, S. B. RNA sequencing and analysis. *Cold Spring Harb. Protoc.* 2015, 951–969 (2015).

3. Head, S. R. *et al.* Library construction for next-generation sequencing: overviews and challenges. *Biotechniques* 56, 61-passim (2014).

4. Reimand, J. *et al.* Pathway enrichment analysis and visualization of omics data using g:Profiler, GSEA, Cytoscape and EnrichmentMap. *Nat. Protoc.* 14, 482–517 (2019).

5. Hwang, B., Lee, J. H. & Bang, D. Single-cell RNA sequencing technologies and bioinformatics pipelines. *Experimental and Molecular Medicine* (2018). doi:10.1038/s12276-018-0071-8

6. Liu, H., Liu, J., Toups, M., Soos, T. & Arendt, C. Gene signature-based mapping of immunological systems and diseases. *BMC Bioinformatics* 17, 171 (2016).

7. Pu, J., Yu, H. & Guo, Y. A novel strategy to identify prognosis-relevant gene sets in cancers. *Genes (Basel).* 13, (2022).

8. Tarazona, S. *et al.* Data quality aware analysis of differential expression in RNA-Seq with Noiseq R/Bioc package. *Nucleic Acids Res.* 43, e140–e140 (2015).

9. Yu, G., Wang, L. G., Han, Y. & He, Q. Y. ClusterProfiler: An R package for comparing biological themes among gene clusters. *Omi. A J. Integr. Biol.* (2012). doi:10.1089/omi.2011.0118

10. Liberzon, A. *et al.* Molecular signatures database (MSigDB) 3.0. *Bioinformatics* 27, 1739–1740 (2011).

11. Kent WJ, Sugnet CW, Furey TS, Roskin KM, Pringle TH, Zahler AM, H. D. The human genome browser at UCSC. *Genome Res* Jun;12(6), 996–1006 (2002).

12. Kumar, M. P. *et al.* Analysis of Single-cell RNA-Seq identifies cell-cell communication associated with tumor characteristics. *Cell Rep.* 25, 1458–1468 (2018).

13. Stuart, T. *et al.* Comprehensive integration of single-cell data. *Cell* 177, 1888–1902 (2019).

14. Butler, A., Hoffman, P., Smibert, P., Papalexi, E. & Satija, R. Integrating single-cell transcriptomic data across different conditions, technologies, and species. *Nat. Biotechnol.* 36, 411–420 (2018).

15. Zilionis, R. *et al.* Single-cell transcriptomics of human and mouse lung cancers reveals conserved myeloid populations across individuals and species. *Immunity* 50, 1317-1334.e10 (2019).

16. Moriguchi, T. *et al.* MafB is essential for renal development and F4/80 expression in

macrophages. *Mol. Cell. Biol.* 26, 5715–5727 (2006).

17. Kumar, V. *et al.* Cancer-associated fibroblasts neutralize the anti-tumor effect of CSF1 receptor blockade by inducing PMN-MDSC infiltration of tumors. *Cancer Cell* 32, 654-668.e5 (2017).

18. Gielen, P. R. *et al.* Elevated levels of polymorphonuclear myeloid-derived suppressor cells in patients with glioblastoma highly express S100A8/9 and arginase and suppress T cell function. *Neuro. Oncol.* 18, 1253–1264 (2016).

19. Veglia, F., Perego, M. & Gabrilovich, D. Myeloid-derived suppressor cells coming of age. *Nat. Immunol.* 19, 108–119 (2018).

20. Sade-Feldman, M. *et al.* Tumor necrosis factor- α blocks differentiation and enhances suppressive activity of immature myeloid cells during chronic inflammation. *Immunity* 38, 541–554 (2013).

21. Alshetaiwi, H. *et al.* Defining the emergence of myeloid-derived suppressor cells in breast cancer using single-cell transcriptomics. *Sci. Immunol.* 5, eaay6017 (2020).

22. Brusa, D. *et al.* Circulating immunosuppressive cells of prostate cancer patients before and after radical prostatectomy: profile comparison. *Int. J. Urol. Off. J. Japanese Urol. Assoc.* 20, 971–978 (2013).

23. Ekiz, H. A. *et al.* MicroRNA-155 coordinates the immunological landscape within murine melanoma and correlates with immunity in human cancers. *JCI insight* 4, (2019).

24. Youn, J.-I., Nagaraj, S., Collazo, M. & Gabrilovich, D. I. subsets of myeloid-derived suppressor cells in tumor bearing mice. *J. Immunol.* 181, 5791–5802 (2008).

25. Tsubaki, T. *et al.* Novel adherent $CD11b^+$ $Gr\text{-}1^+$ tumor-infiltrating cells initiate an immunosuppressive tumor microenvironment. *Oncotarget* 9, 11209–11226 (2018).

26. Ryu, S. H. *et al.* granulocyte macrophage-colony stimulating factor produces a splenic subset of monocyte-derived dendritic cells that efficiently polarize t helper type 2 cells in response to blood-borne antigen. *Frontiers in Immunology* 12, 767037 (2022).

27. Huang, W. *et al.* Calcium/Calmodulin Dependent Protein Kinase Kinase 2 Regulates the Expansion of Tumor-Induced Myeloid-Derived Suppressor Cells. *Frontiers in Immunology* 12, 754083 (2021).

28. Varney, M. L. *et al.* Small molecule antagonists for CXCR2 and CXCR1 inhibit human colon cancer liver metastases. *Cancer Lett.* 300, 180–188 (2011).

29. Zhu, F. *et al.* Tumor-associated macrophage or chemokine ligand CCL17 positively regulates the tumorigenesis of hepatocellular carcinoma. *Med. Oncol.* 33, 17 (2016).

30. Gobert, M. *et al.* Regulatory T cells recruited through Ccl22/Ccr4 are selectively activated in lymphoid infiltrates surrounding primary breast tumors and lead to an adverse clinical outcome. *Cancer Res.* 69, 2000–2009 (2009).

Chapter 3

Proteomic analysis of MLAC and analysis of MLAC marker proteins

Abstract

In this chapter, in order to detect MLACs in tumors using antibodies, I searched for proteins that could be used as cell surface markers for MLACs. I isolated plasma membrane protein from MLACs and MDSCs and performed label-free quantitative shotgun proteomics analysis. After that I integrated the transcriptome analysis from chapter 2 and the proteomics from this chapter by using Rank-rank hypergeometric analysis to yield high confidence marker candidates. I identified that a subset of MLACs express H2-Ab1 and CD11c while these proteins are absent in MDSCs. Flow cytometry analysis of markers also reveal a notable degree of heterogeneity in the surface protein expression profile in MLACs.

3-1. Introduction

3-1.1 Cell surface protein extraction

Cell surface proteins are plasma membrane proteins that are located on the external side of the plasma membrane. Immunophenotyping of leukocyte subsets is dependent on the labeling of specific surface markers[1]. These are essential in discriminating immune cell subsets by flow cytometry analysis. Because of their localization on the cell, cell surface proteins are also sought after due to their utility in isolation of viable cells through FACS and as a therapeutic target.

Cell surface proteins are generally underrepresented in whole proteome analysis because of their hydrophobicity, general low expression, and less trypsin cleavage sites[2]. Plasma membrane proteins have an amphipathic nature, wherein they possess hydrophilic extramembrane regions and hydrophobic segments that span the phospholipid bilayer[3]. They also have varying number of transmembrane domains wherein proteins with more transmembrane domains are more difficult to solubilize. Hence, optimized solubilizing buffers are needed to sufficiently solubilize plasma membrane protein. Furthermore plasma membrane proteins only compose a small percent of the total protein species[4]. This reduces the capacity to identify and accurately measure differentially expressed plasma membrane proteins. The most abundant cellular component is the cytosolic protein[5]. Because of this, there is a need to enrich for plasma membrane proteins. High yield and purity from plasma membrane protein extraction is necessary for proteomic analysis. Hence several methodologies have been developed for this purpose[6].

I used the Mem-per plus plasma membrane extraction kit to purify and isolate plasma membrane proteins. The mechanism of this method involves permeabilizing the plasma membrane to release and remove the cytosolic proteins while a strong detergent buffer is used to solubilize the outer plasma membrane proteins.

3-1-2. LC-MS/MS

The approach to surface marker discovery is a label-free quantitative proteomic analysis. This method does not use any labeling of proteins prior to mass analysis and is a comparative analysis between samples. In this study, high performance liquid chromatography (LC) coupled with high resolution tandem MS (LC-MS/MS) was used for protein quantification. It is a powerful technique that is used to identify and quantify several unknown proteins in a sample through their mass spectra. The addition of LC separates the sample into different components prior to mass analysis[7]. This method involved digesting the proteins into peptides using specific proteases like trypsin and Lys-C. Next the raw mass spectra data of the peptides are computationally "stitched" back together in order to obtain protein polypeptide sequences. These polypeptide sequences can then be annotated and identified through protein databases. These counts of proteins can be further subjected to downstream analysis to extract genes of a particular cellular component or to infer a biological function (Fig. 3-1).

For this workflow, the Proteome Discoverer software (Thermofischer Scientific) was used for proteome data analysis. It is an application made to simplify peptide identification, peptide quantification, and statistical analyses. Afterwards, I analyzed the raw matrix of identified proteins in order to check for the reproducibility of analysis between replicates, determine the abundance of identified plasma membrane proteins and finally differentially expressed proteins.

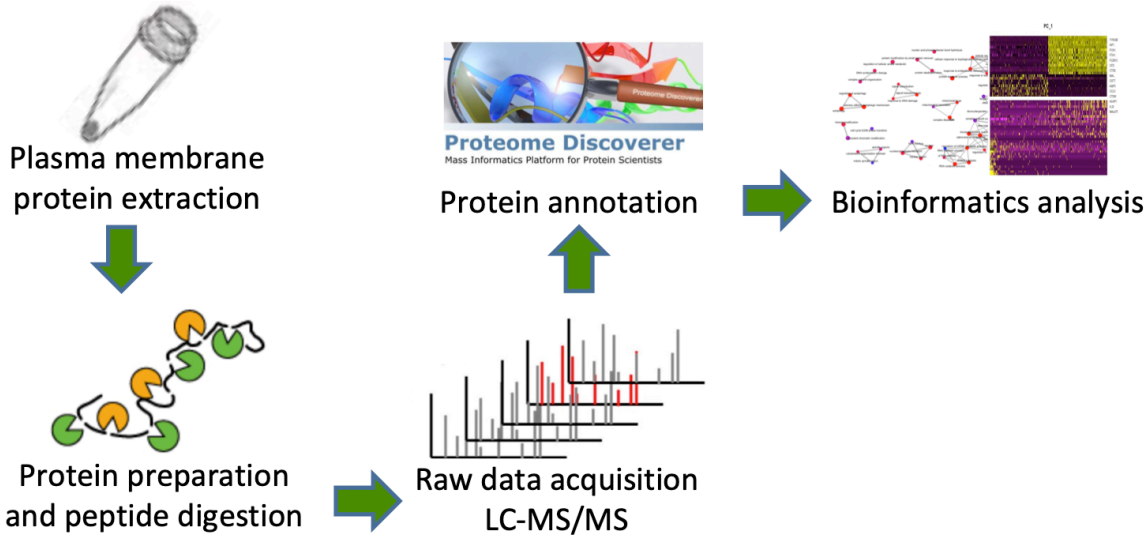

Fig. 3-1. Workflow for LC-MS/MS. Plasma membrane protein was extracted from sorted cells, and then digested into peptides. Proteins were quantified and identified through LC-MS/MS. Finally, differentially expressed proteins were identified.

3-1-3. MHCII subunits

The transcriptome analysis in chapter 2 revealed that several MHCII subunits were found to be upregulated in MLACs. The main function of MHCII is antigen presentation. This surface protein is highly expressed by antigen presenting cells. In mice, there are two dominant MHCII haplotypes mice are I-E and I-A. H2-Ab1, which is one of the top MLAC candidates, belongs to the I-A haplotype and is the B subunit allele (Fig. 3-2). MHC is highly polymorphic as there are many alleles that make up a single MHCII molecule that are spread throughout the human population, though the basic structure remains the same. This variability of alleles allows the variable region of the alpha and beta chain to recognize different antigens.

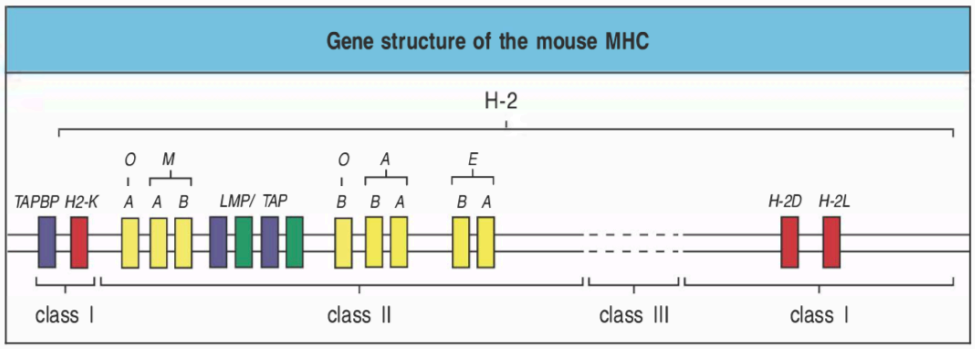

Fig. 3-2. Genetic organization of MHCII genes in mice. Adopted from Janeway, et al[8]. The major haplotypes of MHCII encoding genes (in yellow) are A, E, and M, and they are divided into *A* (α) and *B* (β) subunits. MHC I are in red.

3-1-4. CD11c (Integrin alpha X)

CD11c molecule is the most widely used marker to identify dendritic cells, although CD11c is also expressed in a subset of macrophages and monocytes[9]. CD11c is capable of binding to several ligands such as intercellular adhesion molecule (ICAM)-1 and ICAM-4[10] for the adhesion with other cells, which aids in the process of immune response[11]. It can also bind to fibrinogen and collagen for the adhesion to vascular epithelia[12]. It has also been found that CD11c forms a complex with CD18 and the phosphorylation of this complex facilitates reorganization of the cytoskeleton and increases adhesion[12]. CD11c also has other functions such pairing with integrin beta 2, to bind complement fragment iC3b and aid in phagocytosis and migration of macrophages and dendritic cells[13].

3-2. Materials and Methods

3-2-1. Mice

Male B6(Cg)-*Tyr*$^{c-2J}$/*J* (B6 albino) albino mice were obtained from Charles River Laboratories, Japan (Yokohama, Japan). All mice were housed in specific pathogen free conditions in the animal facilities at Tokyo Institute of Technology. Animal experiments were performed with the approval of the Animal Ethics Committees of Tokyo Institute of Technology (no. D2020008) and in accordance with the Ethical Guidelines for Animal Experimentation of Tokyo Institute of Technology.

3-2-2. Cell culture

LLC cell line was grown in DMEM (Gibco, Thermo Fisher Scientific, Waltham, MA, USA) supplemented with 5% FBS (Gibco), 100 units/mL penicillin, 100 units/mL streptomycin (Nacalai Tesque). RAW264.7 cells were cultured in DMEM supplemented with 10% FBS, 100 units/mL penicillin, 100 units/mL streptomycin (Nacalai Tesque). Cells were cultured in a 5% CO2 incubator at 37°C. The cells were regularly checked for mycoplasma contamination using a mycoplasma detection kit (Takara Bio, Shiga, Japan).

3-2-3. Subcutaneous tumor formation

The experiment was performed using 6 to 9-week-old male B6 albino mice. The mice were anesthetized with pentobarbital sodium (Somnopentyl, Kyouritsu Seiyaku, Japan). Murine Lewis lung carcinoma cell line LLC obtained from ATCC maintained with 5% FBS-DMEM supplemented with penicillin (100 units/mL) and streptomycin (100 mg/mL). The cultured LLC cells were collected by trypsinization and adjusted to a concentration of 1×10^6 cells/ 20 μL.

Cells were mixed with an equal volume of Geltrex® (Thermo Fisher Scientific) and then injected subcutaneously into the ventral part of the hind limb of mice.

3-2-4. Isolation of tumor infiltrating lymphocytes from tumors

Subcutaneous tumors of 15-20 mm in diameter were resected, minced using a scalpel blade and digested in RPMI medium (Thermo Fisher Scientific) supplemented with 2% FBS and 2.6 U Liberase DH (Roche Applied Science) at 37°C for 60 min, and then sequentially passed through 250, 100, and 40 μm strainers (Greiner Bio-One) to obtain single-cell suspensions. Cells were then resuspended in PharmLyse^{TM} solution (BD Bioscience) and incubated for 10 min at room temperature to lyse red blood cells. To select for the adherent cells, the cells were seeded into culture dishes with 2% FBS-RPMI at a seeding density of 2×10^7 cells/10 cm culture dish (Thermo Fischer Scientific) and incubated at 37°C for 20 min to allow adherent cells to attach to the surface of the dish. The non-adherent cells were collected and seeded again onto another culture dish in order to remove more adherent cells. The non-adherent cells remaining from that dish were collected for further analysis as the non-adherent fraction. The plate containing adherent cells were washed three times with PBS containing 0.68 mM EDTA. Strongly adherent cells were dislodged using PBS containing 2.5 mM EDTA and were collected with light scraping: these cells are the adherent fraction. Cells were resuspended in FACS buffer (PBS containing 1.2 mM EDTA and 5% FBS) in preparation for FACS.

3-2-5. FACS

Cells were blocked with anti-FcγRII/III and stained with anti-CD11b (BioLegend), Gr-1 (BioLegend) and anti-F4/80 (Bio-Rad). MLACs and MDSCs were sorted using SH800S (Sony

Biotechnology Tokyo, Japan). Information on antibodies is listed in Table 3-1.

3-2-6. Flow cytometry

Cells were blocked with anti-Fc γ RII/III (Biolegend) for 25 min at 4°C and stained with fluorophore-conjugated antibodies (see Table 3-1 for concentrations and manufacturers of antibodies) for 30 min at 4°C. Cells were washed once with FACS buffer to remove unbound antibodies. The cells were analyzed using the iCyt EC800 (Sony Biotechnology). Flow cytometry results were further analyzed using FlowJo (TreeStar).

Table 3-1. Antibodies used for FACS and flow cytometry analysis

Antibodies	Fluorochrome	Manufacturer	Clone number	Concentration
Gr-1	PE, Pe-Cy7	BioLegend	RB6-8C5	1:100
CD11b	PE/Cy7, AF488	BioLegend	M1/70	1:200
F4/80	AF647, AF488	Bio-Rad	C1:A3-1	1:50
H2-Ab1	PE	BioLegend	AF6-120.1	1:50
CD11c	Pe-Cy7, PE	BioLegend	N418	1:100
Mgl2	PE-Cy7	BioLegend	URA-1	1:100
CD74	Unconjugated	BioLegend	In1	1:100
Klrd1	Pe-Cy7	BioLegend	18D3	1:100
CD209a	PE	BioLegend	MMD3	1:50

3-2-7. Plasma membrane protein extraction

Plasma membrane proteins were isolated through the Mem-Per Plus plasma membrane protein extraction kit (Thermofischer Scientific) as recommended by the manufacturer (Fig. 3-3). In brief, sorted cells were permeabilized using the permeabilization buffer to remove cytosolic proteins. The sample was then centrifuge to pellet the cells and the permeabilization buffer was removed. Plasma membrane proteins were extracted by adding solubilization buffer. The sample was centrifuged to pellet the cell debris. The supernatant, which contains plasma membrane protein was collected and was stored in -80°C.

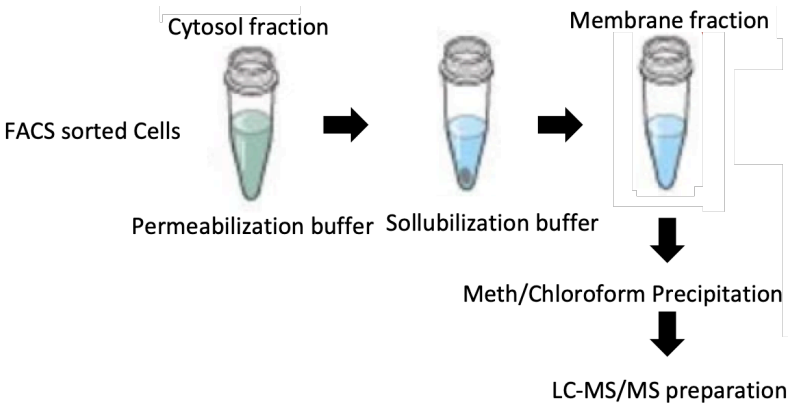

Fig. 3-3. Schematic diagram of extraction of plasma membrane protein from FACS sorted cells.

3-2-8. Methanol chloroform precipitation

The pooled protein was concentrated by methanol chloroform precipitation. The sample was diluted 3-fold with distilled water. Then 4 times the volume of methanol was added and homogenized. Equal volume of chloroform was added to the sample, and the mixture was homogenized. The sample was centrifuged at 14,000×g for 2 min, and then the upper layer was discarded. Methanol (Fujifilm Wako Pure Chemical, Osaka, Japan) was added to dilute the sample 5-fold and the mixture was centrifuged at 14,000×g for 3 min. The solvent was removed as much as possible in order to collect the precipitated protein. The precipitated protein was then washed with methanol and dried.

3-2-9. SDS-PAGE

RAW264.7 were lysed in radioimmunoprecipitation assay (RIPA) buffer (50 mM Tris HCl, pH 8.0, 150 mM NaCl, 1% NP-40, 0.5% sodium deoxycholate, 0.1% sodium dodecyl sulfate) containing protease cocktail inhibitor (Nacalai Tesque) and protein concentration was determined using Pierce BCA protein assay kit (Thermo Fisher Scientific). RAW264.7 lysate, plasma membrane fraction proteins, and cytosolic fraction proteins were separated by

electrophoresis on a 10% acrylamide gel. Silver staining (KANTO Chemical, Co, Tokyo, Japan) was then used to visualize the banding pattern.

3-2-10. Western blotting

After separation of proteins by SDS-PAGE, proteins were transferred to a hydrophilic polyvinylidene fluoride membrane (Merck, NJ, USA) and blocked with 5% skim milk in TBST (20 mM Tris, pH 7.5, 150 mM NaCl, 0.1% Tween 20). The membrane was then probed with relevant primary antibodies: (GAPDH (2118s, 1:1000), H2AII (2578S, 1:300), Cytochrome C (4272S, 1:500) (all from Cell Signaling Technology, Danvers, MA, USA), and CD45 (25386, 1:1000) (Abcam, Massachusetts, USA) and incubated overnight at 4 °C. The membranes were washed with TBST 3 times for 5 min and stained with secondary antibody: anti-rabbit IgG HRP-linked Antibody (7074, 1:5000 Cell signaling Technology). The membranes were washed with TBST 3 times for 5 min and chemiluminescence reaction was carried out using Chemi-Lumi One (Nacalai Tesque) and chemiluminescence detection and image processing was performed using Imagequant 4000 (GE Healthcare Life Sciences, Chicago, IL, USA).

3-2-11. Peptide preparation

Proteins were reduced for 30 min at room temperature using 1 M dithiothreitol (DTT) in 50 mM ammonium bicarbonate (ABC) buffer (1/100 volume of sample), and alkylated for 20 min using 1 M iodoacetamide (Fujifilm Wako Pure Chemical) in 50 mM ABC buffer (1/20 volume of sample). Samples were then diluted five-fold with 50 mM ABC buffer. Tryipsin/Lysyl endopeptidase mix[14] (Trypsin/Lys-C, Mass Spectrometry (MS) grade, Promega, Madison, WI, USA) was added to a final concentration of 0.5 μg/50 μg protein, and samples

were incubated for 3 h at 25°C. Finally, additional 1 μg per 50 μg protein Trypsin/Lys-C, (MS grade, Promega) was added, and samples were digested overnight at 37°C. Detergents were removed through precipitation with ethyl acetate and 0.5% trifluoroacetic acid[14].

3-2-12. LC-MS/MS

To desalt the peptide, 1 mL of Elution solution (0.1% TFA, 80% acetonitrile) was placed on a StageTip (GL Sciences, Tokyo, Japan) and centrifuged at 1,000×g for 2 min at room temperature. Then, 1 mL of Binding solution (0.1% TFA, 2% acetonitrile) was added and centrifuged in the same way. 200 μL of Binding solution was added to the sample and centrifuged at 500×g for 3 min at room temperature on a StageTip. The tube was washed again by adding 200 μL of Binding solution to the empty tube, and the solution was placed on the StageTip and centrifuged at 500×g for 3 min at room temperature. This step was repeated again. 1 mL of Binding solution was placed on the StageTip and centrifuged at 1,000×g for 2 min. The StageTip was transferred to a collection tube, loaded with 300 μL of Elution solution, and centrifuged at 500×g for 2 min to elute. The eluted solution was transferred to a 1.5 mL tube and centrifuged at 500×g for 2 min.

The supernatant was centrifuged at 20,000×g for 5 min at 4°C and analyzed using a nanoLC-mass spectrometer (Quadrupole-Orbitrap, Thermo Fisher Scientific), n=3. MS data were processed using Proteome Discoverer 3.0 (Thermofischer Scientific) and protein IDs were identified through the murine Uniprot protein database[15]. Differentially expressed proteins were identified through calculating the fold-change and P-value.

3-2-13. Analysis of biological process of differentially expressed proteins

The differentially expressed proteins were converted into their corresponding genes subjected to Gene set enrichment analysis (GSEA) through the R ClusterProfiler[16] package by referencing to the Molecular Signatures Database (MSigDB)[17].

3-2-14. Rank-rank hypergeometric overlap (RRHO) analysis

Gene expression counts from RNA-seq data were tabulated with peptide counts from LC-MS/MS by tabulating the corresponding gene IDs with protein IDs. The input score was calculated through using the fold-change of fold-expression and *P*-value of expression from the RNA-seq and proteomics analyses by calculating Cohen's D[18]. Detection and ranking of top correlated candidates were performed through RRHO analysis. The segmented heatmap was generated through the RRHO2 R package[19].

3-2-15. Statistical analysis

All data are presented as mean ± standard deviation and were statistically analyzed with unpaired t-test. *P*-values of 0.05 or less were considered statistically significant.

3-3. Results

3-3-1. Validation of plasma membrane protein extraction method

To test the accuracy of the plasma membrane protein extraction method, RAW264.7 cells, a murine macrophage cell line, were used. I collected RAW246.7 cells and extracted membrane proteins, which includes plasma, mitochondrial, and nuclear membrane proteins, using the MEM-PER plasma membrane extraction kit and collected the membrane fraction, cytosolic fraction, and remaining pellet protein. I compared the protein yield of each fraction with RAW246.7 cells that were lysed in RIPA buffer. The amount of membrane protein yield is about 17% of the unseparated protein (Table 3-2).

I first compared the general composition of these protein fractions through visualizing the difference in banding pattern on SDS-PAGE gel analysis. The plasma membrane fraction and cytosolic fraction had completely different banding pattern (Fig. 3-4). Moreover, the banding pattern cytosolic fraction seemed to be more similar to unseparated sample.

Table 3-2. Protein yield from plasma membrane protein extraction of RAW264.7 cells

Sample*	**Protein yield (μg)**
Membrane fraction	248.4
Cytosolic fraction	438.1
Pellet	258
Unseparated protein	1,395

***Plasma membrane protein was isolated from 3.5×10^6 RAW264.7 cells. The same number of RAW264.7 cells was also used to estimate total protein to produce the unseparated protein sample.

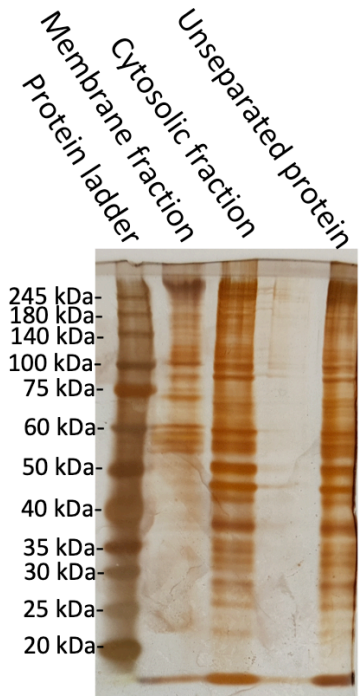

Fig. 3-4. SDS-PAGE gel analysis of protein fractions. Cytosolic fraction, membrane fraction, and unseparated protein from RAW246.7 were shown. Acrylamide gel was stained with silver staining.

To further analyze the protein composition of the different fractions, I performed Western blotting to analyze for proteins of different cellular localizations. This was also used to determine the efficacy of plasma membrane protein extraction. CD45 (common lymphocyte antigen) was analyzed to represent plasma membrane proteins and GAPDH for cytosolic proteins. CD45 was strongly enriched in the membrane fraction and the relative abundance of GAPDH was slightly less in the membrane fraction compared to cytosolic fraction (Fig. 3-5). H2AII (histone) and cytochrome C were analyzed to determine the amount of nuclear and mitochondrial proteins in the samples, respectively. It is interesting to note that H2AII and cytochrome C was not found in the membrane fraction nor cytosol fraction, but was detected in the unseparated sample (Fig. 3-5). This suggests that the permeabilization buffer may not be effective in sollubilizing the membranes of organelles. The solubilization buffer may be acting

mostly superficially to solubilize plasma membrane proteins. Overall, these results suggest sufficient isolation and enrichment of plasma membrane proteins with sufficient purity.

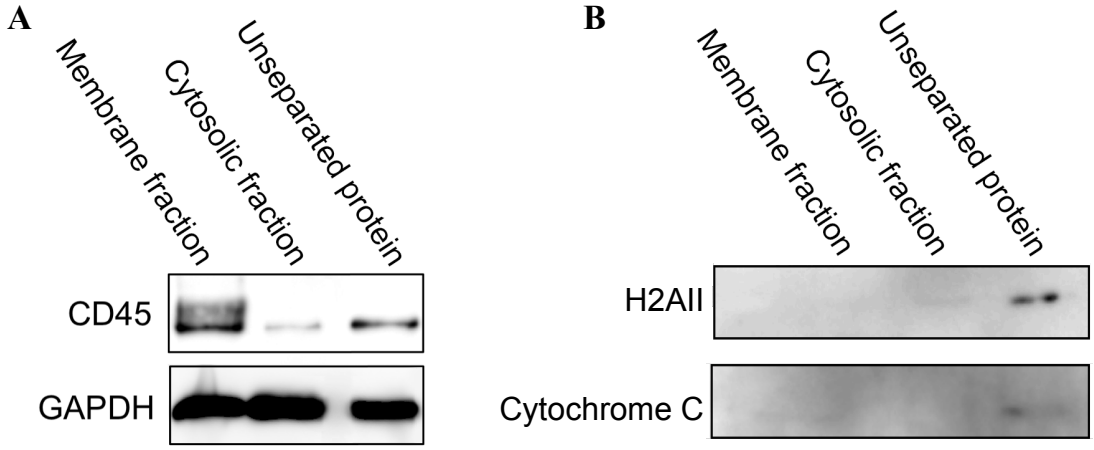

Fig. 3-5. Western blot analysis of membrane fraction, cytosol fraction, and unseparated protein after membrane fractionation of RAW264.7 cells. **A.** Amount of the membrane protein CD45 and the cytosolic protein GAPDH were analyzed. **B.** Amount of nuclear protein H2AII and mitochondrial protein cytochrome C were analyzed. Representative results are shown.

3-3-2. Plasma membrane proteome analysis of MLACs

After optimizing the use of the plasma membrane extraction kit, I isolated plasma membrane proteins from MLACs and MDSCs. Table 3-3 shows the information for the samples collected and the amount of protein yielded.

Table 3-3. Cells isolated and corresponding protein yield for proteome analysis

		MLAC membrane	**MDSC membrane**
Isolated cells ($\times 10^6$)	Trial 1	7.181	5.009
	Trial 2	2.313	1.956
	Trial 3	2.362	2.651
Protein amount (μg)	Trial 1	18.1	14.2
	Trial 2	3.42	3.46
	Trial 3	5.08	4.21

About 2 μg of total protein was the minimum input amount of LC-MS/MS analysis. Trial 1 was first performed with a larger amount of protein (5-7 μg) in order to check if plasma membrane proteins can be detected successfully. Then this was scaled down to about 2 μg. A total of 3 biological replicates were performed (Table 3-4). Out of the 1960 unique proteins detected by LC-MS/MS analysis, plasma membrane proteins were the most abundant at 1506 proteins (Table 3-4). However, proteins from the cytosol, nucleus and cell organelles were also detected but to a lesser extent. It is also possible that some proteins can be found in multiple cellular localizations.

Table 3-4. Number of unique proteins identified in each cellular component through Proteome Discoverer software

Cellular component	Protein number
Plasma membrane	1506
Cytosol	545
Nucleus	720
Organelle	153
Total unique proteins identified	1960

The plasma membrane proteins that were detected were subjected to differential expression analysis. Differentially expressed proteins were filtered as having greater than 3-fold-change (FC) and with a *P*-value of less than 0.05 (Fig. 3-6). The top upregulated plasma membrane proteins for MLACs over MDSCs were histocompatibility 2, class II, locus Dma (H2-Dma), CD11c, histocompatibility 2, class II antigen A, beta 1 (H2-Ab1), histocompatibility 2, class II, I-E alpha chain, and histocompatibility 2, class II, E-D beta chain. The most significantly downregulated plasma membrane proteins for MLACs over MDSCs were CD93, Ighg, Endod1, and Fcgr1. Interestingly, several MHCII subunits were upregulated in MLACs compared to MDSCs and LC-MS/MS detected several peptide fragments derived from the same protein

(Table 3-5). Furthermore, the biological significance analysis of the upregulated plasma membrane proteins for MLAC revealed that there was enrichment for leukocyte mediated immunity, antigen processing and presentation, and positive regulation of cell adhesion (Fig. 3-7). It is possible that these upregulated plasma membrane encoding proteins altogether can contribute to the adhesion properties of MLAC. These results suggest that MLAC may have unique activities in the tumor that are facilitated through its expressed plasma membrane proteins.

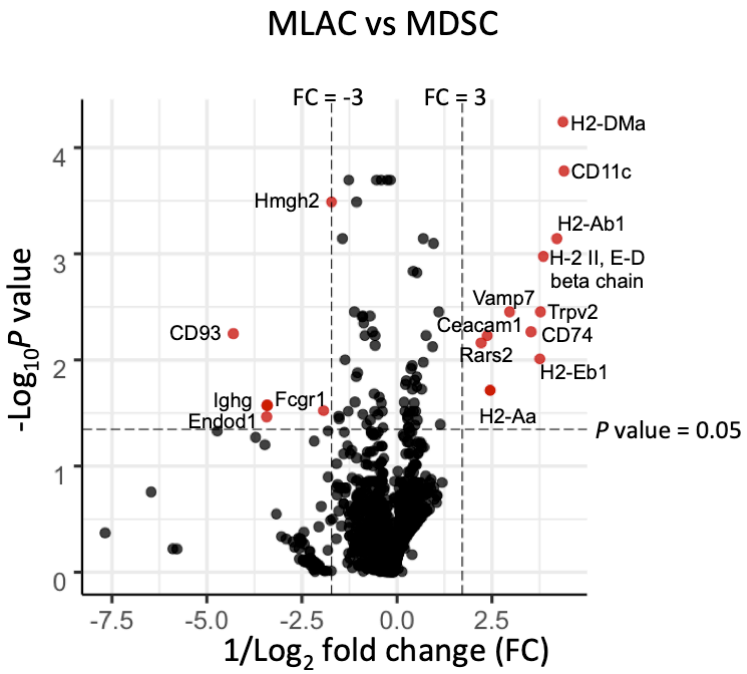

Fig. 3-6. Volcano plot showing the upregulated and downregulated plasma membrane proteins for MLACs. Dashed lines in x- and y-axis indicate the fold-change (FC) > 3 and *P*-value > 0.05, respectively. Red dots with protein names indicate significantly changed proteins.

Table 3-5. MHCII subunits expression ratio from plasma membrane proteome

Protein description	**Protein name**	**Mean abundance ratio of peptide count (MLAC/MDSC)**
H-2 class II histocompatibility antigen, I-A beta chain	H2-Eb1	3.68
H-2 class II histocompatibility antigen, E-S beta chain	H2-Eb1	3.68
H-2 class II histocompatibility	H-2 class II	3.64

antigen, I-E alpha chain	histocompatibility antigen, I-E alpha chain	
H-2 class II histocompatibility antigen, A-R alpha chain	H2-Aa	3.64
H-2 class II histocompatibility antigen, A-S alpha chain	H2-Aa	3.64
H-2 class II histocompatibility antigen, A-Q alpha chain (Fragment)	H2-Aa	3.64
H-2 class II histocompatibility antigen, A-K alpha chain	H2-Aa	3.64
H-2 class II histocompatibility antigen, A-D alpha chain	H2-Aa	3.64
H-2 class II histocompatibility antigen, A-F alpha chain	H2-Aa	3.64
H-2 class II histocompatibility antigen, E-Q beta chain	H-2 class II histocompatibility antigen, E-Q beta chain	3.27
H-2 class II histocompatibility antigen, A-Q alpha chain	H2-Aa	3.25
H-2 class II histocompatibility antigen, I-A beta chain (Fragment)	H2-Eb1	3.04
H-2 class II histocompatibility antigen, I-A beta chain	H2-Eb1	3.04
H-2 class II histocompatibility antigen, E-B beta chain	H2-Eb1	2.67
H-2 class II histocompatibility antigen, E-D beta chain	H-2 class II histocompatibility antigen, E-D beta chain	2.41
H-2 class II histocompatibility antigen, A-U alpha chain	H2-Aa	2.31
H-2 class II histocompatibility antigen, A-B alpha chain	H2-Aa	2.31
H-2 class II histocompatibility antigen, A-F beta chain (Fragment)	H2-Ab1	2.07
H-2 class II histocompatibility antigen, A beta chain	H2-Ab1	2.03
H-2 class II histocompatibility antigen, A-D beta chain	H2-Ab1	1.99
H-2 class II histocompatibility antigen, A-F beta chain	H2-Ab1	1.97
H-2 class II histocompatibility antigen, A-Q beta chain	H2-Ab1	1.91
H-2 class II histocompatibility antigen, A-K beta chain	H2-Ab1	1.68

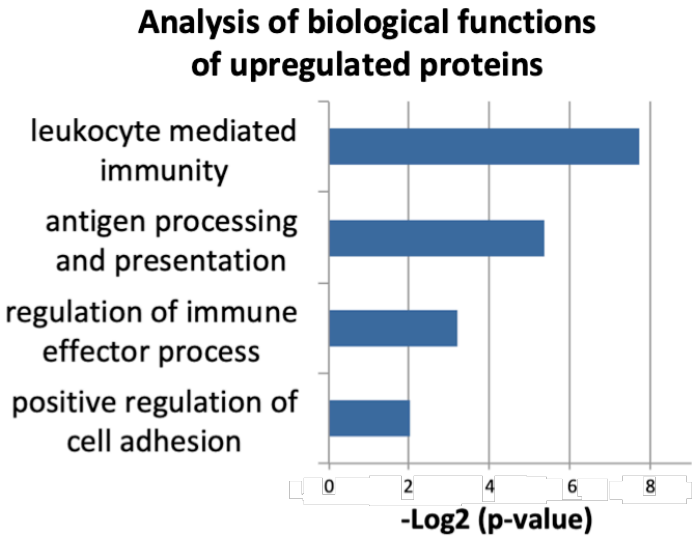

Fig. 3-7. Analysis of enriched biological processes for significantly upregulated plasma membrane proteins for MLAC. The corresponding gene names for the proteins were used in this analysis.

Next, rank-rank hypergeometric overlap analysis (RRHO)[18] was performed to select high-confidence markers and validate correlated hits between the transcriptome and proteome analyses. RRHO analyzes genes based on the rank of differential expression rather than magnitude of differential expression. The composite ranks were determined based on the highest fold-change and lowest *P*-value from differentially expressed genes and proteins. I visualized the correlation between transcriptome and proteome by using a 2D heatmap (Fig. 3-8). The top right quadrant of the 2D heatmap contains the plasma membrane protein candidates that were consistently correlated and upregulated between transcriptome and proteome analyses. CD301a, H2-Eb1, H2-Aa, H2-Ab1, CD74, and CD11c were ranked as the top six most consistent proteins between both datasets (Table 3-6). Then, to test whether these six proteins can be used as MLAC markers, their expression levels on MLAC and MDSC were analyzed by flow cytometry (Figs. 3-9 and 3-10). I found that a significant population of MLACs expressed H2-Ab1 and CD11c, while only a small population expressed CD74. MDSCs did not express any of these proteins.

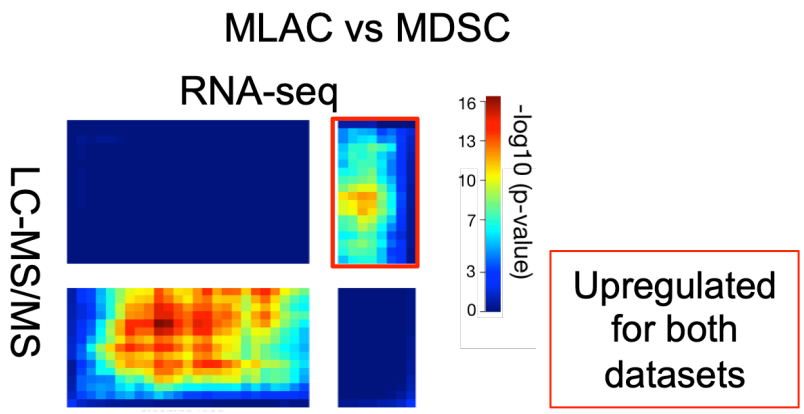

Fig. 3-8. RRHO heatmap comparing rank overlap of differentially expressed genes between transcriptomic and proteomic analyses. Genes were plotted based on correlation of upregulation. The upper right quadrants indicate genes upregulated in both datasets while lower left quadrants indicate genes downregulated in both datasets. Red and dark blue indicate the highest and lowest degree of overlap, respectively.

Table 3-6. Top 25 ranked marker candidates having concordantly enriched expression in MLAC compared to MDSC based on rank-rank hypergeometric analysis

Rank	Gene name	Protein name
1	*Mgl2*	Macrophage galactose N-acetyl-galactosamine-specific lectin 2 (CD301a)
2	*H2-Eb1*	H-2 class II histocompatibility antigen, I-E beta chain (H2-Eb1)
3	*H2-Aa*	H-2 class II histocompatibility antigen, A alpha chain (H2-Aa)
4	*H2-Ab1*	H-2 class II histocompatibility antigen, A beta chain (H2-Ab1)
5	*Cd74*	H-2 class II histocompatibility antigen gamma chain (CD74)
6	*CD11c*	Integrin alpha X (CD11c)
7	*Steap4*	Steap4
8	*Syne1*	Nesprin-1 (Syne1)
9	*Cd177*	CD177
10	*S100a9*	Protein S100-A9 (S100a9)
11	*Rab44*	Ras-related protein Rab-44 (Rab-44)
12	*Fpr2*	Formyl peptide receptor 2 (Fpr2)
13	*Adgrg3*	Adhesion G protein-coupled receptor G3 (Adgrg3)
14	*Il1rap*	Interleukin-1 receptor accessory protein (Il1rap)
15	*Itgb2l*	Integrin beta-2-like protein (Itgb2l)
16	*Mcemp1*	Mast cell-expressed membrane protein 1 (Mcemp1)
17	*Sorl1*	Sortilin-related receptor (Sorl1)
18	*Clec10a*	C-type lectin domain family 10 member A (Clec10a)
19	*Clec7a*	C-type lectin domain family 7 member A (Clec7a)

20	*Rab27a*	Ras-related protein Rab-27A (Rab27a)
21	*Cd300lf*	CMRF35-like molecule 1 (CD300lf)
22	*Sirpb1b*	Signal-regulatory protein beta 1B (Sirpb1b)
23	*Lrg1*	Pleiotropic regulator 1 (Lrg1)
24	*Lcn2*	Neutrophil gelatinase-associated lipocalin (Lcn2)
25	*Itprip*	Inositol 1,4,5-trisphosphate receptor-interacting protein (Itprip)

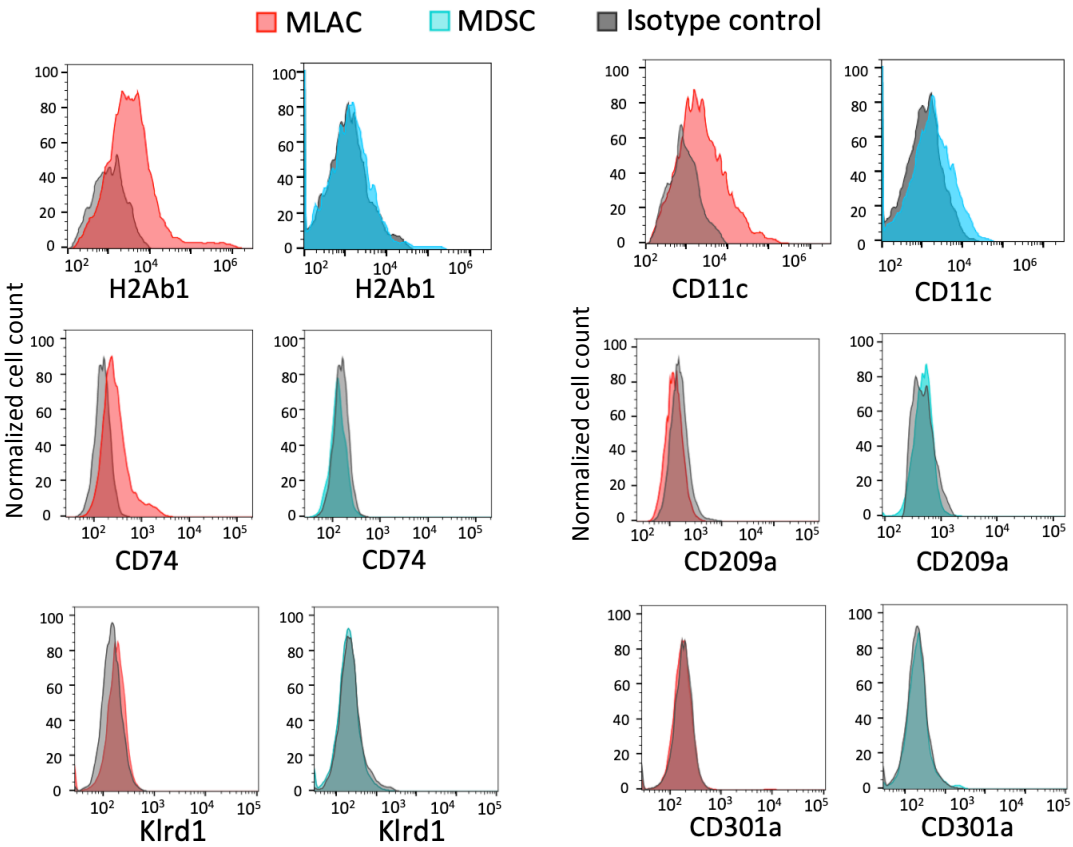

Fig. 3-9. Expression levels of different candidate markers on MLACs and MDSCs. $CD11b^{+}$ $F4/80^{-}$ MLAC and $CD11b^{+}Gr\text{-}1^{+}$ MDSC were prepared from adherent and non-adherent fractions of LLC tumor, respectively. Expression levels of six candidate marker proteins on MLACs and MDSCs were analyzed by flow cytometry.

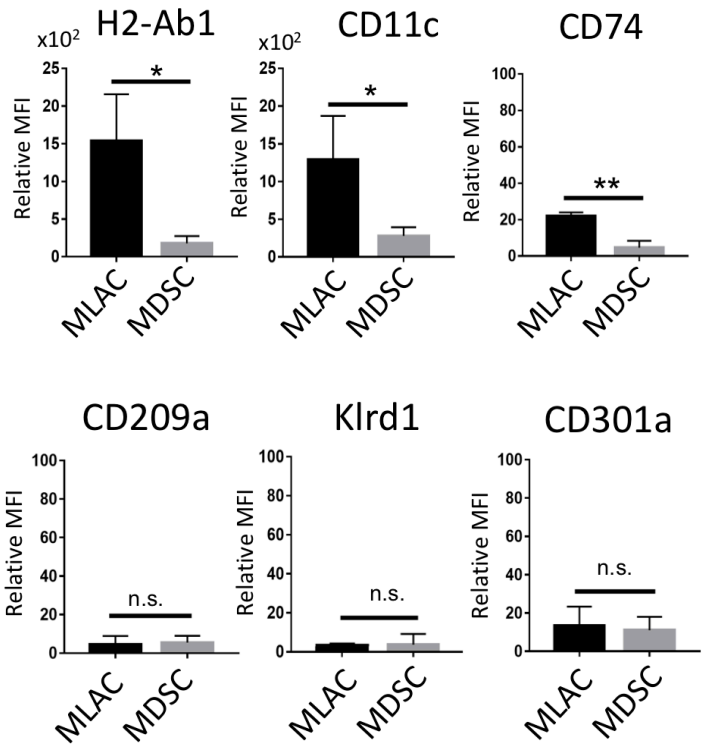

Fig. 3-10. Relative median fluorescence intensity (MFI) of candidate markers. MFI values were obtained from flow cytometric results shown in Fig. 3-9. Relative MFI = $MFI_{stained\ sample} - MFI_{isotype\ control}$. Error bars indicate standard deviation. *$p < 0.05$, **$p < 0.01$, n.s., not significant. $n = 3$.

I then analyzed the co-expression of H2-Ab1 and CD11c as cell surface marker candidates on MLACs obtained by adhesion-based separation (hereinafter referred to as Adh-MLACs). Flow cytometry analysis revealed that combination staining of commercially available antibodies against H2-Ab1 and CD11c could label about 44% (combining H2-Ab1$^+$ and CD11c$^+$ populations) of Adh-MLACs. Approximately 30% and 28% of Adh-MLACs were labeled with H2-Ab1 and CD11c antibodies, respectively, of which approximately 13% to 16% were double positive (Fig. 3-11). These results indicate that, although anti-H2-Ab1 and anti-CD11c antibodies were not capable of labeling all MLACs, H2-Ab1 and CD11c may be used as markers to directly isolate MLAC subsets from the tumor-extracted CD11b$^+$F4/80$^-$ populations.

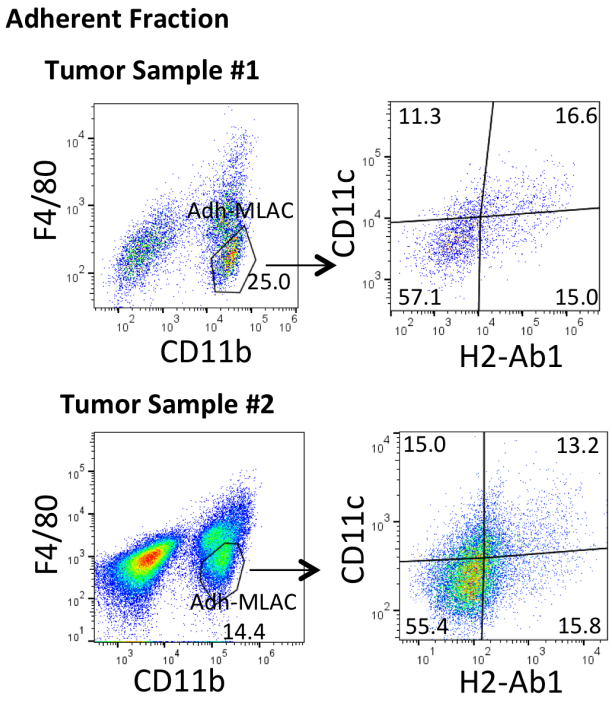

Fig. 3-11. Flow cytometry analysis of H2-Ab1 and CD11c expressing populations of Adh-MLACs.

Table 3-7. Differential expression of CD11c and H2-Ab1 between MLAC and MDSC based on RNA-seq and plasma membrane proteome analysis

Gene name	MLAC (TPM*)	MDSC (TPM)	Fold-change	Protein name	MLAC (APC**)	MDSC (APC)	Fold-change
H2-Ab1	1703.8	496.6	3.43	H2-Ab1	6.12×10^{7}	1.91×10^{6}	32.1
CD11c (Itgax)	86.33	50.08	1.72	CD11c	5.81×10^{5}	1.70×10^{4}	34.2

*Transcript count is expressed in TPM (transcript per million).
**Peptide count is expressed in APC (average peptide count).

Table 3-8. Differential expression of CD11b and CD18 between MLAC and MDSC based on plasma membrane proteome analysis

Protein name	MLAC (APC*)	MDSC (APC)	Fold-change
CD18	3.595×10^{8}	2.522×10^{8}	1.427
CD11b	1.497×10^{9}	1.444×10^{9}	1.037

*Peptide count is expressed in APC (average peptide count).

3-4. Discussion

This chapter presented the plasma membrane proteome analysis of MLAC in order to determine surface markers and identified H2-Ab1 and CD11c as potential MLAC markers. It is common for the quantity of fold-change of RNA expression to not reflect protein expression, which made it challenging to determine the reliability of chosen candidates and to predict the extent of differential expression[20]. Shotgun proteomics was performed to more accurately quantify plasma membrane proteins. LC-MS/MS analysis detected trace amounts of proteins from other cellular components such as cytosolic and nuclear membrane proteins although they were not detected by Western blotting. This is due to the mechanism of the plasma membrane extraction kit which permeabilizes the plasma membrane and removes the cytosol from the cell, and then a strong detergent buffer, the solubilization buffer, is used to solubilize the plasma, mitochondrial, and nuclear membrane proteins. Because of this extraction principle, it is likely that proteins from other organelles could not be completely removed from the membrane fraction. Despite this, plasma membrane proteins could still be accurately and abundantly detected.

RRHO was able to verify that the proteomics analysis was reliable due to the correlation of upregulated and downregulated proteins between transcriptome and proteome analysis. Through this integration, the risk of false positives or false negatives, compared from basing solely from proteome analysis alone, can also be reduced.

Proteomic analysis showed that CD11c expression was 34.2-fold higher in MLACs than in MDSCs, but transcriptome analysis showed less than 2-fold (Table 3-7), suggesting that CD11c may be regulated primarily at the protein level. CD11c protein levels are known to be correlated with pro-inflammatory cytokines[21-23]. Because the TME is associated with a chronic

inflammatory state, the secretion of many inflammatory cytokines is controlled in a context-dependent manner. This potentially explains why not all MLACs are CD11c-positive and the proportion of CD11c-positive MLACs is not constant. MLACs seem to overlap with conventional dendritic cells with respect to expression of MHCII and CD11c. Although the majority of conventional dendritic cells are $F4/80^{+}$, $F4/80^{-}$ subsets of dendritic cells have also been reported[24-26]. In line with scRNA-seq analysis results indicating the association of MLACs with monocyte cell populations, previous studies have also shown that monocytes can upregulate CD11c expression in response to inflammatory stimuli, but did not differentiate nor obtain the antigen presentation activity of dendritic cells[27]. These previous reports suggest that the observed cells might be MLACs. The expression of CD11c and CD74, which both have a function and adhesion[28], might explain the strongly adherent properties of MLAC.

Plasma membrane proteome analysis showed that MLACs have high expression levels of several MHCII subunits, such as H2-Ab1, H2-Eb1, H2-Aa, and H2-Dma. The H2-Ab1 antibody clone used in this study could detect multiple MHC Class II I-Ab alloantigens. However, this antibody did not detect MDSCs. It is possible that previously reported $CD11b^{+}F4/80^{-}$ tumor-infiltrating cell population that highly expressed MHCII[29] may have been MLAC. Hence, MLACs may already be recognized as a poorly characterized subset of tumor-infiltrating myeloid cells. Further studies are required to determine the relationship between MLACs and dendritic cells, as well as to investigate if MLACs possess antigen-presenting capabilities.

The accuracy of the detection of plasma membrane proteins is dependent on the efficiency of solubilization of the proteins. Further optimization and testing of other protein precipitation methods may allow for increased sensitivity of detection of plasma membrane proteins.

MLAC were found to express several adhesion proteins, hence it is also necessary to determine the expression of these other adhesion proteins on MLACs. Given that CD11c is expressed on MLACs, the adhesion function of CD11c is only present when it forms a heterodimer with CD18[30]. There is also an increase in the expression of CD18 based on proteome analysis (Table 3-8), which may suggest the formation of CD18/CD11c heterodimer. In contrast, the expression of CD11b, which can also dimerize with CD18 was not significantly different between MLACs and MDSCs. Furthermore, it is necessary to determine the contribution of these adhesion proteins towards the ability of MLAC to strongly adhere to culture dishes, such as testing the adhesion on dishes with defined extracellular matrix coating such as collagen or fibrinogen.

References

1. Rugg-Gunn, P. J. et al. Cell-surface proteomics identifies lineage-specific markers of embryo-derived stem cells. *Dev. Cell* 22, 887–901 (2012).

2. Vit, O. & Petrak, J. Integral membrane proteins in proteomics. How to break open the black box? *J. Proteomics* 153, 8–20 (2017).

3. Elschenbroich, S., Kim, Y. & Jeffrey, A. Isolation of cell surface proteins for mass spectrometry- based proteomics. *Expert Rev. Proteomics* 7, 1–14 (2010).

4. Kongpracha, P. et al. simple but efficacious enrichment of integral membrane proteins and their interactions for in-depth membrane proteomics. *Mol. Cell. Proteomics* 21, 100206 (2022).

5. Karhemo, P. R. et al. An optimized isolation of biotinylated cell surface proteins reveals novel players in cancer metastasis. *J. Proteomics* 77, 87–100 (2012).

6. Geiger, T., Wehner, A., Schaab, C., Cox, J. & Mann, M. Comparative Proteomic Analysis of Eleven Common Cell Lines Reveals Ubiquitous but Varying Expression of Most Proteins. Mol. Cell. *Proteomics* 11, M111.014050 (2012).

7. Kang, J. Principles and applications of lc-ms/ms for the quantitative bioanalysis of analytes in various biological samples. (2011).

8. Murphy, K., Travers, P., Walport, M., & Janeway, C. Janeway immunobiology. Garland Science, New York 53, (2013).

9. Wu, J., Wu, H., An, J., Ballantyne, C. M. & Cyster, J. G. Critical role of integrin CD11c in splenic dendritic cell capture of missing-self CD47 cells to induce adaptive immunity. *Proc. Natl. Acad. Sci*. U. S. A. 115, 6786–6791 (2018).

10. Ihanus, E., Uotila, L. M., Toivanen, A., Varis, M. & Gahmberg, C. G. Red-cell ICAM-4 is a ligand for the monocyte/macrophage integrin CD11c/CD18: characterization of the binding sites on ICAM-4. *Blood* 109, 802–810 (2006).

11. Ungai-sala, R., Orgova, N., Erdei, A. & Bajtay, Z. CD11c/CD18 Dominates Adhesion of Human Monocytes, Macrophages and Dendritic Cells over CD11b/CD18. 1–17 (2016). doi:10.1371/journal.pone.0163120

12. Uotila, L. M., Aatonen, M. & Gahmberg, C. G. Integrin CD11c/CD18 α -chain phosphorylation is functionally important. J. *Biol. Chem*. 288, 33494–33499 (2013).

13. Sadhu, C. et al. CD11c/CD18: novel ligands and a role in delayed-type hypersensitivity. *J. Leukoc. Biol*. 81, 1395–1403 (2007).

14. Deschoenmaeker, F. et al. The absence of thioredoxin m1 and thioredoxin c in anabaena sp. pcc 7120 leads to oxidative stress. Plant *Cell Physiol*. 59, 2432–2441 (2018).

15. Yuqi Wang, Qinghua Wang, Hongzhan Huang, Wei Huang, Yongxing Chen, Peter B. McGarvey, Cathy H. Wu, C. N. A. A crowdsourcing open platform for literature curation in UniProt. *PLoS Biol* 19, (2021).

16. Yu, G., Wang, L. G., Han, Y. & He, Q. Y. ClusterProfiler: An R package for comparing biological themes among gene clusters. *Integr. Biol*. (2012). doi:10.1089/omi.2011.0118

17. Liberzon, A. et al. Molecular signatures database (MSigDB) 3.0. *Bioinformatics* 27, 1739–1740 (2011).

18. Plaisier, S. B., Taschereau, R. & Wong, J. A. Rank-rank hypergeometric overlap : identification of statistically significant overlap between gene-expression signatures. *Nucleic Acids Res* 38, 1–17 (2010).

19. Cahill, K. M., Huo, Z., Tseng, G. C., Logan, R. W. & Seney, M. L. Improved identification of concordant and discordant gene expression signatures using an updated rank-rank hypergeometric overlap approach. *Sci. Rep*. 8, 9588 (2018).

20. Hoogendijk, A. J. et al. Dynamic transcriptome-proteome correlation networks reveal human myeloid differentiation and neutrophil-specific programming. *Cell Rep*. 29, 2505-2519.e4 (2019).

21. Wong, E. et al. Langerhans Cells Orchestrate the Protective Antiviral Innate Immune Response in the Lymph Node. *Cell Rep*. 29, 3047-3059.e3 (2019).

22. Puig, K. L., Swigost, A. J., Zhou, X., Sens, M. A. & Combs, C. K. Amyloid precursor protein expression modulates intestine immune phenotype. *J. NeuroImmune Pharmacol*. 7, 215-230 (2012).

23. Han, C. et al. NOX4 promotes mucosal barrier injury in inflammatory bowel disease by mediating macrophages M1 polarization through ROS. *Int. Immunopharmacol*. 104, 108361 (2022).

24. Sheng, J. et al. A discrete subset of monocyte-derived cells among typical conventional type 2 dendritic cells can efficiently cross-present. *Cell Rep*. 21, 1203–1214 (2017).

25. Hotblack, A. et al. tumor-resident dendritic cells and macrophages modulate the accumulation of TCR-engineered t cells in melanoma. *Mol. Ther*. 26, 1471–1481 (2018).

26. Soncin, I. et al. The tumour microenvironment creates a niche for the self-renewal of tumour-promoting macrophages in colon adenoma. *Nat. Commun*. 9, 582 (2018).

27. Drutman, S. B., Kendall, J. C. & Trombetta, E. S. Inflammatory spleen monocytes can upregulate CD11c expression without converting into dendritic cells. *J. Immunol*. 188, 3603–3610 (2012).

28. Beswick, E. J. & Reyes, V. E. CD74 in antigen presentation, inflammation, and cancers of the gastrointestinal tract. *World J. Gastroenterol*. 15, 2855–2861 (2009).

29. Huang, W. et al. Calcium/Calmodulin Dependent Protein Kinase Kinase 2 Regulates the Expansion of Tumor-Induced Myeloid-Derived Suppressor Cells. *Frontiers in Immunology* 12, 754083 (2021).

30. Abdel-Salam, B. K. A. & Ebaid, H. Expression of CD11b and CD18 on polymorphonuclear neutrophils stimulated with interleukin-2. *Cent. J. Immunol.* **39**, 209–215 (2014)

Chapter 4

Analysis and validation of H2-Ab1- and CD11c-positive MLAC subsets

Abstract

H2-Ab1 and CD11c are expressed in populations of MLACs, while none of these proteins are expressed in MDSCs. A FACS gating strategy using these surface markers was developed to isolate MLAC populations from $CD11b^{+}F4/80^{-}$ cells without adhesion-based separation. The equivalence of the $CD11b^{+}F4/80^{-}H2\text{-}Ab1^{+}$ ($H2\text{-}Ab1^{+}$) and $CD11b^{+}F4/80^{-}CD11c^{+}$ ($CD11c^{+}$) populations to MLACs obtained by adhesion-based separation (Adh-MLACs) was verified by analyzing key characteristics of MLACs. $H2\text{-}Ab1^{+}$ and $CD11c^{+}$ populations, like Adh-MLAC, were confirmed to express the MLAC gene signature, exhibited potent cancer growth promoting ability, and had no immunosuppressive activity. These results highlight that H2-Ab1 and CD11c can be utilized for detection and isolation of MLACs directly from tumors. The use of these markers can contribute to determine the role of MLACs in the development of an immunosuppressive TME.

4-1. Introduction

4-1-1. T cell activation

The T cell receptor (TCR) complex is utilized by T cells for the recognition of foreign antigen peptides displayed on MHC (MHC-antigen peptide complex) and T cell activation. The TCR complex is made up of TCR for antigen recognition and CD3 complex for signal transduction (Fig. 4-1). The TCR or CD3 complex is composed of several subunits, TCR-α and TCR-β chains or CD3γ, CD3δ, and CD3ε subunits, and ζ-chain, respectively, and they are collectively called CD3. Each CD3 subunit has immunoreceptor tyrosine-based activation motifs (ITAMs) which are involved in signal transduction[1]. CD4 and CD8 are co-receptors that also bind to the MHC-antigen peptide complex and aid in activation by recruiting lymphocyte-specific protein tyrosine kinase (Lck), which phosphorylates ITAMs (Fig. 4-2). When the TCR recognize and bind an MHC-antigen peptide complex expressed by antigen presenting cells, the ITAMs become phosphorylated by Lck, and ZAP-70 bind to them. This causes the activation of multiple downstream signaling pathways such as activation of mitogen activated protein kinase (MAPK), which activates transcription factors necessary for proliferation[2].

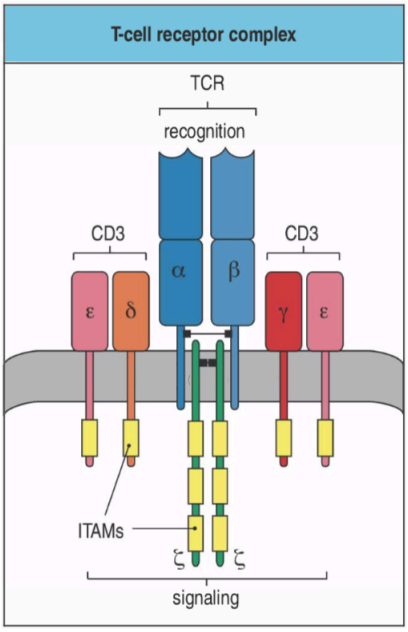

Fig. 4-1. Structure of the TCR complex. Recognition site and signaling domain of the TCR complex is indicated. ITAMs are indicated by the yellow rectangles. Adopted from Janeway, et al[3].

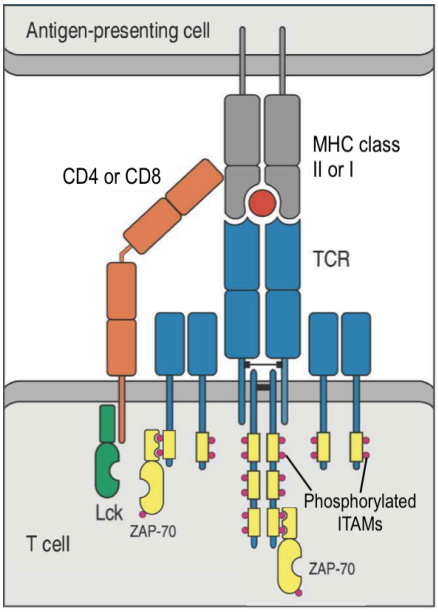

Fig. 4-2. Activation of T cell through interaction with antigen presenting cell. The interaction of the MHC molecule of an antigen presenting cell with CD4 or CD8 and TCR of a T cell is shown. ITAMs (yellow rectangles) are phosphorylated (red circles). Adopted from Janeway, et al[3].

The signaling through the TCR complex alone may not be sufficient to activate a naive T cell. This can be aided by co-stimulatory molecules like CD28 which further enhances proliferation, cytokine production, and survival of T cells. CD28 is present on the surface of all naive T cells and binds the co-stimulatory ligands CD80 or CD86, which are expressed on some antigen-presenting cells (Fig. 4-3). After binding, the cytoplasmic domain of CD28 is phosphorylated and activates phosphoinositide 3-kinase, which generates phosphatidylinositol (3,4,5)-trisphosphate (PIP_3), which also leads to similar downstream signaling pathways to the pathways used by ZAP70[3].

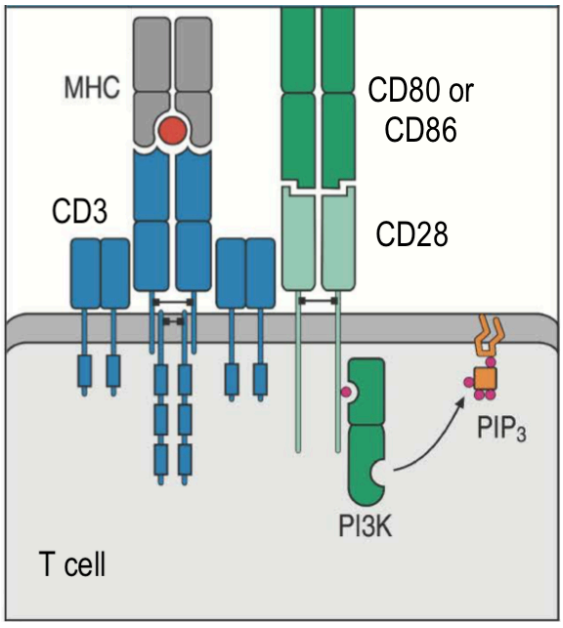

Fig. 4-3. Binding and signaling of co-stimulatory ligand CD28 in T cell interaction with antigen presenting cell. Adopted from Janeway, et al[3].

Anti-CD3ε and anti-CD28 antibodies are used to provide antigen-independent signaling and stimulation for T cells. Treatment with anti-CD3ε and anti-CD28 antibodies mimic the binding of the MHC-antigen peptide complex to the TCR complex and CD80 to CD28, respectively. The extent of stimulation is more greatly dependent on the concentration of anti-CD3ε than anti-

CD28[4]. Culture plates that are pre-coated with anti-CD3ε and anti-CD28 are used for T cell activation assays. This method of activation is used for both CD4 and CD8 T cells[5].

Carboxyfluorescein succinimidyl ester (CFSE) is a fluorescent dye with an excitation of 494 nm and emission of 521 nm that can be used to trace cells and observe proliferation[6]. When cells are stained with CFSE and divide, the daughter cells contain half of the fluorescence dye. This "dilution" is repeated with every cell division. Hence, cells with high CFSE signal have not divided while cells with stepwise lower CFSE signal have divided multiple times[7]. This assay leads to a more accurate method of determining proliferation when compared to simply quantifying the cells, because the quantity of cells for every generation of division and the number of rounds of division can be quantified (Fig. 4-4).

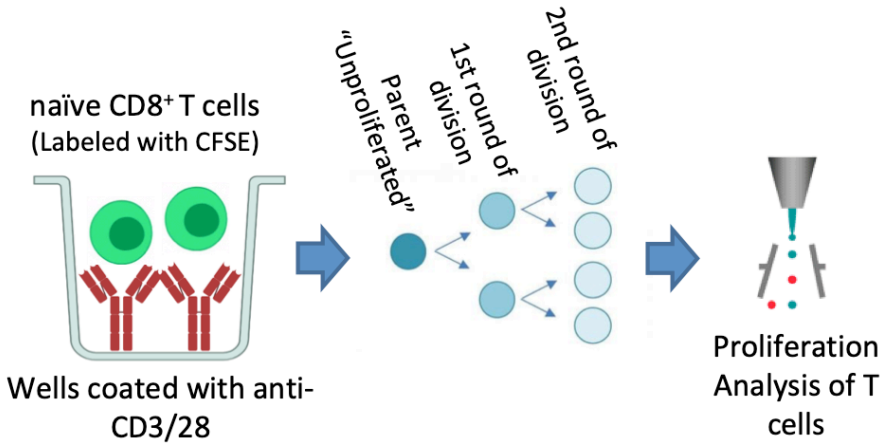

Fig. 4-4. Schematic diagram of stimulation of T cells using anti-CD3/CD28 antibodies and analysis of proliferation.

4-2. Materials and Methods

4-2-1. Mice

Male B6(Cg)-*Tyr*$^{c\text{-}2J}$/*J* (B6 albino) albino mice were obtained from Charles River Laboratories, Japan (Yokohama, Japan). All mice were housed in specific pathogen free conditions in the animal facilities at Tokyo Institute of Technology. Animal experiments were performed with the approval of the Animal Ethics Committees of Tokyo Institute of Technology (no. D2020008) and in accordance with the Ethical Guidelines for Animal Experimentation of Tokyo Institute of Technology.

4-2-2. Subcutaneous tumor formation

The experiment was performed using 6 to 9-week-old male B6 albino mice. The mice were anesthetized with pentobarbital sodium (Somnopentyl, Kyouritsu Seiyaku). Murine Lewis lung carcinoma cell line LLC obtained from American Type Culture Collection (ATCC) (Maryland, USA) maintained with 5% fetal bovine serum-Dulbecco's Modified Eagle's medium (FBS-DMEM) (Nacalai Tesque) supplemented with penicillin (100 units/mL) and streptomycin (100 mg/mL). The cultured LLC cells were collected by trypsinization and adjusted to a concentration of 1×10^6 cells/ 20 μL. Cells were mixed with an equal volume of Geltrex® (Thermo Fisher Scientific) and then injected subcutaneously into the ventral part of the hind limb of mice.

4-2-3. Isolation of tumor infiltrating lymphocytes from tumors

Subcutaneous tumors of 15-20 mm in diameter were resected, minced using a scalpel blade and digested in RPMI medium (Thermo Fisher Scientific) supplemented with 2% FBS and 2.6 U Liberase DH (Roche Applied Science) at 37°C for 60 min, and then sequentially passed through

250, 100, and 40 μm strainers (Greiner Bio-One) to obtain single-cell suspensions. Cells were then resuspended in PharmLyse^{TM} solution (BD Bioscience) and incubated for 10 min at room temperature to lyse red blood cells. To select for the adherent cells, the cells were seeded into culture dishes with 2% FBS-RPMI at a seeding density of 2×10^7 cells/10 cm culture dish (Thermo Fischer Scientific) and incubated at 37°C for 20 min to allow adherent cells to attach to the surface of the dish. The non-adherent cells were collected and seeded again onto another culture dish in order to remove more adherent cells. The non-adherent cells remaining from that dish were collected for further analysis as the non-adherent fraction. The plate containing adherent cells were washed three times with PBS containing 0.68 mM EDTA. Strongly adherent cells were dislodged using PBS containing 2.5 mM EDTA and were collected with light scraping: these cells are the adherent fraction. Cells were resuspended in FACS buffer (PBS containing 1.2 mM EDTA and 5% FBS) in preparation for FACS.

4-2-4. FACS

Cells were blocked with anti-FcγRII/III and stained with anti-CD11b (BioLegend), Gr-1 (BioLegend) and anti-F4/80 (Bio-Rad). MLACs and MDSCs were sorted using SH800S (Sony Biotechnology Tokyo, Japan). Information on antibodies is listed in Table 4-1.

4-2-5. Flow cytometry

Cells were blocked with anti-FcγRII/III (Biolegend) for 25 min at 4°C and stained with fluorophore-conjugated antibodies (see Table 4-1 for concentrations and manufacturers of antibodies) for 30 min at 4°C. Cells were washed once with FACS buffer to remove unbound

antibodies. The cells were analyzed using the iCyt EC800 (Sony Biotechnology). Flow cytometry results were further analyzed using FlowJo (TreeStar).

Table 4-1. Antibodies used for FACS and flow cytometry analysis

Antibodies	Fluorochrome	Manufacturer	Clone number	Concentration
Gr-1	PE, Pe-Cy7	BioLegend	RB6-8C5	1:100
CD11b	PE/Cy7, AF488	BioLegend	M1/70	1:200
F4/80	AF647, AF488	Bio-Rad	C1:A3-1	1:50
H2-Ab1	PE	BioLegend	AF6-120.1	1:50
CD11c	Pe-Cy7, PE	BioLegend	N418	1:100

4-2-6. FACS

Disaggregated tumors and spleen samples were blocked with anti-Fc γ RII/III and stained with fluorophore-conjugated antibodies. Splenocytes were stained with anti-CD8 (BioLegend, 53-6.7, 1:100) and $CD8^+$ T cells were isolated through SH800S (Sony Biotechnology).

4-2-7. qRT-PCR

cDNA was generated from using the ReverTra Ace (Toyobo Co.) reverse transcriptase. The reaction mixture included 4 μL reaction buffer, 200-300 ng total RNA sample, 2 μL $Oligo(dT)_{20}$ primers (10 pmol/μL), 2 μl dNTP (10 mM), 40 U RNase inhibitor, 100 U reverse transcriptase, and the total volume was made up to 20 μL with nuclease free water. Reverse transcription was performed using the following conditions: 30°C for 10 min, 42°C 20 min, and 99°C for 5 min WK0232 Thermal cycler (Wako).

The Thunderbird SYBR qPCR mix (Toyobo Co.) was used to quantify the expression levels of various genes. The reaction mixture contained 0.4 μM of each primer, 5 μL of diluted cDNA and nuclease free water for a total volume of 20 μL. The reaction mixtures were preheated at 95°C for 10 min to activate the enzyme and then underwent 40 cycles of melting at

95°C for 15 sec, and annealing/extension at 60°C for 1 min in a TP800 Thermal Cycler Dice Real Time System (Takara Bio). The primers used are listed in Table 4-2-1.

Table 4-2-1. Primers used in qRT-PCR

Gene name	Sequence
Mgl2	F: ACTTCCAGAACTTGGAGCGG
	R: CTGGGAAGGAACTGTTAGAGCA
CD209a	F: CACTGCCTGCCACAATGT
	R: CCCAGTACCATGTAGACTCC
CD74	F: CCGAAATCTGCCAAACCTGTG
	R: CAGGCCCAAGGAGCATGTTA
Klrd1	F: CAGGAAGTTTCTGAATGC TGTGT
	R*:* TGGATTGGGGCTGAAGAAGG

4-2-8. In vitro co-culture assay

Boyden-chamber assays were performed using a 6.5-mm transwell® with 0.4-μm pore membrane insert (Greiner Bio-One). Fire fly-expressing LLC (LLC/Fluc) cells[8] (2.4×10^4 in 1.44 mL DMEM+5% FBS medium) were seeded into the bottom chamber, while myeloid cells sorted from tumors (3.6×10^4 in 100 μL RPMI+10% FBS medium) were seeded in the upper chamber of the transwell®. After 48 hrs of co-culture at 37°C, LLC/Fluc cells were lysed with Passive Lysis Buffer (Promega), then the luciferase activity was measured using a Luciferase Assay Kit (Promega) and luminometer (GL-210A, Microtec Co., Ltd, Chiba, Japan).

All recombinant DNA experiments were performed with the approval of the recombinant DNA advisory committees of the Tokyo Institute of Technology. All methods were performed in accordance with relevant guidelines and regulations.

4-2-9. T cell suppression assay

$CD8^+$ T cells were sorted from splenocytes of healthy C57BL/6 mice and labeled with 2.5 μM carboxyfluorescein succinimidyl ester (CFSE) (Thermo Fisher Scientific) for 10 min. The cells were then washed and resuspended in RPMI supplemented with 10% FBS and 50 μM β-mercaptoethanol. T cells (5×10^4) were seeded into each well of a 96-well U-bottom plate (Corning, Corning, NY, USA) that was pre-coated with anti-CD3 ε (0.75 μg/mL, BioLegend, 145-2C11) and anti-CD28 (2 μg/mL; BioLegend, 37.51) for stimulated set-ups. T cells were then co-cultured with sorted MLACs or MDSCs and incubated for 3 days. Cells were then collected, blocked with anti-mouse CD16/32 (BioLegend, 93, 1:200), and stained with anti-CD8 (BioLegend, 53-6.7, 1:100). T cell proliferation was assessed by flow cytometry (iCyt EC800).

4-2-10. Statistical analysis

All data are presented as mean $\pm$ standard deviation and were statistically analyzed with unpaired t-test. *P*-values of 0.05 or less were considered statistically significant.

4-3. Results

H2-Ab1 and CD11c are expressed in populations of MLACs, while none of these proteins are expressed in MDSCs. The FACS gating strategy using these surface markers was developed to isolate MLAC populations from $CD11b^{+}F4/80^{-}$ cells without adhesion-based separation (Fig. 4-5). When cells were isolated by this method, about 15% and 13% of the $CD11b^{+}F4/80^{-}$ cells were $H2\text{-}Ab1^{+}$ and $CD11c^{+}$, respectively, and these percentages were about half of those gated from the MLACs obtained by adhesion-based separation (Adh-MLAC) (Fig. 3-11). To validate the molecular characteristics of the $CD11b^{+}F4/80^{-}H2\text{-}Ab1^{+}$ and $CD11b^{+}F4/80^{-}CD11c^{+}$ cells (hereafter abbreviated as $H2\text{-}Ab1^{+}$ and $CD11c^{+}$, respectively, and their negative counterparts as $H2\text{-}Ab1^{-}$ and $CD11c^{-}$) were sorted directly from tumor single cell suspensions and analyzed for expression of the MLAC signature gene by qRT-PCR. The expression of *Mgl2*, *Cd209a, Klrd1, and Cd74* were highly elevated in Adh-MLACs, $H2\text{-}Ab1^{+}$ cells, and $CD11c^{+}$ cells, but low in $H2\text{-}Ab1^{-}$ cells, and $CD11c^{-}$ cells, and MDSCs isolated from the NA-MDSC (Fig. 4-6).

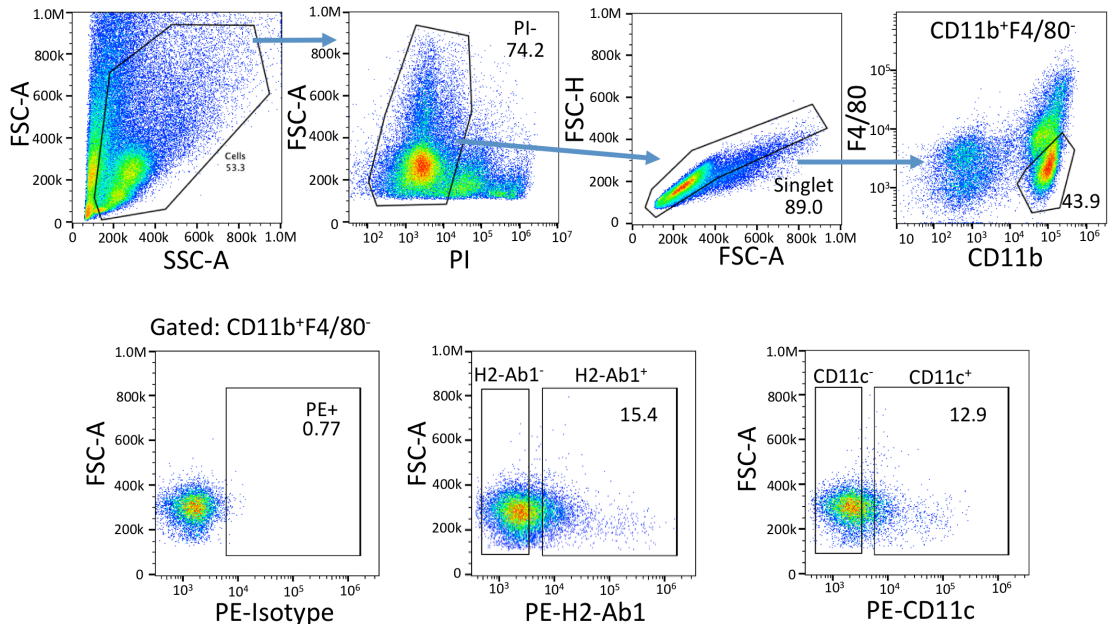

Fig. 4-5. Gating strategy for H2-Ab1$^+$ and CD11c$^+$ MLACs from LLC tumor-extracted cells. CD11b$^+$F4/80$^-$ cells were first gated (upper) and analyzed for H2-Ab1 (bottom center) and CD11c (bottom right) expression by flow cytometer. Positive gates were set based on isotype controls (bottom left).

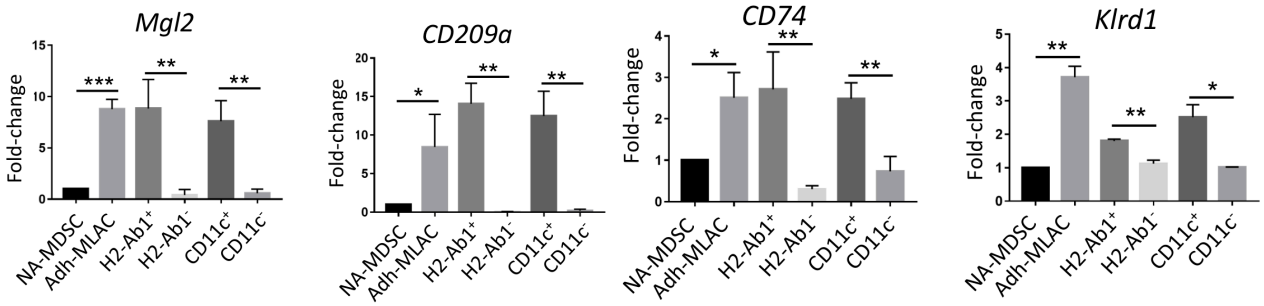

Fig. 4-6. Expression analysis MLAC signature genes in H2-Ab1$^+$ and CD11c$^+$ MLAC. H2-Ab1$^+$ cells, CD11c$^+$ cells, H2-Ab1$^-$ cells, CD11c$^-$ cells, Adh-MLAC, and NA-MDSCs were sorted by FACS and subjected to qRT-PCR. Expression levels of target genes were normalized to actin and fold-change of target cell population over NA-MDSC expression was calculated. Error bars indicate standard deviation, $n = 3$. * $p < 0.05$, ** $p < 0.01$, *** $p < 0.001$, n.s.

Then, H2-Ab1$^+$ and CD11c$^+$ MLAC subsets were investigated for functional characteristics previously identified in MLACs: direct growth promotion and lack of immunosuppression[66]. H2-Ab1$^+$ and CD11c$^+$ cells showed significant LLC growth-promoting activity to the similar

extent as Adh-MLACs, while H2-Ab1$^-$ and CD11c$^-$ cells showed weak growth-promoting activity similar to NA-MDSCs (Fig. 4-7).

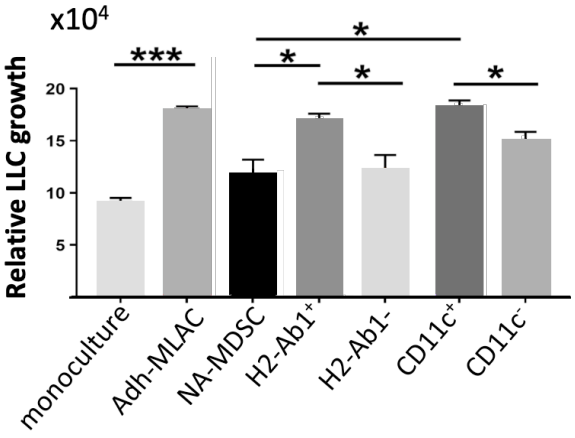

Fig. 4-7. Direct growth-promoting effects of H2-Ab1$^+$ and CD11c$^+$ MLACs on cancer cells. LLC/Fluc cells were co-cultured with test cells. After co-culture for 48 hrs, the luciferase activity of the LLC/Fluc cells was measured. The growth rate of LLC/Fluc cells without co-culture was indicated as monoculture. Relative LLC/Fluc growth is expressed as relative luminescence units. Error bars indicate standard deviation, $n = 3$. *$p < 0.05$, *** $p < 0.001$, n.s, not significant.

Then the immunosuppressive activity of MLAC and MDSC were examined by a co-culture immunosuppression assay, in which Adh-MLACs and NA-MDSCs were co-cultured with polyclonally stimulated CD8$^+$ T cells. T cell proliferation rates were examined by CFSE dilution. The results suggest that Adh-MLACs did not suppress T cell proliferation, while NA-MDSCs showed significant suppression of T cell proliferation (Fig. 4-8A), confirming the T-cell immunosuppressive activity of MDSCs and lack of such activity in MLACs[66]. When H2-Ab1$^+$ cells, CD11c$^+$ cells, and their corresponding marker negative populations were examined for immunosuppressive activity, CD8$^+$ T cell proliferation was not affected by H2-Ab1$^+$ or CD11c$^+$ cells, but was significantly inhibited by H2-Ab1$^-$ and CD11c$^-$ cells (Fig. 4-8B), indicating that H2-Ab1$^+$ and CD11c$^+$ cells lack T-cell immunosuppressive activities. These results confirmed that H2-Ab1$^+$ and CD11c$^+$ subsets possess functional properties of MLACs.

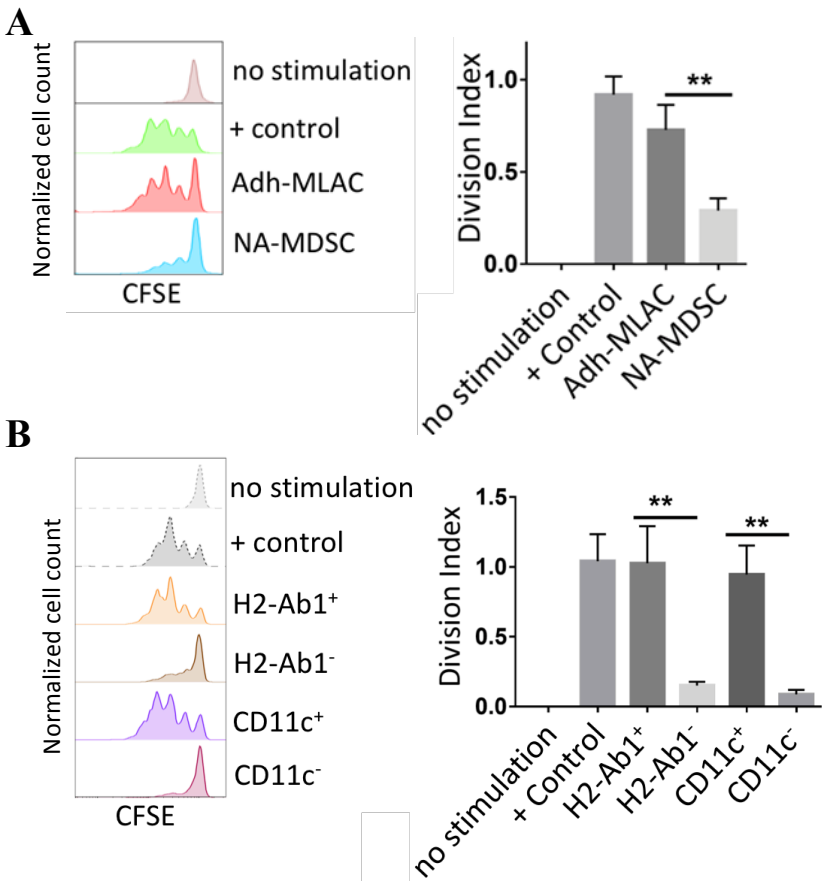

Fig. 4-8. Immunosuppressive activity of H2-Ab1$^+$ and CD11c$^+$ cells. **A, B.** CFSE-labeled and stimulated CD8$^+$ T cells were co-cultured with Adh-MLACs or NA-MDSC (A) and with H2-Ab1$^+$ cells or CD11c$^+$ cells (B). T cell proliferation was analyzed by flow cytometry and indicated by division index. Error bars indicate standard deviation, $n = 3$; $^{**}P < 0.01$.

4-4. Discussion

This chapter presented the equivalence of the H2-Ab1$^+$ and CD11c$^+$ MLAC subsets to Adh-MLACs verified by analyzing key characteristics of MLACs. The scRNA-seq analysis and validation of surface markers, in the previous chapter, have highlighted the heterogeneity within MLACs. Thus, it was challenging to identify marker proteins that could label the entire MLAC population, with uncharacterized subsets remaining among Adh-MLAC. Only 13%-16% of Adh-MLAC co-expressed both H2-Ab1 and CD11c (Fig. 3-12), with some populations of Adh-

MLAC expressing only one marker. Therefore, when sorting using only one marker, H2-Ab1$^-$ and CD11c$^-$ cells could have been mixed with considerable number of MLACs. Nevertheless, H2-Ab1$^-$ and CD11c$^-$ cells did not show clear MLAC properties, except that they had slightly higher growth-promoting activity than MDSCs (Fig. 4-7). The "residual" MLAC population is potentially very minute among the CD11b$^+$F4/80$^-$ population, as they were hardly detected by qRT-PCR analysis (Fig. 4-6). Because the use of either marker would be sufficient to isolate and label cells with MLAC characteristics, utilizing H2-Ab1$^+$ and CD11c$^+$ subsets sorted directly from tumor-extracted cells will facilitate further investigation of MLACs. Additional studies are needed to more deeply explore the other CD11b$^+$F4/80$^-$ Adh-MLAC subpopulations and determine the relationship and potential differences between H2-Ab1$^+$ and CD11c$^+$ MLAC subsets.

Many of the genes and proteins that were upregulated in MLACs have a role in antigen presentation. Moreover, there were several subunits of MHCII that were more highly expressed in MLACs than in MDSCs. Therefore, it is important to clarify whether MLACs have any immunostimulatory activity. It is also important to determine the full extent of MHCII expression in MLACs by intracellular flow cytometry.

Although this study focused on plasma membrane proteins, cytosolic and nuclear proteins may be excellent markers for isolating specific cell populations. Investigating these proteins in future studies may identify marker proteins that enable the isolation of the entire MLAC population from tumor-extracted cells. In the meantime, studies using the H2-Ab1$^+$ and CD11c$^+$ subsets are expected to provide sufficient information to advance the understanding of MLACs, leading to the development of therapeutic strategies to inhibit or delay the formation of an immunosuppressive TME.

References

1. Love, P. E. & Hayes, S. M. ITAM-mediated signaling by the T-cell antigen receptor. *Cold Spring Harb. Perspect*. Biol. 2, a002485 (2010).

2. Ngoenkam, J., Schamel, W. W. & Pongcharoen, S. Selected signalling proteins recruited to the T-cell receptor-CD3 complex. *Immunology* 153, 42–50 (2018).

3. Murphy, K., Travers, P., Walport, M., & Janeway, C. Janeway immunobiology. Garland Science, New York 53, (2013).

4. Yang, H., Parkhouse, R. M. E. & Wileman, T. Monoclonal antibodies that identify the CD3 molecules expressed specifically at the surface of porcine gammadelta-T cells. *Immunology* 115, 189–196 (2005).

5. Bashour, K. T. et al. CD28 and CD3 have complementary roles in T cell traction forces. *Proc. Natl. Acad. Sci*. 111, 2241–2246 (2014).

6. Carson, M. J. & Wilson, E. H. Visualizing chemokine-dependent T cell activation and migration in response to central nervous system infection. *Methods Mol. Biol*. 1013, 171–183 (2013).

7. Quah, B. J. C. & Parish, C. R. New and improved methods for measuring lymphocyte proliferation in vitro and in vivo using CFSE-like fluorescent dyes. *J. Immunol. Methods* 379, 1–14 (2012).

8. Tsubaki, T. et al. Novel adherent $CD11b^{+}$ $Gr\text{-}1^{+}$ tumor-infiltrating cells initiate an immunosuppressive tumor microenvironment. *Oncotarget* 9, 11209–11226 (2018).

Chapter 5

Conclusions and Future Prospects

Myeloid cells are a highly diverse immune cell population that abundantly infiltrate tumors and contribute to the development of a complex TME. Among them, MLACs are a recently identified subpopulation of myeloid cells that infiltrate tumors early in development and promote tumor growth. Because of these functions, MLACs play an important role in establishing an immunosuppressive TME. However, MLAC can only be isolated through adhesion-based separation, and share several surface markers with MDSCs such as Ly6C and Ly6G. Hence, the lack of MLAC-specific markers has hindered further characterization of MLACs and *in vivo* studies on the precise functions of MLACs have been limited. In this study, I aimed to investigate cell surface markers of MLACs by comparing them with MDSCs using a combination of RNA-seq and plasma membrane proteomics analyses.

Chapter 2 describes the transcriptome analysis of MLACs. In order to discover surface markers to isolate MLAC by FACS and gain a deeper understanding of their functions, transcriptome analysis was performed through a combination of RNA-seq analysis and analyzing public scRNA-seq data. Because of the similarity of surface markers between MLACs and MDSCs, the transcriptome profile of these two cell populations was compared. GSEA of these upregulated genes for MLAC suggest that MLACs are involved in unique biological processes compared with MDSCs, such as inflammation through cytokine production and granulocyte migration. The differentially expressed genes of MLACs were further applied to a public scRNA-seq dataset, which allowed for the identification a cell cluster that corresponds to MLACs. This MLAC cluster expressed all the top plasma membrane protein encoding genes found from RNA-seq and also had low expression of MDSC gene markers. These analyses revealed that MLACs are distinct from MDSC and other intratumoral myeloid cells. This also identified *CD209a, Mgl2, CD74,* and *Klrd1* as MLAC gene markers. Because these four genes

were validated to be consistently upregulated in MLACs compared to MDSCs, they were assigned as a MLAC gene signature; a set of genes that can identify cells as MLACs.

Chapter 3 describes the plasma membrane proteome analysis of MLACs in order to discover high confidence surface markers for MLACs. Because mRNA expression level does not always correlate to protein expression, plasma membrane proteome analysis was also performed to supplement transcriptome analysis. This analysis was performed by isolating plasma membrane proteins from MLACs and MDSCs and subjecting them to LC-MS/MS. Several plasma membrane proteins were detected and their expression correlated to transcriptome analysis. RRHO analysis was then performed as a statistical tool to combine and integrate proteome analysis with RNA-sequencing data, and obtain the top correlated plasma membrane protein candidates from both analyses. The expression of candidate protein markers between MLACs and MDSCs were then tested by flow cytometry analysis by staining with commercially available antibodies. An MHCII subunit H2-Ab1 and an adhesion protein CD11c were highly expressed in a significant population in MLACs while they were not expressed in MDSCs. Approximately 32% and 28% of MLACs could be labeled with H2-Ab1 and CD11c antibodies. When used together, these markers could label about half of the MLAC population.

Chapter 4 validated H2-Ab1 and CD11c as MLAC markers through sorting and testing of marker-positive populations. H2-Ab1 and CD11c was employed in sorting MLAC populations directly from tumors instead of relying on adhesion-based isolation. H2-Ab1^{+} and CD11c^{+} cells were sorted from the CD11b^{+}F4/80^{-} tumor population by FACS. By performing qRT-PCR, these H2-Ab1 and CD11c expressing MLAC subsets expressed high levels of MLAC signature genes. The growth promoting activity of these MLAC subsets were confirmed by performing co-culture growth assay with LLC cells and the absence of immunosuppressive activity was confirmed by

co-culture immunosuppression assay with naïve $CD8^+$ T cells. These were comparable to the characteristics of MLACs collected by adhesion-based isolation (Adh-MLACs). In contrast, the corresponding $CD11b^+F4/80^-H2\text{-}Ab1^-$ and $CD11b^+F4/80^-CD11c^-$ cell populations had low expression of MLAC signature genes, had weak cancer growth promoting activity and were immunosuppressive. This showed the equivalence of $H2\text{-}Ab1^+$ and $CD11c^+$ cells with MLACs isolated using adhesion-based separation. This confirmed the use of H2-Ab1 and CD11c as marker proteins for the isolation of MLAC populations from tumors.

Investigation of MLACs defined by surface markers can further facilitate the study of MLACs, leading to a better understanding of the function of myeloid cells in TME and malignant progression. Determining whether MLACs are also present in humans is important for understanding tumor immunity. Humans possess several CD11c and MHCII expressing cell subpopulations[1]. Human orthologs for all the MLAC markers such as HLA-DQB2 for H2-Ab1[2] exist and can be used as a framework to determine the MLAC counterparts in humans.

Further *in vivo* analysis is required to examine the universality of MLAC markers and the MLAC gene signature across different tumor models and tissues, such as spleen, blood, and bone marrow. The dynamics and pattern of MLAC accumulation in early tumors could also be determined using a mouse model with fluorescent reporters, such as Kikume Green-Red, which changes color from green to red upon violet light-irradiation[3]. The spleen or bone marrow may be irradiated following tumor formation, and the presence of MLACs within the photoconverted cells can be detected to determine the origin, tissues of accumulation, and fate of MLACs.

References

1. S. K. Wculek, F. J. Cueto, A. M. Mujal, I. Melero, M. F. Krummel, D. Sancho, Dendritic cells in cancer immunology and immunotherapy, *Nat. Rev. Immunol*. 2020, 20, 7–24.

2. J. A. Blake, J. T. Eppig, J. A. Kadin, J. E. Richardson, C. L. Smith, C. J. Bult, The mouse genome database community knowledge resource for the laboratory mouse*, Nucleic Acids Res*. 2017, 45, D723–D729.

3. H. Tsutsui, S. Karasawa, H. Shimizu, N. Nukina, A. Miyawaki, Semi-rational engineering of a coral fluorescent protein into an efficient highlighter,.*EMBO Rep*. 2005, 6, 233–238.

Achievements

Publications

Diem Thi Phuong Tran, Takahiro Kuchimaru, Mongkol Pongsuchart, Kha The Nguyen, **John Clyde Co Soriano**, Tetsuya Kadonosono, Shinae Kizaka-Kondoh. ROR2 regulates the survival of murine osteosarcoma cells in lung capillaries. *J. Cancer Metastasis Treat.* 6, 47 (2020).

Hitomi Miyabara, Ryuichiro Hirano, Shigeaki Watanabe, **John Clyde Co Soriano**, Hitomi Watanabe, Takahiro Kuchimaru, Nobuo Kitada, Tetsuya Kadonosono, Shojiro A. Maki, Gen Kondoh, Shinae Kizaka-Kondoh. In vivo optical imaging of tumor stromal cells with hypoxia-inducible factor activity. *Cancer Science* Oct;114(10):3935-3945 (2023).

John Clyde Co Soriano, Shiho Tsutsumi, Daiya Ohara, Keiji Hirota, Gen Kondoh, Tatsuya Niwa, Hideki Taguchi, Tetsuya Kadonosono, Shinae Kizaka-Kondoh. Identification of surface markers and functional characterization of myeloid derived suppressor cell-like adherent cells. *Advanced Biology* (2023). [In press]

Poster Presentations

John Clyde Co Soriano, Shiho Tsutsumi, Tetsuya Kadonosono and Shinae Kondoh. Determination of MDSC-like Adherent Cell Marker by Analysis of Adhesion Proteins. IVIS user Imaging Forum 2019.

John Clyde Co Soriano, Daiya Ohara, Keiji Hirota, Gen Kondoh, Tatsuya Niwa, Tetsuya, Kadonosono and Shinae Kizaka-Kondoh. Identification of Surface Markers and Functional

activities of MDSC-like Adherent Cells (MLAC). 45th Annual Meeting of the Molecular Biology Society of Japan 2023.

Acknowledgements

I would like to express my deepest thanks to my supervisor, Dr. Shinae Kondoh of the Faculty of Life Science and Technology, the School of Life Science and Technology, Tokyo Institute of Technology, who gave me the opportunity to study PhD. I would like to thank Dr. Tetsuya Kadonosono for his essential advice in the development of this study.

I would like to acknowledge the technical assistance of the FACS Core Laboratory, Institute of Medical Science, Tokyo University for helping in the designing of gating scheme and providing essential advice for cell sorting. I would also like to thank Shiho Tsutsumi for assistance with cell sorting, optimization of isolation conditions and mouse tumor experiments.

I would like to thank Dr. Keiji Hirota and Daiya Ohara for their analysis of raw RNA-seq data, Gene Ontology analysis and essential advice in transcriptomes analysis. I would also like to acknowledge the Open Research Facilities for Life Science and Technology, Tokyo Institute of Technology for allowing me to use their qPCR thermocycler and FACSmelody.

I would like to thank the Cell Biology Center Research Core Facility at Tokyo Tech for the TripleTOF 6600 mass spectrometer measurements.

Additionally, I would like to thank the former members of Kondoh laboratory and members of Kadonosono laboratory for supporting me in my endeavors. Finally, I would like to thank my parents and friends for constantly encouraging me.

John Clyde Co Soriano

2023